THERMODYNAMIC STUDIES

OF

INCLUSION COMPOUNDS

A thesis submitted for the Degree of Doctor
of Philosophy of the University of London

by

Henry John Francis STROUD

B.Sc., A.R.C.S.

Physical Chemistry Laboratories,
Department of Chemistry,
Royal College of Science,   October 1969.
Imperial College,
London, S.W.7.

TO MY WIFE

ABSTRACT

Experimental and theoretical aspects of the thermodynamics of the sorption of simple molecules in a molecular sieve zeolite are studied. Relationships are derived which express certain bulk thermodynamic properties of these systems in terms of the molecular parameters by means of a grand partition function. Numerical calculations are presented for methane sorbed in a synthetic zeolite, Linde Molecular Sieve type 5A. The various canonical partition functions and related summations required in these calculations are estimated using the Monte Carlo method; those for close packed systems are obtained indirectly. These results show that over an extensive temperature range the heat capacity of the sorbed phase is dominated by the effects of the redistribution of the sorbate both in and among the cavities which occur in the zeolite.

Experimentally, families of isotherms in the temperature range $194 - 300^{\circ}K$ for methane, ethane and krypton in the above zeolite are reported. Each is of the simple Langmuir form and no hysteresis is observed. The methane-Linde 5A system is studied further by measuring its heat capacity over the temperature range $12 - 300^{\circ}K$ with two different concentrations of methane. Several slow relaxation effects are observed, which are accompanied by either cooling or warming temperature drifts. The molar heat capacity of sorbed methane is dependent on its concentration within the zeolite. Analysis of this data shows qualitative, but not satisfactory quantitative,

agreement with the results obtained from the above theory when a simple spherically symmetric potential for the cavity is used. Better agreement is obtained when the zeolite oxygen atoms are taken as being more ionic and the sorbate-sorbent potential is summed over each sorbent atom independently.

A description is given of the vacuum-type adiabatic calorimeter used in these investigations. The calorimeter vessel and attached heater are especially designed to withstand temperatures over $300^{\circ}K$ during the outgassing of the zeolite. The development of a three channel fully automatic shield control system to maintain the adiabaticity of the vessel during heat capacity measurements is reported.

ACKNOWLEDGEMENTS

CONTENTS

Chapter 1

THERMODYNAMIC STUDIES OF SORPTION
IN A SYNTHETIC ZEOLITE

1.1.   Introduction.

Much work has been done in recent years on the
inclusion of a great variety of molecules in zeolite
minerals. A zeolite is an aluminosilicate which
has a three dimensional tetrahedral framework en-
closing cavities occupied by large cations and
water molecules, both of which are capable of movement
in and removal from the framework. When the water
has been removed by evacuation at high temperatures,
the dehydrated or 'activated' rigid framework remains
as the 'host' lattice which is penetrated by regular
micro-porous channels capable of occluding 'guest'
molecules. The channels are said to be micro-porous
since their cross sectional free diameter (see
Chapter 2) is only of the order of a few interatomic
distances, about 4 - 11 A in the zeolite used in this
work. This means that thermodynamic properties
will not be affected by surface tension phenomena, as
they are in systems containing larger diameter pores.

Many zeolites occur naturally, but that which
was chosen for use in this work is a synthetic
variety first made by the Linde Company. It is
ideally suited to detailed experimental and theoret-
ical studies for several reasons. Its structure,
which has been studied in several laboratories and

is very well characterized, consists of three different
types of cavity. Two of these are too small to be
of any importance in these studies, but the other
type can contain a number of small occluded mole-
cules. These cavities are very nearly spherical
and they are joined together to form the micro-
porous channels by the way of near circular openings,
or windows, bounded by eight oxygen atoms in a very
nearly flat ring. These cavities occur in simple
cubic symmetry so that each is joined to six neigh-
bouring cavities. Thus small molecules which are
able to pass through the restrictions in the channels
can migrate over the entire framework.

This is not the case in most other systems
where 'guest' molecules are occluded in a different
'host' species. In these the guest molecules are
confined to a void when the inclusion compound is
synthesized from which they cannot ordinarily
migrate to other similar voids or away from the
structure altogether without complete distruction
of the compound.

Thus in the inclusion compound formed when
long hydrocarbon chains are occluded in the long
channels of one of the crystal modifications of
urea, the molecules in one channel cannot migrate
into a neighbouring channel; in fact they cannot
even change places with adjacent molecules in the same
channel. More akin to the zeolite inclusion compounds
are the quinol and water clathrates because the
guest molecules are occluded in definite cavities.
However there are important differences. The cavities
are much smaller in the former and are only singly

occupied. Also the crystalline modification of the
host which contains these large voids is thermo-
dynamically unstable when the bulk of the cavities
are not occupied and tends to convert to a different
crystalline form.

It is interesting to study the motions of the
molecules which are occluded in these voids since
the intermolecular forces which govern them can
be formulated with reasonable precision. This is
not the case in the pure condensed phase of the
guest molecules where the molecules have a compar-
able amount of freedom, that is the liquid state,
because there the intermolecular forces on a part-
icular molecule are due to its interactions with
its neighbouring molecules which themselves are
moving extensively. In these occlusion compounds
the positions of the atoms which make up the host
structure are known accurately because the structure
is quite rigid.

A theoretical model of the liquid state was
given by Lennard-Jones and Devonshire (1937) in
which each molecule was assumed to be trapped in a
hypothetical cage or cell composed of its neigh-
bouring molecules. The intermolecular energy of
this caged molecule was calculated by averaging
or 'smearing' out the nearest neighbouring molecules
over a spherical surface such that the average
intermolecular distance was preserved to give a
spherically symmetric potential well in which each
molecule moved.

The cavities of β-quinol and the synthetic

zeolite used in the work reported in this thesis
are in fact nearly spherical and the atoms which
make up the cavity walls are very nearly uniformly
distributed in the spherical surface. Thus the
Lennard-Jones and Devonshire potential can be used
quite satisfactorily to describe the energy vari-
ation within these cavities, and this would simplify
enormously any theoretical calculations.

Van der Waals and Platteeuw (1959) described
a statistical thermodynamic treatment of the occlusion
of simple molecules in quinol type compounds in
which the energy of the molecules within the cavities
was described by the above method. Experimental
thermodynamic data for various species occluded in
quinol were obtained, mainly by Staveley and co-
workers (Grey and Staveley 1963, and references
therein), which gave good foundation to this theoret-
ical approach.

If such an approximation describes satisfactorily
the motion of the molecules in that system, it
would seem worthwhile to see if a similar treatment
could be applied to molecules occluded in zeolites.
Clearly the theory would be more involved because
of the increased complexity of the system, namely
the multiple occupancy of the cavities and the
allowable inter-cavity migration. Another difficulty
in the interpretation of the results would be that
the actual potential in the zeolite cavities is
more heterogeneous than in those systems discussed
earlier and so the assumption of a spherical potential
might be less well founded.

In this chapter the zeolite complexes have so far been thought of as being analogous to host-guest inclusion compounds. They can equally well be considered as consisting of a solid sorbent to which the sorbate molecules are joined by physical forces. Indeed, by far the most common means used to study the behaviour of these complexes is the measurement of sorption isotherms. The usual methods are used, and the results are often interpretated in the formalisms primarily adopted for use with adsorption of molecules on a surface and not molecules filling a fixed volume. In these systems, as opposed to the above mentioned occlusion compounds, the sorbed and gaseous phases of the guest species can remain in thermodynamic equilibrium. At moderate temperatures this is also true for zeolite systems, but in later chapters important effects will be described caused by non-equilibrium states at low temperatures. In these states the molecules cannot migrate through the windows between cavities, and so each molecule is trapped in a cavity like those in clathrates.

Zeolites behave like normal sorbents in that one crystalline form is quite stable thermodynamically whether or not it contains guest molecules. Accordingly, throughout this thesis the zeolite is referred to as a sorbent and the occluded molecules as sorbate. Detailed theoretical accounts of the motions of molecules in normal adsorbed films is lacking. There are two factors responsible for this. Firstly, equilibrium sorption isotherms do not give unequivocally the detail required to characterize the motion of the sorbed molecules. Secondly, the properties of the surface on which the sorption takes

(place

are not easily established. For any crystallite the outer surface will be composed of many crystal planes, and surface imperfections will be present. Thus the data is often indicative more of the nature of the sorbent surface than the sorbate molecular motions. This second point does not apply to zeolite sorption because this does not occur on the outer surfaces of the crystallites but within the cavities. The atoms which make up the surfaces of these are crystallographically arranged, and all the cavities are identical.

The nature of the motions of molecules in the sorbed state has been investigated by heat capacity calorimetry (see Sec. 3.2). This technique has also been used to investigate the properties of molecules occluded in voids of host structures and the ensuing results have yielded significant information on their motions and elucidated many interesting effects. However the data which have been reported of the heat capacity over narrow ranges of tamperature of adsorbed films on the outer surfaces of crystals, mainly of titanium dioxide, have not been interpreted with any degree of success because of the unknown character of the sorbent surface (Pace 1967).

In this thesis a description is given of the determination of the heat capacity of a sorbed phase in a synthetic zeolite at different sorbate concentrations over a wide range of temperatures. The results are discussed both qualitatively and quantitatively, in terms of a statistical thermodynamic theory.

1.2.   This Thesis.

This thesis is concerned, in the main, with
the thermodynamic properties of pure methane sorbed
in Linde Molecular Sieve type 5A. The experimental
data found for this system include a family of iso-
therms determined at temperatures in the range 194 -
300°K (Chapter 4) and the heat capacity of the sorbent
containing two different concentrations of methane
(Chapter 8). The heat capacity of the sorbed methane
is calculable because the heat capacity of the sorbent
containing no sorbate is also obtained (Chapter 7).
These calorimetry experiments are conducted over the
temperature range 12 - 300°K, using a vacuum type
adiabatic calorimeter system. The adiabaticity of
the calorimeter vessel is maintained by means of a
fully automatic shield control system, the development
of which is fully described (Chapter 5).

Linde 5A was used as the zeolite sorbent for
several reasons. Its near spherical cavities made the
above thermodynamic properties particularly amenable
to theoretical calculation. All Linde zeolites
designated type A have identical aluminosilicate
frameworks and hence cavity geometry. The various
types are different in the cations which they contain,
Thus type 4A contains all sodium ions, whereas 5A
has some of these exchanged for calcium ions.
Clearly one calcium ion replaces two sodium ions in
order to maintain electrical neutrality for the whole
structure. This exchange process can easily be continued
to the point where two thirds of the sodium ions have
been replaced. This causes the effective size of the
windows (see Sec. 2.1) between cavities to increase

so that molecules with cross sections of up to about 5A instead of 4A can migrate. More extensive exchange, or exchange with other cations, does not increase the effective size of the windows any further.

The rate at which methane can migrate between cavities is determined by the window size and the temperature. Linde 5A was chosen for use in these studies because its large windows would allow this migration to the lowest temperatures, and so postpone to as low a temperature as possible the complications which arise when this process is slow (Chapter 8).

A description is given of a special calorimeter vessel heater assembly which allowed the vessel to be heated to over $300^\circ C$ during the outgassing of the zeolite sample without removal of the heating element, as was the custom in earlier similar calorimeters.

The thermodynamics of molecules sorbed in Linde 5A are discussed and the derivations of several new relationships are given (Chapter 3). These are applied to calculate numerical results for methane in Linde 5A, and these are compared with the experimental data obtained (Chapter 9).

Also given are families of isotherms for both ethane and krypton in the laboratory sample of Linde 5A. The relevant temperature range is $194 - 300^\circ K$. Theoretical calculations on these systems have yet to be accomplished, as have ~~to to~~ the experimental heat capacity determinations.

CHAPTER-2

SORPTION IN ZEOLITES

2.1.   The Sorbent Structure.

The sorbent used throughout this work is a
Linde molecular sieve, designated type 5A, which
was first reported in 1956 (Breck et al. 1956,
Reed and Breck 1956). This synthetic zeolite is an
aluminosilicate mineral which has a tetrahedral
framework enclosing cavities occupied by large cations
and water molecules, both of which are capable of
movement in and removal from the rigid framework.
The idealised formula is

$$\tfrac{1}{3}Na_2O. \quad \tfrac{2}{3}CaO. \quad Al_2O_3. \quad 2SiO_2. \quad xH_2O \quad .$$
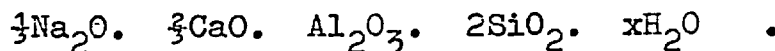
The positions of the water molecules in the framework
do not concern us since the sample in these studies
is always used in the dehydrated form; although
note is made that the size of the unit cell and the
positions of the framework atoms is not very dependant
on the water content (Barrer and Meier 1958, Broussard
and Shoemaker 1960).

The dehydrated structure, excluding the sodium
and calcium atoms and the identity of the silicon
and aluminium atoms, belongs to space group O_h^1-Pm3m
with a lattice constant of 12.30 ±.02A (Reed and
Breck 1956, Lewis 1959, Howell 1960). Density
measurements show that the number of atoms in the unit
cell corresponds to six times that indicated in the

formula. The structural unit can be taken as the 'so-
dalite cage': this is a cubooctahedron consisting of
36 oxygens with interstices among them for 24 silicon
or aluminium atoms, the oxygens forming six four-
membered (4-M) rings and eight 6-M rings. These
sodalite cages can be linked to one another in
various ways resulting in different structures as
in the zeolites type A and X (Meier 1967). The
former structure is formed by joining through 'bridge'
oxygen atoms the 4-M rings producing very small
cubic cages. More significantly, much larger cavities
are produced which are truncated cubo-octahedra.
Each one is surrounded by eight sodalite cages
whose centres fall at the corners of a cube
(Fig.2.1). This large cavity is enclosed by twelve
4-M, eight 6-M, and six 8-M rings. It is these
large volumes in which sorption generally takes
place, it is common to call them α-cavities.
Each such cavity is linked to six others octahedrally
through the six large 8-M rings, thus forming large
micro-porous channels which intersect perpendicularly.

  -       These cavities are almost spherical with a
free diameter of 11.4A.   The six large openings
are commonly called 'windows', each of these near
circular windows has a free diameter of 4.2A.
By free diameter is meant the interatomic distance
less the collision diameter, σ, of the species con-
cerned.   The two free diameters mentioned above
are enclosed by oxygen atoms for which the collision
diameter is taken as 2.70A.

Fig. 2.1.   The Arrangement of the Sodalite Cages
in Linde type A zeolites.
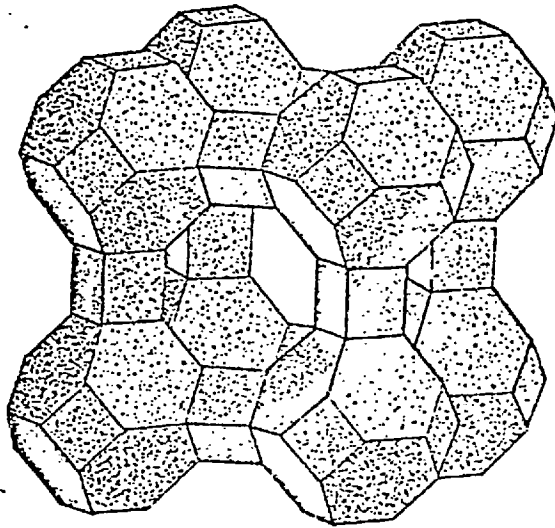
Illustration taken from Meier (1967).

The sodalite cages, of free diameter 6.6 A, are
referred to as β-cavities. Since the largest ring
of oxygen atoms which enclose them is only six-
membered, 2A free diameter, these spaces are of no
great importance in sorption studies. They are
relevant to the present studies because our sample
of the zeolite, like that of Barrer and Meier (1958),
has a high aluminium to silicon ratio (1.058:1,
see Sec. 4.3). They allocated equal numbers of these
atoms to the framework and suggested that the remain-
ing aluminium atoms are occluded as AlO_2^- at the centres
of the β-cavities. Our sample would thus have about
70% of these cavities so filled. Since it is thought
that Al-O-Al bridges with four-coordinate aluminium
are unlikely to exist (Loewenstein 1954) the frame-
work must have the silicon and aluminium atoms
arranged rigorously alternatively. The true unit cell
constant is then double that given above and X-ray
photographs should show superstructure lines, as in
ordered alloy structures. Evidence that these in
fact occur has been presented (Barrer and Meier
1958). Although reference has been made above
to aluminium, silicon and oxygen atoms, obviously
these will all carry some electrical charge.

Owing to the freedom of movement which is
allowed to the cations, thermal excitation and
positional disorder cause there to be much controversy
still concerning their positions. It would seem that
there are two kinds of location, I and II. Ion
exchange, the supported by sorption evidence, suggests that the
latter are much more easily moved, and that they
occupy positions in or near the 8-M windows; it also
suggests that there are eight type I cations, probably

all sodium. These type I cations were first thought
to occupy the 8-fold positions at the centres of
the 6-M rings (Reed and Breck 1956). Lewis (1959)
supported this, and Broussard and Shoemaker (1960)
who alone used hydrated samples came to a similar
conclusion. However it has been postulated that these
cations in fact randomly occupy positions off this
3-fold axis, hence in 24-fold positions (Howell 1960).
The type II positions are more troublesome to locate
precisely. Reed and Breck placed them in the
3-fold positions in the plane of the 8-M ring,
that is balanced between two adjacent α-cavities.
Lewis's work indicated positions 2.5 A along the
axis of the 8-M ring into the cell; whilst Howell
followed the earlier work in placing these cations
in the 8-M ring but increased the degeneracy of these
positions to 12-fold and assumed that in Linde 5A they
were occupied at random by four cations.

Thus it can be seen there exists uncertainty
as to the cation positions. However since the
actual difference in the various proposed structures
is small, parameters which are accurate enough
for the calculation of molecular forces can be
quoted. Also it is quite possible that in the
sorption complexes to be studied here, the cation
locations are slightly dependent on the amount of
material sorbed and the temperature. Averaged
atomic parameters were chosen for the earlier
calculations (Limcharoen 1968) and these are adhered
to in this work in order to make intercomparision
of results posible; they are given in Tables 2.1
and 2.2.

TABLE 2.1.   ATOMIC COORDINATES OF LINDE 5A as fractions
of the lattice constant (from Broussard and
Shoemaker 1960).

Lattice Constant taken as 12·31 A.

Atom	Number in unit cell	Coordinates (Origin at m3m)		
		x	y	z
(Si,Al)	24	0.0000	0.1972	0.3727
O_1 (bridge)	12	0.0000	0.2280	0.5000
O_2 (single)	12	0.0000	0.2878	0.2878
O_3 (4-ring)	24	0.1118	0.1118	0.3482
(Na,Ca)	8	0.1950	0.1950	0.1950

TABLE 2.2.   PARAMETERS FOR α-CAVITY in absolute units (A).

Atom	Number	Distance from cavity centre
(Si,Al)	48	0.5983
O_1 (bridge)	24	0.5692
O_2 (single)	24	0.5832
O_3 (4-ring)	24	0.5695
(Na,Ca)	8	0.5283

2.2 The Sorbed State in Zeolites.

A wide variety of molecules, ranging from
non-polar inert gases to strongly dipolar water and
ammonia, including those as small as helium to
those as large as long-chained normal paraffins,
can enter the cavities of Linde Molecular Sieve
type 5A and hence become 'sorbed' molecules. If
possible, sorption will always take place in the
cavities and not on the outer surface of the cry-
stallites because of the much more favourable heat
of sorption in the cavities where the sorbed molecule
can interact to some degree with sorbent molecules
on all sides. The motions of the sorbed molecules
will depend on the temperature, the amount of cavity
filling, the molecular size and the type of interactions
it has with the sorbent.

The main factors which determine whether a
molecule will be sorbed in Linde 5A are its size,
its structure and the temperature. Breck and Smith
(1959) found that molecules of minimum collision
diameter of up to .5A larger than the zeolite window
could be sorbed because of the bond vibration of
atoms making up the window, however molecules that
were 1A larger could not enter the zeolite at all.
This is partly determined by temperature, since
sorption equilibrium will be hastened by increasing
the temperature due to the increase both in the
kinetic energy of the sorbate and of the increased
vibrations of the atoms of the framework which
form the windows. It is worth noting here that ions
near to the windows reduce their effective size.
For example, putting sodium ions near the windows
of type A zeolites decrease the effective window

diameter from about 5A to 4A, whilst replacing these with potassium ions reduces the size still further. Under comparable conditions, sorption is more profuse for molecules which can interact specifically (Kiselev and Lopatkin 1967) with the sorbent. For instance, ethene is more readily sorbed than ethane because its high polarisability attracts it to the cations.

The physical state of the sorbed molecule is different from guest molecules in clathrate complexes (e.g. water and quinol clathrates) in three ways. First, the cavities are of such a size that multiple occupancy can occur, a Linde 5A cell being capable of holding up to 25 H_2O, 14 to 16 Ar, N_2 or O_2, but only about 4 n-C_4H_{10} (Barrer 1964). A long sorbed molecule can be in two cells at the same time, or a molecule may sit in the window between two cavities. Second, the molecules can diffuse from one cell to another through the windows formed by rings of eight oxygen atoms. Naturally the rate of the process is temperature dependent and might for all practical purposes cease at low temperatures. Third, the sorbed molecule can approach near to dehydrated cations (Ca^{++} and Na^+ in 5A) giving strong ion-induced dipole and perhaps ion-dipole interactions.

Multiple occupancy means that the sorbate-sorbate interactions will have some bearing on the state of the sorbed molecules, and that thermodynamic properties, like the molar heat capacity of the sorbed phase, will probably not be independent of the amount of guest in a fixed amount of host as

is generally the case for clathrates (Parsonage
and Staveley 1959, Stepakoff and Coulter 1963).
This together with the mobility of the molecules through
all the cavities, causes complications in the inter-
pretation of the data on the zeolite sorbed phase.
Thus not only is there multiple occupancy, but the
distribution of the sorbate among the cavities
will change with temperature. Since, when a re-
distribution occurs, it is, in the main, only the
inter-sorbate potential energy which changes,
careful study is required to characterize this
aspect of zeolite sorption.

The motion of the molecules within the cavities,
the inter-cavity motion, is also more complex in
zeolites than in the normal clathrates because
the intermolecular potential is less homogeneous.
This is due to the presence of the exchangeable
cations which, in the activated zeolite, are not
contained in hydration sheaths but are only partially
held by the framework oxygens. In Linde 5A, the
small divalent calcium ions produce large electro-
static fields and field gradients in their neighbour-
hood. At low temperatures it would be expected
that sorbed molecules would become localised in these
environments, causing their motion to be drastically
curtailed. This effect seems to be evident even
for the non-polar, spherically symmetrical molecule
methane (see Ch. 8). These localised molecules
become more mobile about the cavity as the temperature
is elevated, and this process, which is a diffusion
one, can be characterized by an activation enery.
Clearly this 'hopping' process will have a lower
activation energy than the 'hopping' process of the

molecules between cavities since it must always
precede it. Due to the extra potential barriers
within the cell, the 'rattling' vibrational ex-
citation of the molecule in the cavity is thus not
as simple as that of molecules trapped in clathrates.

The rotational motion of the sorbed molecule
will also be affected when it is near a cation.
Clearly dipolar molecules will be most affected,
but calculations show (see later) that for methane
the barrier hindering at least two of its degrees of
rotational freedom is appreciable. Such effects are
only important in clathrates if the molecule is non-
spherical, or its size approaches that of the host
cage. Thus methane in β-quinol rotates freely above
150°K, and is hardly restricted below this temperature
(Parsonage and Staveley 1960, Coulter et al. 1963),
although in this case all three degrees of rotational
freedom are affected.

By far the most extensive data on the zeolite
sorbed state are isotherms. Many studies have been
reported on a wide variety of molecules sorbed in
Linde 5A. Although simple to obtain, the information
which they yield on the sorbed phase is limited
basically to heats and entropies of sorption.
The information retrieved by fitting the data to
theoretical equations is rarely un-ambiguous.
This is because the data are generally imprecise,
and,more subtely, the theoretical equations are
insensitive to changes in the assumed model. For
example, often the constancy of the free energy
of sorption (or a related equilibrium constant)
with the amount of sorption is taken as a criterion

of various models, but this can be constant because
unpredicted changes in the heat and entropy of
sorption with the amount sorbed almost exactly
cancel each other. In any event isotherm data
can give no information about the sorbed state
below the temperature at which the windows become
so small that equilibrium cannot be obtained.

2.3. Sorption and Intermolecular Forces.

For the molecules concerned in this work,
namely methane, ethane, and krypton, the forces
under which the sorbate moves are purely physical.
These forces can be thought to result from several
distinct effects. A general account of these forces
has been presented by Moelwyn Hughes (1961), whilst
Young and Crowell (1962) have reviewed the subject
from the standpoint of physical sorption. In most
studies the forces between the constituent atoms and
ions of the sorbent are ignored and assumed unchanged
during the sorption process; the sorbent is considered
inert and just provides a constant potential in which
the sorbate is placed. This is never strictly true,
but is a very good approximation in physical sorption
studies. It is obviously not valid in chemisorption.
In the work described here. the sorbate does not
affect the rigid zeolite framework, but the cations
could well move slightly when sorption takes place.

The above intermolecular forces can be considered
to be of four types; these are summarized below,
1) A sorbed molecule with a permanent dipole or
quadrupole will tend to orientate itself so that it

can interact attractively with the fields or field
gradients respectively which are present due to the
sorbent. Also these permanent multipoles will interact
mutually to give an extra inter-sorbate attraction.
In this study with molecules which have no permanent
dipoles these forces are ignored. However slight
interactions should occur with ethane and nitrogen
due to their small quadrupole moments and with
methane because of its slight octapole moment.
2) The same fields and field gradients due to the
sorbent will always induce dipoles and quadrupoles in
approaching molecules. The only significant interaction
is the field-induced dipole, where the attractive
potential is given by:

$$E = -\tfrac{1}{2}\alpha F^2$$

where α is the polarisability of the sorbate molecules
and F is the resultant field at the molecule. For the
particular case of zeolitic sorption considered here
the field is due to the cations and oxygens of the
framework. In the theoretical calculations on the
cell model (Sec.2.4), mathematical convenience
necessitates that the total electrostatic charge is
'smeared out' over the whole of the cavity wall.
It is well-known in electrostatics theory that a
sphere with a uniformly charged surface has no field
within it. Thus these calculations do not allow for
any field-induced dipole interactions. In reality
the field within the cavity approaches uniformity
except near the wall and especially near the cations.
At least at low temperatures when the sorbate becomes
virtually non-mobile, the molecules probably reside
very near to the cations for significantly long
periods. Simple calculations show (see later)
that for polyatomic species these forces could restrict

markedly the motion of the molecules.

3) Regardless of whether any pair of molecular species mutually interact in the two ways outlined above, they will always be attracted together by dispersion or 'London' forces. These are the long range interactions of the instantaneous dipoles and multipoles which are mutually induced by the continuous variations which occur in the electron distribution of each system. The most important term is that due to the induced dipole-induced dipole interactions which obeys the relationship.

$$E = -\frac{C}{r^6}$$

where E is the energy, r is the distance between the two atoms, and C is a constant. It is usually assumed that this interaction is additive for each significant pair of atoms. So the total contribution of this interaction type to the sorption potential is the sum of the above terms for all the pairs of atoms, one in the sorbate and one in the sorbent. Pitzer (1959) and Young and Crowell (1962) have reviewed the ways in which the constant C can be evaluated. For two interacting mono-atomic species, the equation of Slater and Kirkwood is frequently used:

$$C = \frac{3eh}{4\pi m_e^{\frac{1}{2}}} \frac{\alpha_1 \alpha_2}{(\frac{\alpha_1}{N_1})^{\frac{1}{2}} + (\frac{\alpha_1}{N_2})^{\frac{1}{2}}}$$

where e is the electronic charge, h Plank's constant, and m_e is the mass of the electron. α_1 and α_2 are the polarisabilities of the two species while N_1 and N_2 are related to the number of electrons in the outer

shells. If an interacting species is polyatomic,
it can be regarded as one entity for this calculation
where α and N then refer to the molecular para-
meters.

Dispersion forces also result from the inter-
action between mutually induced dipoles and quadrupoles
or two quadrupoles, but these are generally quite
small. They are generally ignored because the
equations characterizing them corresponding to the
one above for dipole-dipole interactions are not
well-known. They are often allowed for empirically
(see below).

4) Lastly there are repulsion forces. If the distance
between two species becomes so small that their
electron orbitals overlap, then strong repulsion
forces result. The form of this potential is not
well known and consequently it is chosen so as to
be mathematically tractable. It increases positively
very rapidly as the inter-molecular distance becomes
small, and is realistically represented by an
exponential term. A more convenient form is the
inverse relationship, Rr^{-n}, where R is a constant
and r the inter-species separation. R could be
chosen to make the total potential minimum occur
at the known equilibrium separation. n is nearly
always given the value 12 .

In practice, if the only attractive forces
in the system are of the induced dipole-dipole
type, the total potential is of the form given
by Lennard-Jones:

$$E = -\frac{C}{r^6} + \frac{R}{r^{12}}$$

It is convenient to express the potential in terms
not of C and R, but of ϵ and σ which are energy at
the equilibrium separation and the finite distance
at which the potential is zero, respectively.
The resultant equation is

$$E = -4\epsilon\left((\frac{\sigma}{r})^6 - (\frac{\sigma}{r})^{12}\right)$$

If it is required to calculate intermolecular
forces based on this equation, the only problem
is to decide on suitable values of the parameters ϵ
and σ for each pair of interacting atoms or molecules.

Firstly the interaction between identical
species is considered. Tables have been compiled
(Hirshfelder et al. 1954) of the parameters for
gases found empirically from second virial co-
efficients. These parameters take into account
implicitly the contribution of dispersion forces
from higher multipoles than dipoles. From these tables
the sorbate-sorbate interaction can immediately be
formulated. For spherical species like the inert
gases and methane the resulting potential is quite
accurate, the error would be larger for the non-
spherical ethane, where the true potential is
dependent on the angles of the molecular axes to
the line joining the molecule centres. Previous

calculations of zeolite sorption by Limcharoen
(1968) and those presented in this work are for
krypton and methane only.

Also needed are the corresponding parameters
for the oxygens and cations of the framework.
These are required not because the interest is in
the interactions among the sorbent directly, but
in order to estimate the parameters for the sorbent-
sorbate potential (see below). Since the Lennard-
Jones parameters for cation-cation and oxygen-
oxygen ions are not obtainable from experimental
data like the inter-sorbate parameters, they are
determined by using the theoretical equations.
Thence the maximum interaction energy, ϵ, is calculated
using the Slater-Kirkwood formula given above for
C and the following equations:

$$C = -4\epsilon\sigma^6$$

$$r_o^6 = 2\sigma^6$$

where r_o is the equilibrium separation, i.e. the
separation where the total interaction is ϵ.
There is some controversy over the values to be taken
in the Slater-Kirkwood expression for the polaris-
abilities and effective number of electrons for the
oxygen since they depend on its charge and coordination.

The values used in the calculations here assume
that the charge on the cations is balanced by placing
.25 of the electronic charge on each oxygen; these
values are tabulated and discussed elsewhere
(Limcharoen 1968). The corresponding values were
chosen as those with which the above values for C
gave the correct equilibrium separation.

For two identical species, the Slater-Kirkwood
equation given above simplifies to

$$C = \frac{3eh}{8\pi m_e^{\frac{1}{2}}} \alpha^{\frac{3}{2}} N^{\frac{1}{2}}$$

N is the effective number of electrons , which is
assumed to be the average of the total number in
the atom or ion and the number in the outer sub-shell
(Pitzer 1959). The values for the polarisabilities
for the cation are given directly in the literature
(Landolt-Bernstein 1950). For the oxygen ions the
best value of the polarisability appears to be that
used by Barrer and associates (Barrer and Peterson
1964, Rees and Williams 1964). This value is derived
from the experimental refractivity measurement of
K-felspar, a 3-dimensional aluminosilicate, in which
the oxygens are in a similar environment to those
in zeolites. The value is slightly larger than
the polarisability of neutral oxygen, but much
smaller than that of the oxygen in CrO, CaO, or
MgO. This point is also discussed by Kiselev and
Lopatkin (1967) who found that α varied linearly
with the charge of the oxygen for O, O^- and O^{--}.
Therefore they found the value for $O^{x-}(x = .25)$ by

interpolation.

As mentioned above these parameters are required
in order to calculate the sorbate-sorbent interaction.
If this is assumed to be of the Lennard-Jones type,
then the parameters ϵ and σ are needed for the
interaction between non-identical species. These
are calculated from the corresponding parameters
for the interaction between like species using
'combination rules' (Rowlinson and Townley 1957).

$$\epsilon_{12} = (\epsilon_{11} \epsilon_{22})^{\frac{1}{2}}$$

$$\sigma_{12} = \frac{1}{2}(\sigma_{11} + \sigma_{22})$$

where the subscripts refer to the nature of the
interacting species.

Having arrived at values for all the above
parameters. and knowing the crystallographic data
for the zeolite, in principle the total interaction
can be calculated for any number of molecules in a
cavity for any arrangement of the sorbate. Since
for Linde 5A, each cavity wall can be taken as 72
oxygens and 8 cations, this calculation would be
very tiresome. Since at least the oxygens are
arranged more or less regularly on a near spherical
surface, it is a good approximation to 'smear-out'
all the sorbent interaction centres uniformly on
such a surface. This procedure was proposed by

Lennard-Jones and Devonshire (LJD) (1937) in connection with the theory of the cell model of condensed phases. The resulting spherically symmetrical LJD potential for the sorbate-sorbent interaction is given by

$$U = \Lambda^{\ast}\left((\frac{v^{\ast}}{v_o})^4 \; 1(\frac{r^2}{a^2}) \; - 2(\frac{v^{\ast}}{v_o})^2 \; m(\frac{r^2}{a^2}) \right)$$

where $\Lambda^{\ast}$ = the energy parameter, corresponding to ϵ in the Lennard-Jones potential,

$v^{\ast} = \sigma^3$

$v_o = a^3 2^{-\frac{1}{2}}$

a = radius of the spherical cavity (taken here as the mean distance from the cavity centre of the oxygens),

r = distance of the particular sorbate molecule from the cavity centre,

$1(y) = (1+12y+25.2y^2+12y^3+y^4)(1-y)^{-10}$

$m(y) = (1+y)(1-y)^{-4}$.

This potential function has been closely examined by Wentorf et al. (1950), and used by van der Waals and Platteeuw (1959) to describe the potential in the cavities of clathrates.

Figures 2.2 and 2.3 which are taken from the calculations of Limcharoen (1968) clearly indicate the potential profile for methane in a Linde 5A α-cavity. Figure 2.2 shows the potential along the C_2, C_3 and C_4 axes with the cations and oxygens in their true positions, whilst figure 2.3 is based on the calculation where just the framework oxygens

Fig. 2.2. The Total Interaction Potantial for Methane in a Linde 5A α-cavity.

Fig. 2.3. The Total Interaction Potential for Methane in a Linde 5A -cavity with the Oxygen atoms sphericalized.
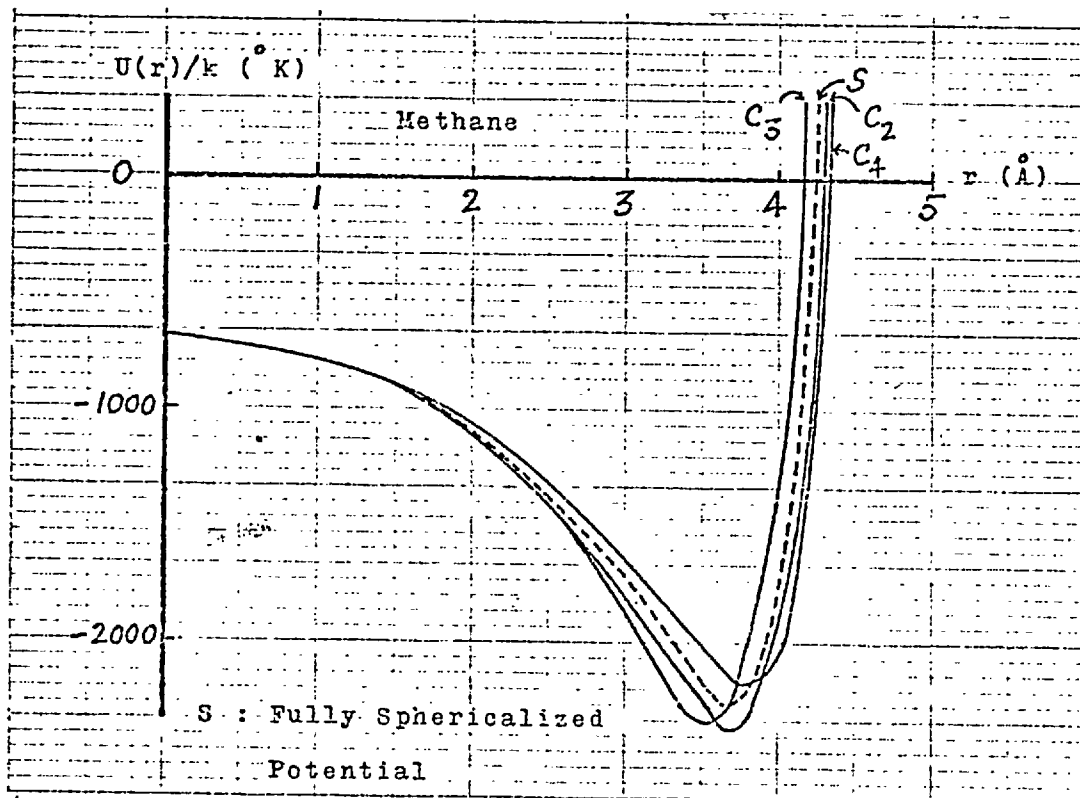
are 'smeared out'. Both diagrams indicate the shape
of the fully sphericalized potential which is used
in the main statistical mechanical calculations
(see Sec. 3.4.4). It is seen that this potential
does in fact give a good representation of the true
potential except along the C_4 axis. This is the
axis of the eight membered rings which connect
neighbouring α-cavities. The true potential only
offers a small energy barrier (about 550 cal/mole)
to sorbate molecules moving into an adjacent cavity
whereas the fully sphericalized potential presents
an infinite barrier around the cavity in all directions.
Thus the latter potential cannot be used to describe
inter-cavities diffusion processes.

CHAPTER 3

THERMODYNAMICS OF ZEOLITIC SORPTION

3.1.   Introduction.

The nature of the sorbed phase in zeolites can
be probed by measuring the change in one or more of
its equilibrium thermodynamic properties when a
different property is altered under known conditions.
These thermodynamic properties include pressure,
temperature, the sorbate to sorbent ratio, heat
capacity or heats of sorption. For example, in
isotherm studies the variation in pressure is noted
when the amount of sorbate in a fixed amount of sorbent
is altered at constant temperature. In order to
interpret the data obtained, the relationship must
be known between the observed macroscopic or molecular
properties. This is the role of statistical
thermodynamics. Two such approaches will be described
below (Sec.3.4).

Firstly the kind of thermodynamic data which can
be obtained will be mentioned. As noted previously
in Section 2.2, by far the most extensive data
available are isotherms, Since these are equilibrium
measurements, at constant amount sorbed, the pressure
and temperature variables are linked through an
equation of the Clausius-Clapeyron type, so that
heats and entropies of sorption can be estimated.
Also models of the sorbed state can be tested by
using the methods of statistical thermodynamics

to derive the corresponding equilibrium constants,
and the constancy of these over a wide range of
pressure can be tested. (Barrer 1958, Garden and
Kington 1956, Garden et al. 1956). However the
imprecision of the experimental data and the insen-
sitivity of the calculated data to changes in the model
often causes this procedure to be of little value
(see Sec.2.2).

This technique is also limited if there is not
complete thermal or mechanical equilibriun throughout
the system, or if any of the sorption processes are
not between true equilibrium states, since the
thermodynamic equations are then no longer valid.
Thus considering the specific case of methane sorbed
in Linde 5A, equilibrium isotherm data cannot be
obtained below the temperature at which the sorbate
can no longer pass at a reasonable rate through the
cavity windows. Yet at these low temperatures the
motions and interactions of the sorbed phase can
be of great interest.

3.2. Calorimetric Data.

Calorimeters have been constructed in many
laboratories to measure heats of sorption or the heat
capacity of the sorbed phase, or occasionally both.
The actual heat of sorption primarily obtained
depends on the apparatus and the manner in which it
is used. This resulted in much confusion in this
field intil it was clarified in papers by Hill (1959),
Kington and Aston (1951), and it has been more

recently reviewed by Pace (1967). For example
a different heat of sorption arises if the sorbate
is added to the sorbent isothermally or adiabatically,
since in the first case a heat of decompression
has been included. These different heats of sorption
can easily be related, and each can be measured
very accurately in precision calorimeters. Also
the heat of sorption for irreversible sorption
processes which cannot be derived from isotherm
data can be measured in this way. Clearly in itself
this could be useful in systems which exhibit
hysteresis to determine whether the sorption or
desorption process is irreversible. For the reversible
step the measured heat of sorption should equal
within the known errors the corresponding value for
the isotherm data.

The problems encountered in measuring significantly
the heat capacity of an sorbed gas are formidable
(Pace 1967), the main problem being that the contri-
bution of the heat capacity of the sorbed gas is
only a small fraction of the gross heat capacity.
Clearly, the more accurate results will be obtained
with the more active sorbents and the most precise
calorimeters. Such are the problems that this type
of heat capacity measurements have only been reported
in recent years, the vast majority of the work being
done by workers in the laboratories of Morrison and
Pace. All the early work (see ref. 4,6,7,20,21,
22,23, and 24 in Pace (1967)) was concerned with
the inert or other simple gases sorbed on the outer
surface of one of two of the three crystal forms
of titanium dioxide. These are rutile and anatase,
both of which are sorbents of large surface area.

Several interesting effects were encountered. In
the nitrogen-rutile system, a relaxation phenomenon
caused long heating drifts at around $35^{o}K$ (Morrison
and Szasz 1948), whilst in the nitrogen trifluoride-
anatase system (Siebert and Pace 1956) a transition
was reported at about $60^{o}K$ at high sorbate concen-
trations only. Unfortunately the interpretation
of these results is hindered by the high heterogeneity
of the surface due to surface defects and also the
various crystals planes which can form exposed surfaces.

To surmount this problem, Pace extended his
work to gases sorbed on a surface which was not
only much more homogeneous but also had a large
surface area (Bobka et al. 1957). The heat capacity
of argon sorbed on highly graphitised carbon (Graphon)
in the range $55-88^{o}K$ was measured at various coverages.
The results were interesting because generally the
heat capacity decreased with increasing temperature
indicating a peak below $55^{o}K$. It would clearly be
interesting to study this system in greater detail.

Each of these studies used an adiabatic calorimeter
with the sample vessel joined by a thin metal tube
to a remote dosing apparatus. This enabled the amount
of sorbate in the vessel to be altered very easily
and the sorbent could be speedily outgassed since there
was no need to remove the vessel from the calori-
meter system. This process needed the adiabatic
shields to be removed, after which the thermometer
and heater were taken from the vessel. The vessel
could then be heated to the required temperature
(usually about $200^{o}C$) whilst its contents were under
vacuum. This experimental arrangement has much to

commend it for convenience of use, its limitations
are also obvious. First, since the vessel heater
has to be removed between runs, it cannot be rigidly
attatched to the vessel. Thus heat exchange will
be relatively slow and large thermal gradients will
exist in the system. There inevitably lead to errors,
particularly at high temperatures. A fuller discussion
of this point is presented in Section 5.4.1.

Second, the main objection to this experimental
procedure is that the vessel is always open. When
the pressure above the sorbent is appreciable, the
amount of gas actually in the vessel is a matter of
doubt. In precise calorimetry, it is necessary to be
able to account accurately for all the energy which
is delivered to or taken from the sample vessel.
The usual practice is to isolate the vessel as much
as possible from the surrounding adiabatic shields
by, amoung other things, making all the connecting
wires as thin as possible and suspending the vessel
by some very poor conductor like nylon cord. In the
above systems the vessel is joined to the shields by
a substantial metal tube, which at the higher temp-
eratures contains gas molecules. Such an arrangement
can have a very high effective thermal conductivity,
especially at very low temperatures (metal conduction)
and near or above the boiling point of the gas. This
last effect is very convincingly exhibited in the
'heat pipe' devices (Eastman 1968). This limits
the working range of the apparatus to the region below
about $150^{o}K$ for acceptable results. As Pace (1967)
comments, the critical part of the apparatus design
is a copper ring just above the shields which counter-
acts these heat links by bringing the temperature

of the metal tube and its contents to the shield
temperature.

The apparatus described in chapter 5 of this
thesis was designed to overcome these problems.
Briefly it can be said here that a closed vessel is
used so that the amount of sorbate in it is definitely
constant and no metal connecting tube is incorporated.
Also, as the heater was designed to withstand the
outgassing temperature (over $300^{\circ}C$ in our case), it
could be fixed permanently to the vessel. Clearly
these modifications improve the attainable precision
of the apparatus over those described earlier, but the
price is paid in that a more complicated outgassing
and sorbate dosing procedure is necessary.

The heat capacity results presented later should
be more amenable to interpretation than those mentioned
above not only because of these apparatus changes,
but also because of the nature of the sorbent used.
On a microscopic scale, the surface of a crystal is
quite non-uniform, indeed the presense of a surface
could be regarded as a defect in the solid state.
It is that part of the material for which the bulk
and periodic crystallographic properties which
characterize the solid become invalid descriptions.
It can be seen then that studies of the nature of a
surface will be very difficult to understand from a
molecular viewpoint. In zeolitic sorption the sorbed
phase does not extend over the crystal surfaces but
penetrates the crystallographic structure. This means
that the environment of this sorbed phase is known
exactly, making a microscopic explanation of its
properties more meaningful. For example, in as much

as a zeolite cavity can be regarded as a sorption site,
all such sites are crystallographically identical.
For surface sorption, this would only be an approxi-
mation even on a very homogeneous surface.

3.3. Heat Capacity of the Sorbed Phase: Thermodynamic Considerations.

3.3.1. Introduction.

The bulk thermodynamic relationships used later
for dealing with the experimental data will now be
formally derived. The conventional symbolism is used,
a bar and a wavy line over an extensive variable
indicating a partial molar and molar quantity
respectively. The sorbent and calorimeter are
considered inert; their thermodynamic functions
are taken to be independent of the amount of sorbate
present. Thus the total heat of sorption is allocated
to the sorbate molecules. A full derivation of the
Clausius-Clapeyron equation is given to show clearly
the relationship between the isosteric heat of sorption
and the differential heat of sorption used to interpret
the heat capacity data. The last section deals with
the calculation of the pressure in the calorimeter
vessel. Thermodynamic equilibrium is assumed through-
out.

3.3.2. The Clausius-Clapeyron Equation.

In any sorption system, the sorbate is always
present in two phases, the sorbed and non-sorbed
states, the actual amount in each phase being

determined by its pressure and the temperature. The general equation for the small change, dG, in the Gibb's free energy, G, in a closed system is

$$dG = VdP - SdT \quad ,$$

The corresponding equations for the sorbed (s) and non-sorbed (q) phases of the sorbate are, per mole of sorbate

$$d\widetilde{G}_g = \widetilde{V}_g dP - \widetilde{S}_g dT$$

and

$$d\bar{G}_s = \bar{V}_s dP - \bar{S}_s dT \quad .$$

Partial molar quantities are required in the second equation because the corresponding molar quantities $\widetilde{V}_s$ and $\widetilde{S}_s$ are dependent on n, the number of moles of sorbate in the sorbent. If the two phases are to remain in equilibrium when changes in pressure and temperature are imposed on the system

$$d\widetilde{G}_g = d\bar{G}_s \quad .$$

So

$$\frac{dP}{dT} = \frac{\widetilde{S}_g - \bar{S}_s}{\widetilde{V}_g - \bar{V}_s} = \frac{\widetilde{H}_g - \bar{H}_s}{T(\widetilde{V}_g - \bar{V}_s)} \quad .$$

Also

$$\widetilde{H}_g = \widetilde{E}_g + P\widetilde{V}_g \quad \text{and} \quad \bar{H}_s = \bar{E}_s + P\bar{V}_s \quad ,$$

For a two component system (sorbate, sorbent) in which the sorbent is considered inert, the total energy of the sorbed phase is written

$$E_s = \tilde{E}_s n$$

$$\frac{dE_s}{dn} = \bar{E}_s = \tilde{E}_s + n\left(\frac{d\tilde{E}_s}{dn}\right)_T \quad .$$

This gives

$$\tilde{H}_g - \bar{H}_s = \tilde{E}_g - \tilde{E}_s - n\left(\frac{d\tilde{E}_s}{dn}\right)_T + P(\tilde{V}_g - \bar{V}_s) = q_{st} \quad .$$

Since $\tilde{V}_g \gg \bar{V}_s$,

$$\frac{dP}{dT} = \frac{q_{st}}{T\tilde{V}_g} \quad .$$

This equation applies at constant amount sorbed because each phase was assumed a closed system. q_{st} is the isosteric heat of sorption. It is usually found from equilibrium isosteres (P – T curves) by assuming ideality of the gaseous phase, that is

$$\tilde{V}_g = \frac{RT}{P} \quad ,$$

and simplifying the equation to

$$\frac{d \ln P}{d(1/T)} = -\frac{q_{st}}{R} \quad .$$

Thus at a fixed sorbate to sorbent ratio, $\ln P$ is plotted against $1/T$, the gradient giving q_{st} directly.

The above approximation also simplifies the expression for q_{st}:

$$q_{st} = \tilde{E}_g - \tilde{E}_s - n\left(\frac{d\tilde{E}_s}{dn}\right)_T + RT \quad .$$

3.3.3.   Heat Capacity Relationships.

Consider a calorimeter vessel of fixed volume containing a sorbate and a fixed amount of sorbent. That is to say the vessel forms a closed system. The energy, E, of the whole system can be expressed as

$$E = E_b + E_s + E_g$$

E_b =   energy of the calorimeter vessel and sorbent (this is assumed independent of the sorbate-sorbent ratio),

E_s =   energy of the n moles of the sorbed phase, and

E_g =   energy of the $(N - n)$ moles of the gaseous phase, that is the non-sorbed molecules.

Clearly,

$$E = E_b + \widetilde{E}_s\, n + (N - n)\widetilde{E}_g \quad .$$

The equation can be differentiated with respect to temperature, remembering that

$$\widetilde{E}_s = \widetilde{E}_s(n,T) \quad ,$$

$$\frac{dE}{dT} = \frac{dE_b}{dT} + n\left\{ (\frac{\partial E_s}{\partial n})_T \frac{dn}{dT} + \frac{d\widetilde{E}_s}{dT} \right\}$$

$$+ \widetilde{E}_s \frac{dn}{dT} + (N - n)\frac{d\widetilde{E}_g}{dT} - \widetilde{E}_g \frac{dn}{dT}$$

$$= C_c + C_{vg} + C_{vs} - q_d \frac{dn}{dT}$$

where

$$q_d = q_{st} - RT = \widetilde{E}_g - \widetilde{E}_s - n(\frac{\partial E_s}{\partial n})_T \quad .$$

In the above equation

C_c is the heat capacity of the vessel and sorbent,

C_{vg} is the heat capacity at constant volume of the non-sorbed gas, and

C_{vs} is the heat capacity of the sorbed phase.

The last term represents the correction which has to be applied for the heat required to desorb dn moles of sorbate to maintain thermodynamic equilibrium when the vessel is heated. The relation between the heat of sorption used in this equation, q_d, and the isosteric heat of sorption for an ideal gas is clearly shown. q_d corresponds to Hill's differential heat of sorption (Hill 1949).

In practice, a known amount of electrical energy, Q, is added to the vessel which produces a measured rise in temperature, ΔT. The heat capacity of the sorbed phase is then given by

$$C_{vs} = \frac{Q}{\Delta T} - C_c - C_{vg} + q_d \frac{dn}{dT}$$

The heat capacity of the sorbent and vessel is found by taking measurements with no sorbate present (see Chapter 7). It has been assumed here that the volume of the sorbent is constant. Clearly, this is not true but the correction term is small and is the same in runs with and without sorbate. The differential heat of sorption is found from isotherm data obtained from measurements on the same sorbent sample. Its multiplier in the above equation, dn/dT, is also found using this data, the details are given in the next section.

3.3.4.   The Pressure within the Calorimeter Vessel.

For the calculations in the previous section, the amount of sorbate desorbed, or the pressure

within the calorimeter vessel, is required to be
known at different temperatures. Since the vessel
is a closed system, at all temperatures the number
of moles of sorbate present (N) is given by

$$N = \frac{RT}{P\tilde{V}_g} + g\, n(P,T)$$

The first term represents that which is in the
gaseous phase, i.e. non-sorbed. The second term
is the measured isotherm expressed as the moles
sorbed per unit weight of sorbent as a function
of pressure and temperature; g is the weight of
sorbent in the vessel. The free volume accessible
to the non-sorbed gas, V_g, is found by helium expansion.
The total dose, N, is also known accurately. Thus
if the isotherm relationship is known at any temperature,
the corresponding pressure can be calculated. This
can be done either by fitting the measured isotherm
points to one of the well
known isotherm equations
and to solve the above
equation algebraically,
or, more directly, by the
following graphical method.
The amount of sorbate act-
ually sorbed is given by
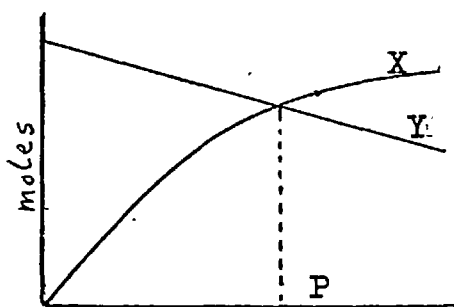
$$X = g\, n(P,T)$$

and
$$Y = N - RT/P\tilde{V}_g$$

X and Y are plotted against P at the temperatures
at which isotherms have been determined; the equi-
librium pressure is the point where the two curves
intersect. A graph can then be plotted of equilibrium
pressure against temperature, from which the amount
desorbed at any temperature can be ascertained.

3.4. Statistical Thermodynamics of Zeolite Sorption.

3.4.1. Introduction.

It has been mentioned earlier that the molecular
properties can be related to the bulk thermodynamic
data by the methods of statistical thermodynamics.
Such calculations have been performed analytically
only for very simple systems like ideal gases and
simple solids, and for the internal motions of
polyatomic molecules. Clearly the bulk thermodynamic
properties depend on the available energy levels and
the way in which these levels are occupied. These
are conveniently correlated to the bulk properties
through a compact mathematical function – the partition
function. The form of this function depends on
the physical restraints which are imposed upon the
system. For a closed system at constant temperature
and volume, the canonical partition function is the
most easy to use.

This function for the particular case of
zeolitic sorption is now considered. Later this
same system will be discussed in terms of a grand
partition function (Sec. 3.4.2). If N molecules
of sorbate are sorbed in a fixed amount of sorbent

which consists of B cavities, and the temperature
of the whole system is T, then the canonical partition
function is given by

$$Z'(N,B,T) = \sum_{l} \exp(-E_l/kT)$$

where E_l is an energy level of the system, and the
summation is over all the energy levels available
to the sorbate within the prescribed conditions.

As a first approximation in performing this
summation, the internal motion of the sorbate
molecules can be factorised out because these
degrees of freedom are usually independent of the
space and momentum coordinates. The equation then is,
in the form of classical mechanics,

$$Z(N,B,T) = h^{-3N} \int \exp(-H(\bar{N})/kT)\ d\bar{N}$$

where $H(\bar{N})$ is the classical total energy of the
configuration in which the N molecules have space and
momentum coordinates $\bar{N}$. The integration is taken
over all phase space. h is Planck's constant.

In classical mechanics, the form of the energy
is given in rectangular coordinates by

$$H(\bar{N}) = \frac{1}{2m}\sum_{i=1}^{i=N}(p_{xi}^2 + p_{yi}^2 + p_{zi}^2) + E(\tilde{N})$$

where m is the mass of a sorbate molecule,
$\bar{p}_{xi}$, p_{yi}, p_{zi} are the momenta, and

$E(\widetilde{N})$ is the potential energy for the sorbate at point $\bar{N}$ in the phase space. $\widetilde{N}$ are just the space coordinates for the point; $E(\widetilde{N})$ is a function of these only. Since in these equations the first kinetic term is only dependent on the momenta and the second configuration term on the space coordinates, the integration of the expression for $Z(N,B,T)$ can be performed separately to give

$$Z(N,B,T) = \Lambda^{-3N} Q(N,B,T)$$

where

$$Q(N,B,T) = \int_{\Delta} \exp(-E(\widetilde{N})/kT) \, d\widetilde{N} \quad .$$

Δ is the total space volume of the sorbent and

$$\Lambda = h/(2\pi mkT)^{\frac{1}{2}} \quad .$$

h is Planck's constant and k is Boltzmann's constant. Λ is the part of the partition function concerned with one kinetic degree of freedom. Note that Q and Λ are not partition functions in themselves.

The assumption has been made that after the sorption process the internal molecular motions are unchanged. This is exact for monatomic species and probably nearly so for other simple molecules if the sorbent potential in each cavity is approximately spherically symmetrical, as is the case in decationated molecular sieves. In Linde 5A at low temperatures the sorbate molecules can become non-mobile adjacent to the cations and appreciable

barriers to the internal motions can occur due to
ion-induced dipole forces (see Sec.2.3). In this
case the above partition function is no longer valid
and a different approach is necessary to examine
the experimental data. This is described in Section
3.4.5.

When the internal motions can be ignored the
above equation can be used: this approach is dis-
cussed in the next section.

3.4.2. The Canonical Partition Function.

The problem: is to perform the integration
denoted by Q in the previous section. That is the
configuraional integral part of the canonical
partition function. This cannot be done directly
since it is a 3N dimensional integration of a
complicated function, and N is a very large number.

For zeolites, Bakaev (1964) and Limcharoen
(1968) have discussed solutions using the cell model
approach which was used by Lennard-Jones and
Devonshire (1937) as a model of the liquid state.
Van der Waals and Platteeuw (1959) applied the same
approach to clathrate complexes where a small molecule
is trapped in a cavity formed in the crystal structure
of another species.

In this model, the configurational space is
divided into 'cells' and the molecular motion is
considered as taking place solely within them.
In the original application these cells were

hypothetical and of no fixed nature, being simply
the 'cage' of neighbouring liquid molecules. In
clathrates and molecular sieves true crystallographic
cavities exist and these are taken as the cells.

Consider just a portion, Δ^*, of the 3N
dimensional space volume when c_1, c_2,........c_B
molecules are in the cavities numbered $1,2,....B$.
The contribution to Q of this part of space volume is

$$Q^*(N,B,T) = \int_{\Delta^*} \exp\,(-E(\widetilde{N})/kT)\ \ d\ \widetilde{N}$$

and

$$E(\widetilde{N}) = \sum_{i=1}^{B} E_i \quad + \quad E_{in} \quad ,$$

where for a particular configuration in Δ^*, E_i is
the potential energy of the c_i particles in the
i th cavity and E_{in} is the potential energy due to
interactions between the different cells.

Progress is more readily made if the last term
is considered zero. This means in effect that the
energy of the molecules in a cavity due to its inter-
actions with the sorbent and other molecules in the
cell are much larger than the corresponding inter-
actions with particles in other cells. The cells
are thus said to be 'quasi-independent'. They are
not completely independent because they must be at
the same temperature and together they form a thermo-
dynamic system with measurable pressure, entropy, etc.
Now, with this assumption, the above equation for
Q^* simplifies to

$$Q^* (N,B,T) = \int_{\Delta^*} \exp \left(\sum_{i=1}^{B} \left(\frac{-E_i}{kT} \right) \right) \, d\widetilde{N} \quad .$$

Since for this part of space volume the molecules are constrained in their cells

$$Q^* (N,B,T) = \prod_{i=1}^{B} q_i$$

where q_i is the configurational integral for the molecules in the i th cell. These molecules are considered distinguishable at this stage in the argument.

As this part of the space volume is quite typical, the integration over the whole volume will simply be a sum of terms similar to Q^*, i.e.

$$Q(N,B,T) = \sum Q^*(N,B,T)$$

where the summation is over all possible and allowed sets of Q^*'s.

Two problems then remain. The configurational integrals of the molecule or molecules within a particular cell have to be calculated, and the relationship between these functions and the configurational integral, Q, must be forged. The first problem should be solvable because the summations involved are only over a small number of dimensions. This is dealt with in Section 3.4.4. For the second problem, Bakaev and Limcharoen suggested different approaches in performing the summation in the above equation.

This problem is dealt with below.

At the outset it is assumed that the molecules are distinguishable and can move around in the sorbent, as is true at high temperature. Consider N molecules sorbed in B cavities with b_n cavities containing exactly n molecules. The number of ways of arranging the B clusters of molecules in the B cavities is

$$B! \; / \; \prod_{n=0}^{G} b_n!$$

where G is the greatest possible number of molecules which can be accommodated in one cavity.

Given such an arrangement on the sorbent lattice, the N distinguishable molecules of the sorbate can now be distributed among the clusters in the following number of ways:

$$N! \; / \; \prod_{i=1}^{B} c_i!$$

This assumes that there is no interest in the order in which the molecules are inserted in the cavities. Thus the total configurational integral for distinguishable molecules is

$$Q(N,B,T) \; = \; \sum_{\substack{all\ allowed \\ sets\ of\ b_n}} \frac{B!}{\prod_{n=0}^{B} b_n!} \frac{N!}{\prod_{i=1}^{G} c_i!} \prod_{i=1}^{B} q_i$$

Since due to the quasi-independence of the cavities,

$$q_m = q_n$$

if $\quad c_m = c_n \quad ,$

then

$$Q(N,B,T) = \sum_{\substack{\text{all allowed} \\ \text{sets of } b_n}} \frac{B!}{\prod b_n!} \cdot \frac{N!}{\prod_{n=0}^{G} n!^{b_n}} \prod_{n=0}^{G} q_n^{b_n}$$

$$= \sum_{\substack{\text{all allowed} \\ \text{sets of } b_n}} t \, b_n$$

where n is the number of molecules in the cavity. In what follows, the summations will be represented by

$$\sum_{b_n}$$

and is taken to mean summation over all sets of b_n which satisfy the following conditions:

$$\sum_{n=0}^{G} n \, b_n = N \quad , \quad \text{and} \quad \sum_{n=0}^{G} b_n = B \qquad \bullet$$

This equation is the basis of the methods used to find the configurational integral suggested by both Bakaev and Limcharoen. The difference between these two approaches arises when allowance is made for the indistinguishability of the sorbate molecules. Bakaev assumed that since they could all move over the entire sorbent, there is no way to distinguish

any one from all the others. Consequently he reduced the value of Q by the number of ways of arraⱥnging N distinguishable particles on N sites to obtain

$$Q_{Bak}(N,B,T) = Q(N,B,T) / N! = \sum_{b_n} t_{Bak} \quad .$$

On the other hand Limcharoen considered that only molecules within a cavity were indistinguishable. Thus

$$Q_{Lim}(N,B,T) = \sum_{b_n} t_{b_n} \Big/ \prod_{n=0}^{G} (n!)^{b_n} = \sum_{b_n} t_{Lim} \quad .$$

Clearly,

$$Q_{Lim}(N,B,T) = \sum_{b_n} \frac{t_{b_n}}{\prod_{n=0}^{G}(n!)^{b_n}} = \sum_{b_n} \frac{N!}{\prod_{n=0}^{G}(n!)^{b_n}} t_{Bak} \quad .$$

$$Q(N,B,T) > Q_{Lim}(N,B,T) \gg Q_{Bak}(N,B,T) \quad .$$

The form proposed by Bakaev seems more reasonable since it is known that all the sorbate can move over the whole cavity volume of the sorbent. Furthermore, this equation should represent the equilibrium configuration at all temperatures. In fact, it probably ceases to do this at low temperatures because of the difficulty, or even impossibility, of transfer of molecules from one cavity to another. The distribution

of the molecules among the cavities will then be
fixed and will depend on the rate of cooling of the
sample. The slower the cooling process is, the
more opportunity there is for redistribution. That
is to say the final frozen-in distribution will be
the equilibrium distribution corresponding to a lower
temperature than if fast cooling was employed.
For zeolitic sorption, an equation has now been
derived for the configurational integral which is
valid at high temperatures. The region of temp-
erature in which this description of the system
becomes invalid depends on both the size of the
sorbate molecules and the size of the windows of the
zeolite cavities. The behaviour in this temperature
region where redistribution becomes extremely slow
has not been considered. Here, unless it has been at
the temperature for a long period, the system will
not be in a equilibrium state, and therefore it cannot
be described adequately by the methods of equilibrium
statistical thermodynamics.

3.4.3. The Grand Partition Function.

3.4.3.1. The Function Proper.

In the last section the configurational integral was given as

$$Q_{Bak}(N,B,T) = \sum_{b_n} \frac{B!}{\prod_n b_n!} \prod_n \left(\frac{q_n}{n!}\right)^{b_n}$$

where the summation is over all possible sets of b_n ($n = 0,1,\ldots.G$) which satisfy the conditions

$$\sum_n n\, b_n = N \quad, \quad \text{and} \quad \sum_n b_n = B \quad.$$

The summation over all sets of b_n is difficult. It could be replaced by the largest term or solved by using the method of steepest descents. This last method was used by Bakaev (1964) in his treatment of this problem. Here thermodynamic association is achieved by means of the grand partition function method (Rushbrooke 1949a).

By definition the grand partition function is

$$\Xi = \Xi(B,T,\lambda) = \sum_{N=0}^{N=BG} \lambda^N\, Z(B,T,N)$$

where λ is the absolute activity, which is related to the chemical potential, μ, by

$$\lambda = \exp(\mu/kT) \; .$$

It is recalled that the canonical partition function, Z_N, can be split into two contributions:

$$Z_N = \Lambda^{-3N} \, Q_N \; .$$

If A, defined as the activity, is given by

$$A = \Lambda^{-3} \lambda \, ,$$

then

$$\Xi(B,T,\lambda) = \Xi(B,T,A) = \sum_{N=0}^{GB} A^N \, Q(N,B,T) \; .$$

Consider the following polynomial expansion,

$$\Xi^*(B,T,A) = (1 + Aq'_1 + \dots A^n q'_n \dots + A^G q'_G)^B .$$

The coefficient of the term with A to the power N is

$$\sum_{b_n} \frac{B!}{\prod_{n=1}^{G} b_n!} \prod_{n=1}^{G} (q'_n)^{b_n} \; .$$

For ease of notation $q_n/n!$ is replaced by q_n' in these equations. Clearly this summation is the canonical partition function for N molecules. The left hand side is the sum of all such terms for N (N = 0,1,... BG) and is therefore, in fact, the grand partition function; that is

$$\Xi(B,T,A) = \Xi^*(B,T,A) \ .$$

If the petite partition function is defined as

$$\Xi_b = 1 + A\,q_1' + A^2 q_2' \ \cdots\cdots\cdots + A^G\,q_G' \ ,$$

it has been shown above that

$$\Xi(B,T,A) = \Xi_b^{\,B} \qquad .$$

By the use of the grand partition function, the difficult summation in the expression for Z(B,T,N) has been circumvented. Since the activity can be readily calculated, once the configurational integrals denoted by q_n(n = 0,1, ... G) have been calculated, the grand partition function will be known. It then remains to express the thermodynamic properties in terms of the grand partition function. In the following sections this is attempted. Throughout the convention is used that quantities marked $\bar{X}_n$ and $\langle X \rangle$ refer to the average of the property X obtained from the configurational integral for a cell of given

occupancy n, q_n, and the grand partition function respectively.

3.4.3.2. The Average Number of Molecules Sorbed.

The average number of molecules sorbed per cavity, $\langle n \rangle$, is given by

$$\langle n \rangle = \frac{\langle N \rangle}{B} = \frac{1}{B} \sum_{N=0}^{BG} \frac{N \lambda^N z_N}{\boxminus}$$

$$= \frac{1}{B} \left\{ \frac{\partial \ln \boxminus}{\partial \ln \lambda} \right\}_T = \left\{ \frac{\partial \ln \boxminus_b}{\partial \ln \lambda} \right\}_T$$

$$\therefore \quad \langle n \rangle = \sum_{n=0}^{G} n A^n q_n' \ \boxminus_b$$

Thus, knowing A and q_n (n = 1,2,...G), $\langle n \rangle$ can be calculated.

3.4.3.3. The Internal Energy of the Sorbed Molecules.

The average internal energy per cavity is ~~cavity~~ given by (Rushbrooke 1949a)

$$\frac{\langle \bar{E} \rangle}{B} = + \frac{kT^2}{B} \left\{ \frac{\partial \ln \boxminus}{\partial T} \right\}_\lambda$$

$$= kT^2 \left\{ \frac{\partial \ln \Box_b}{\partial T} \right\}_\lambda = \frac{\sum_n kT^2 A^n \left(\dfrac{\partial q_n}{\partial T}\right)_A}{\Box_b}$$

but

$$\bar{E}_n = kT^2 \left(\frac{\partial \ln q_n'}{\partial T}\right)$$

so

$$\frac{\langle \bar{E} \rangle}{B} = \frac{\sum_n \bar{E}_n A^n q_n'}{\Box_b}$$

The average internal energy can be found from values of $\bar{E}_n$ and q_n where n runs from 1 to G. It will be seen later that the average energy for n molecules in a cavity, $\bar{E}_n$, can easily be found.

3.4.3.4.   Sorption Isotherms and Isosteric Heats.

The sorption isotherm is the relationship between the average number of molecules sorbed, $\langle n \rangle$, and the hydrostatic pressure, P, at constant temperature (and constant amount of sorbent).

In Section 3.4.3.2., the average amount sorbed was found to be

$$\langle n \rangle = \sum_n n\, A^n q_n' \,/\, \Box_b$$

where

$$A = \Lambda^{-3} \lambda = \Lambda^{-3} \exp(\mu/kT) \quad .$$

It follows that

$$\mu = kT \ln A\Lambda^3 \quad .$$

Now for an ideal gas (Rushbrooke 1949b)

$$-\mu = kT \ln(P\Lambda^3/kT)$$

which gives

$$A = P / kT \quad .$$

The isotherm is therefore given by

$$\langle n \rangle = \sum_n n \left(\frac{P}{kT}\right)^n q_n^t \; / \Xi_b \quad .$$

The equation only applies for an ideal gas. This is a satisfactory approximation for the simple gases discussed in this thesis, especially since only low pressures are employed.

The isosteric heat is defined by the following equation (see Sec. 3.3.2.)

$$q_{st} = -k\left(\frac{\partial \ln P}{\partial (1/T)}\right)_{\langle n \rangle} = kT^2\left(\frac{\partial \ln P}{\partial T}\right)_{\langle n \rangle} \quad .$$

Experimentally this quantity is found by plotting ln P against 1/T, the pressure and temperature values used being those for constant amount sorbed. The above equation assumes that the gaseous phase obeys the ideal gas equation.

Theoretical values can be obtained using the equation now to be derived. The theoretical isotherm equation can be rewritten as

$$\sum_n \left(\frac{P}{kT}\right)^n q'_n \ (n - \langle n \rangle) = 0 \ .$$

Since P and q_n are dependent on temperature, differentiation with respect to this variable yields

$$0 = \sum_n \frac{(n - \langle n \rangle)}{k^n} \left[\frac{-nP^n q'_n}{T^{n+1}} + \frac{nP^{n-1}}{T^n} \frac{dP}{dT} q'_n + \left(\frac{P}{T}\right)^n \frac{dq'_n}{dT} \right]$$

i.e.

$$0 = \frac{\langle n^2 \rangle - \langle n \rangle^2}{- T} + \frac{1}{P} \frac{dP}{dT} (\langle n^2 \rangle - \langle n \rangle^2) + \frac{\langle n \bar{E}_n \rangle - \langle n \rangle \langle \bar{E}_n \rangle}{k T^2}$$

$$\therefore \frac{d \ln P}{dT} = \frac{1}{T} - \frac{\langle n \bar{E}_n \rangle - \langle n \rangle \langle \bar{E}_n \rangle}{kT^2 (\langle n^2 \rangle - \langle n \rangle^2)}$$

When this equation is compared with the one above defining the isosteric heat, the result obtained is

$$q_{st} = kT - \frac{\langle n\,\bar{E}_n\rangle - \langle n\rangle\langle\bar{E}_n\rangle}{\langle n^2\rangle - \langle n\rangle^2} \quad .$$

Again, all the quantities in this equation can be determined.

3.4.3.5.   Heat Capacity of the Sorbate.

The relationship between the heat capacity of the sorbed molecules and the grand partition function is complex. Basically this is because there are two contributions to the heat capacity. First, there is the increase in the average internal energy of the molecules due to their interactions within the cavities. Secondly, the average energy per molecule will change due to the redistribution of the molecules throughout the whole sorbent. Clearly the heat capacity is the rate of change with respect to temperature of the internal energy averaged over the sorbent. Thus

$$\langle\bar{E}_n\rangle = \sum_{n} \bar{E}_n\, g_n$$

where

$$g_n = \frac{\lambda^n z_n}{\boxed{}_b} = \frac{A^n q'_n}{\boxed{}_b}$$

z_n is the canonical partition function for n molecules in a cavity and g_n is the probability that a particular cavity will contain exactly n molecules. It can also be regarded as the fraction of cavities containing exactly n molecules.

If the volume of the system is constant and the amount sorbed is also unchanging, then

$$C_{vs} = \left(\frac{\partial \langle \bar{E}_n \rangle}{\partial T}\right)_{V, \langle n \rangle} = \sum_n C_n \, g_n + \sum_n \bar{E}_n \left(\frac{\partial g_n}{\partial T}\right)_{\langle n \rangle}$$

$$= \qquad C_1 \quad + \quad C_2 \quad .$$

The calculation of C_1, the first contribution mentioned above, is now considered. This is reasonably straight-forward. The probabilities, g_n (n = 0,1...G), can be found from the equation which defines it above, the the cavity heat capacity, C_n (n = 1,2...G), is a function of the cavity partition function z_n. There are two terms: thermal (or kinetic) and configurational. The thermal heat capacity, C_{kin}, is not dependent on the number of molecules in the cavities but is a function of the total amount sorbed, N, and so this can be ignored for the present and can

be added on later. The configurational heat capacity, C_n' , is a function of the configurational integral q_n.

By definition, the average internal energy for n molecules in a cavity, $\bar{E}_n$, is given by

$$\bar{E}_n \;=\; \sum E_n \exp\,(-E_n/kT) \;/\; q_n$$

where E_n is the energy at some configuration, and the summation is over all configurations of the molecules within the cavity. Differentiating with respect to temperature gives

$$C_n' \;=\; \left(\frac{\partial \bar{E}_n}{\partial T}\right)_V \;=\; \frac{q_n' \sum \frac{E_n^2}{kT^2} \exp(-E_n/kT)}{(\,q_n'\,)^2}$$

$$-\; \frac{\left[\frac{E_n}{kT^2}\exp(-E_n/kT)\right]^2}{(\,q_n'\,)^2}$$

$$=\; \frac{1}{kT^2}\,(\,\overline{E_n^2} \;-\; \overline{E_n}^2\,) \qquad .$$

Thus C_n' can be calculated if the mean square of the average internal energy and the average internal energy itself are known for each value of n. These are calculable. The equation is a standard result in the theory of fluctuations, and gives some quantitative indication of the spread of the internal energy for different configurations within the cavity. It is clear that the configurational heat capacity

should depend on this since it is the spread in possible energies which the molecules can experience which allows the average internal energy to vary with temperature, that is for the heat capacity not to be zero.

Thus the heat capacity contribution from the molecular motions within the cavities is

$$C_1 = \frac{1}{kT^2} \sum_n g_n \left(\overline{E_n^2} - \overline{E_n}^2 \right) + \langle n \rangle C_{kin}$$

$$= \frac{1}{kT^2} \left[\overline{E_n^2} - \overline{E_n}^2 \right] + \langle n \rangle C_{kin}$$

where C_{kin} is the kinetic heat capacity per molecule, which classically is given by $3/2 \, k$.

The calculation of C_2, the redistribution heat capacity, is now discussed. It is defined above as

$$C_2 = \sum_n \overline{E_n} \; \left(\frac{\partial g_n}{\partial T} \langle N \rangle \right)$$

The differential coefficients in the equation cannot be calculated directly, so the expression is modified as follows.

At constant B and V,

$$g_n = g_n(\lambda, T)$$

$$\left(\frac{\partial g_n}{\partial T}\right)_{\langle N \rangle} = \left(\frac{\partial g_n}{\partial T}\right)_\lambda + \left(\frac{\partial g_n}{\partial \lambda}\right)_T \left(\frac{\partial \lambda}{\partial T}\right)_{\langle N \rangle}.$$

However

$$\langle N \rangle = N(\lambda, T)$$

$$\left(\frac{\partial \langle N \rangle}{\partial T}\right)_{\langle N \rangle} = 0 = \left(\frac{\partial \langle N \rangle}{\partial \lambda}\right)_T \left(\frac{\partial \lambda}{\partial T}\right)_{\langle N \rangle} + \left(\frac{\partial \langle N \rangle}{\partial T}\right)_\lambda.$$

This gives

$$\left(\frac{\partial g_n}{\partial T}\right)_{\langle N \rangle} = \left(\frac{\partial g_n}{\partial T}\right)_\lambda - \frac{\left(\frac{\partial \langle N \rangle}{\partial T}\right)_\lambda}{\left(\frac{\partial \langle N \rangle}{\partial \lambda}\right)_T} \left(\frac{\partial g_n}{\partial \lambda}\right)_T.$$

Thus from the definition of g_n,

$$\Xi_b^2 C_2 = \sum_n \overline{E_n} \left(\lambda^n \left(\frac{\partial z_n}{\partial T}\right) \Xi_b - \lambda^n z_n \sum_n \lambda^n \frac{\partial z_n}{\partial T}\right)$$

$$- \sum_n \overline{E_n} \left(\Xi_b \sum_n n \lambda^{n-1} z_n - \lambda^n z_n \sum_n n \lambda^{n-1} z_n\right) W$$

and

$$W = \left(\frac{\partial \langle N \rangle}{\partial T}\right)_\lambda \Big/ \left(\frac{\partial \langle N \rangle}{\partial \lambda}\right)_T$$

But

$$\frac{\left(\dfrac{\partial \langle N \rangle}{\partial T}\right)_\lambda}{\left(\dfrac{\partial \langle N \rangle}{\partial \lambda}\right)_T} = \frac{\sum_\lambda n \lambda^n \dfrac{\partial z_n}{\partial T} \Xi_b - \sum_n n \lambda^n z_n \sum_\lambda n \lambda^n \dfrac{\partial z_n}{\partial T}}{\sum_\lambda n z_n \lambda^{n-1} \Xi_b - \sum_n n \lambda^n z_n \sum_\lambda n \lambda^{n-1} z_n}$$

From the definition of $\langle \bar{E}_n \rangle, \langle \bar{E}_n^2 \rangle, \langle n \rangle, \langle n^2 \rangle,$ and $\langle n \bar{E}_n \rangle$,

$$C_2 = \frac{1}{kT^2} \left(\langle \bar{E}_n^2 \rangle - \langle \bar{E} \rangle^2 \right) -$$

$$\frac{1}{kT^2} \frac{\left(\langle n \bar{E}_n \rangle - \langle \bar{E}_n \rangle \langle n \rangle \right)^2}{\langle n^2 \rangle - \langle n \rangle^2}$$

The heat capacity of the sorbed phase at constant amount sorbed can now be written as

$$C_{vs} = \frac{1}{kT^2}\left(\left\langle \overline{E_n^2}\right\rangle - \left\langle \overline{E_n}\right\rangle^2\right) + \left\langle n\right\rangle C_{kin}$$

$$+ \frac{1}{kT^2}\left(\left\langle \overline{E_n}^2\right\rangle - \left\langle \overline{E}\right\rangle^2\right) - \frac{1}{kT^2}\frac{\left(\left\langle n\overline{E_n}\right\rangle - \left\langle n\right\rangle\left\langle \overline{E_n}\right\rangle\right)^2}{\left\langle n^2\right\rangle - \left\langle n\right\rangle^2} .$$

All the terms in this equation can be evaluated.
At low temperatures there is no redistribution and
then the heat capacity reduces to the first two terms
only.

Lastly it should be mentioned that if in the
construction of the potentials the sorbate species
has been considered to be spherically symmetric, then
the above equation will not include the rotational
term. For a monatomic it is zero, for a polyatomic
it is k and 3/2 k for linear and non-linear molecules
respectively.if it is rotating freely.

Grateful acknowledgement is made to Dr N.G.
Parsonage for the derivation.presented in this
section, and also the equation for the isosteric heat
given in Section 3.43.4.

3.4.4. The Configurational Integral.

3.4.4.1. Introduction.

By means of the grand partition function method various useful thermodynamic properties of the sorbed phase in zeolites have been expressed in terms of the activity of the sorbed molecules, A, and sets of G parameters which are functions of the cavity configurational integrals, q_n, where for the entire set n runs from zero to G. These parameters include n and q_n themselves, but also related quantities like $\bar{E}_n$ and $\overline{E_n^2}$. The evaluation of these parameters should evidently be much simpler than evaluating the corresponding parameters of the canonical partition function, $Z(N,B,T)$, because the number of dimensions over which integration must be performed is only 3 to about 30 as opposed to 10^{20}.

The general expression for q_n is

$$q_n = \int_{\Delta_n} \exp(-E_n/kT) \, d(\tilde{n}) = q_n' \, n!$$

where E_n is the potential energy when the n molecules in the cavity are at the positions in the 3n space volume denoted by $\tilde{n}$. The integration is taken over the entire space volume of the cavity. The expression is reduced by n! to obtain q_n'. The potential energy, E_n, is determined by the intermolecular forces which act on the molecules within the cavity, and these are summarized in section 2.3. There it was pointed out that E_n consisted of a sorbate-sorbent term and, if $n > 1$, a sorbate-sorbate term.

The latter was readily formulated as a Lennard-Jones potential but the first was found to be best treated as follows. The sorbate molecules are assumed to move in a spherically symmetrical potential of the form given by Lennard-Jones and Devonshire. The magnitude of the sorbate-sorbent energy is then determined solely by the distance of the molecule from the cavity centre. The limitations of this potential in describing the properties of the sorbed phase were discussed earlier (Sec.2.3) but it was shown generally to represent the potential in the zeolite cavities due to the sorbent quite adequately.

Thus for any configuration of the n molecules within a cavity, the total internal energy can be calculated. The above integration must then be performed to give the partition function. The Boltzmann average of any parameter, X , is found by the same method except that the integrand is now changed:

$$\bar{X} = \frac{1}{q_n} \int_{\Delta r} X \exp(-E_n/kT) \; d(\tilde{n})$$

Limcharoen (1968) found values for the partition function and the heat capacity for methane and krypton in Linde 5A for up to 5 molecules per cavity, at temperatures between 100 and 300°K. These results were found using a digital computer. For n = 1 and 2, Simpson's rule was the technique used for the integration, while a simple Monte Carlo technique gave values for n = 2 to 5. The two sets of values for n = 2 were in good agreement. The Monte Carlo technique is briefly described in the next section.

3.4.4.2.   The Monte Carlo Method.

With the advent of modern high speed digital computers, the Monte Carlo method of performing numerical integration has made possible many summations which occur in problems in statistical mechanics. In the present example, two types of summation are required. First, there is the configurational integral which is just one summation:

$$q_n = \int_{\Delta n} \exp(-E_n/kT) \; d(\tilde{n}) \quad .$$

Second, there are the parameters like the average energy or the average square of the energy which are the ratio of two integrals or summations, one of these being the configurational integral. For example

$$E_n = \frac{\int_{\Delta n} E_n \exp(-E_n/kT) \; d(\tilde{n})}{\int_{\Delta n} \exp(-E_n/kT) \; d(\tilde{n})}$$

This distinction is important as the methods applicable to the solution of the two can be different. It will be recalled that the configurational integral and related quantities involve 3n dimensional integrations when the concern is with n molecules in the cavity.

The Monte Carlo technique has been discussed by Metropolis et al.(1953) and Fosdick (1963), in whose papers reference is made to other work in the literature. What is required is the sum of a mathematical function at every point in a multi-dimensional space. Since the integrand is complex, this cannot

be done by analytical methods, and so resort is made
to a numerical approach. The simple Monte Carlo
technique is simply a sum over many points in the
space, care being taken to sample the whole con-
figurational space uniformly. Thus the points
are chosen completely at random, but such that
their density in the configurational space is
rectangularly uniform. If the points are specified
by a set of random numbers taken from the random
number facility of a modern computer, then this
criterion is satisfied.

It can be shown that the required summation,
s, is given by

$$s = \frac{\triangle}{m} \sum_{m} f(m)$$

where $\triangle$ is the configurational volume, m is the
number of points, or trials, taken, and f(m) is the
integrand.

Clearly the simple Monte Carlo method is
applicable to both types of summation mentioned above.
However the convergence of the summation becomes
progressively poorer the larger the number of
dimensions over which the summation is taken.
This is because for a given amount of computing
time, the number of points in the configurational
space which can be taken will decrease. Also the
system is becoming more close-packed which means
that most of the random points picked will have at
least one very small intermolecular distance
(i.e. molecule overlap will occur) giving a very

positive energy. The contribution of such points
to the configurational integral is negligible.

An improved method is Monte Carlo with importance
sampling, introduced by Metropolis. The theory of this
technique is covered in the papers mentioned previously
and by Wood and Parker (1957) who related it to Markov
chains. This method is only applicable to the second
type of summation mentioned above, namely those which
are the ratio of two integrals, like the average
internal energy. The procedure is as follows.
Initially a point is chosen in the configurational
space; that is the n molecules are placed within
the cavity. The energy of this state is then calculated.
Then either one or all of the molecules are moved such
that each coordinate changes by an amount ΔC, and

$$\Delta C = c \, \alpha$$

Here α is the maximum allowed displacement and c is
a random number between -1 and $+1$. Another set of
random numbers is chosen if a molecule leaves the cavity.
The energy of the new configuration is then cal-
culated, and the difference in energy, ΔE, between this
and the previous configuration also. If the new
configuration has a lower energy it is unconditionally
accepted. If this is not the case it is accepted
provided $\exp(-\Delta E/kT)$, the transition probability,
is greater than a number, between 0 and 1, chosen
at random. If the move is not accepted the system
is returned to the previous configuration. After
each such trial, the value of the required parameter
is calculated. The process is then repeated.
It can be shown that the Boltzmann average of the
parameter is the arithmetric mean of all the values

calculated after each trial.

This is to say that after a large number of
trials have been taken, the frequency with which a
particular configuration occurs in the sum is
directly proportional to exp(-E/kT) where E is the
potential energy corresponding to that configuration
and the temperature $T^{o}K$. The mathematical theory
of random processes proves that if an infinite number
of trials are taken, then the system would reach
every part of the configurational space. The method
is thus ergodic. For a very large, but finite, number
of trials, the method will be ergodic if there
are no great energy barriers within the system, in
this/the zeolite cavity. The configurational space,
which is the space being sampled, does consist of
loosely connected regions. However it does not matter
if only one of these happened to be sampled in a part-
icular calculation because with a spherical potential
all these regions are identical.

The maximum displacement, α , has to be chosen
with some care. If it is too large then most moves
will be forbidden, whilst too small a value will
cause the configuration not to change enough to
represent the whole space adequately. The sum from
this procedure converges far more rapidly than that
for the simple Monte Carlo method, and thus reliable
averages can be obtained even for close packed
systems amd multi-dimensional space. The precision
of the average obtained can be investigated by
starting from a different configuration and, for
simple systems, by comparing them with the values
obtained by the simple Monte Carlo procedure.

3.4.4.3. Calculations For Close-Packed Systems.

The efficiency of the simple Monte Carlo procedure in estimating the configurational integral will depend on the number of molecules in the cavity and on the ratio of sorbate molecular diameter to cavity diameter. For methane and krypton, Limcharoen (1968) was able to compute the configurational integral for up to 5 molecules per cavity at temperatures between 100 and $300^{\circ}K$. In these calculations the inter-sorbate and the sorbate-sorbent potential were modified by introducing hard core cut-offs. Using the inportance sampling procedure he also calculated the average internal energy for up to 10 molecules per cavity. By a linear extrapolation process estimates were obtained of the configurational integral for 6 and 7 molecules per cavity. The uncertainty of the values increases with n, the number of molecules in the cavity. The probable error in the $n = 5$ case shown by the fluctuation in the average values of the parameters calculated decrease the reliability of the results, and this also effects the results quoted for $n = 6$ and 7.

For a complete description of the sorbed state in terms of the grand partition function, values of the configurational integral are required for n up to G, which is the maximum number of molecules per cavity which can be accommodated. From now on only methane sorption is considered, where G is about 9 or 10. Thus values are needed for the configurational integral q_n for $n = 5$ to 10. The method used to calculate these close packed integrals will now be considered.

This technique will be called the 'integration over temperature' method, although it is akin in principle to the coupling parameter method used in the treatment of dense fluids (see Hill 1956).

. Consider the following general expression which is, when C = T, the configurational integral for n molecules in a cavity at a temperature T.

$$q_n(T) = \int_{\Delta n} \exp\left(\frac{-E_1}{kT} - \frac{E_2}{kC}\right) \, d(\tilde{n})$$

where the energy, quite arbitrarily at this stage, has been divided into two contributions. Suppose the configurational integral is known for an identical system but when one of these contributions, E_2, is always non-existent or zero. For that system the integral would be

$$q_n(T)_0 = \int_{\Delta n} \exp\left(\frac{-E_1}{kT}\right) \, d(\tilde{n}) \quad .$$

This is named the primary integral, it is also the configurational integral for the original system when the degrees of freedom or whatever contributes to E_2 is at infinite temperature, that is $C = \infty$. This concept of considering the E_1 term at temperature T and the E_2 term at a different temperature is, of course, simply a hypothesis. It is not connected with or based on the knowledge of transient states in which molecules can exist, say in the pressure front in a shock tube, where the vibrational, rotational

and translational degrees of freedom are considered
to be excited to different temperatures.

The expression for $q_n(T)$ can be differentiated
with respect to $1/C$

$$\frac{d\ q_n(T)}{d(1/C)} = \int_{\Delta_n} - \frac{E_2}{k} \exp\left(\frac{-E_1}{kT} + \frac{-E_2}{kC}\right)\ d(\tilde{n})$$

or

$$\frac{d\ \ln(q_n(T))}{d\ (1/C)} = \frac{\bar{E}_2(C)}{k}$$

If this equation is integrated with respect to
$1/C$ from $C = \infty$ to $C = T$, the following is obtained

$$\ln\left(\frac{q_n(T)}{q_n(T)_o}\right) = \int_{C=\infty}^{C=T} - \frac{\bar{E}_2(C)}{k}\ d\ (1/C)$$

$$\bar{E}_2(C) = \frac{\displaystyle\int_{\Delta_n} E_2 \exp\left(-\frac{E_1}{kT} - \frac{E_2}{kC}\right)\ d(\tilde{n})}{\displaystyle\int_{\Delta_n} \exp\left(-\frac{E_1}{kT} - \frac{E_2}{kC}\right)\ d(\tilde{n})}$$

These equations indicate a means of calculating
q_n for all values of n. The configurational integral

can be estimated if it is known for another similar
system at the same temperature. As will be seen
later this last restriction can be removed if the
integral denoted by $q_n(T)_0$ is independent of temperature.
The integration of $\bar{E}_2(C)$ over $1/C$ is done graphically.
$\bar{E}_2(C)$ is found at different values of C by using the
Monte Carlo method of importance sampling as $\bar{E}_2(C)$
is a ratio of two integrals.

For precise results the graphical integration
should represent only a fairly small 'correction'
to $q_n(T)_0$, and the energy term, E_2, should not have
too large a range of permitted values. This is
because the values obtained for $\bar{E}_2(C)$ when C is
very large are weighted virtually only by the E_1
exponential term, so that extreme values of E_2
are not rejected if the corresponding E_1 term has
no unfavourable contributions. This means the value
obtained for $\bar{E}_2(C)$ is large and converges to its
limit very slowly.

Consider as a typical example the calculation
of the configurational integral for n molecules
in a cavity at temperature T. For a given configur-
ation the total potential energy is

$$E_n = \sum E_{LJ} + \sum E_{LJD}$$

The summations represent the $\frac{1}{2}n(n-1)$ inter-sorbate
Lennard-Jones potentials and the n sorbate-sorbent
Lennard-Jones and Devonshire potentials respectively.

The method described above can be employed
if each of these potentials is slightly modified
to a three parameter potential with hard core cut-
offs. This potential can then be divided into two
contributions as below:

$$E'_n = E_1 + E_2$$

where

$$E_1 = \infty \left.\begin{array}{c} \text{any} \\ \end{array}\right\} r_j < \sigma_j \gamma$$

$$E_1 = 0 \left.\begin{array}{c} \text{all} \\ \end{array}\right.$$
$$E_2 = E_n \left.\begin{array}{c} \\ \end{array}\right\} r_j \geqslant \sigma_j \gamma$$
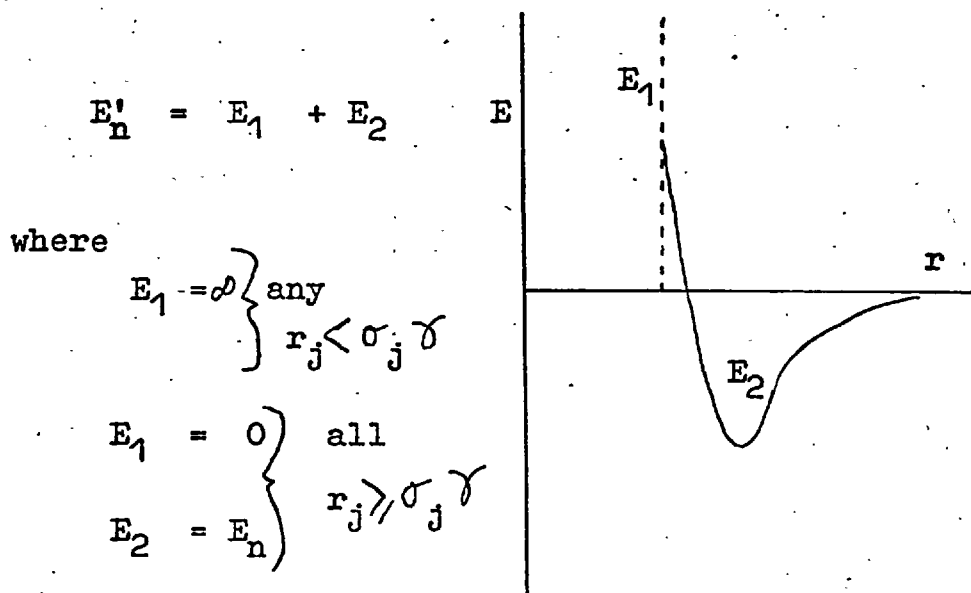
and r_j is an intermolecular distance which influences
E_n, and σ_j is the corresponding σ parameter in the
original potential for that particular intermole-
cular separation. γ is the cut-off parameter which
can sensibly range fron zero to unity. The sorbate
molecules and the cavity wall are thus assumed to
behave as if they have hard cores and a definite
thickness respectively. Clearly the smaller γ is
made, the closer E'_n will be to E_n, but also the
greater is the range of values that it is possible
for E_2 to take. As noted above, too extensive a
range causes the graphical integration to be difficult
and inaccurate. In fact for the calculations reported
here $\gamma = .9$. When these calculations were initiated,
the values $\gamma = .55$ and 6 were assumed, but the

fluctuation in $\bar{E}_2(C)$ for high C values were very
large. This Lennard-Jones type potential modified
with a cut-off does not necessarily describe the
true potential less accurately than the basic
Lennard-Jones potential. The parameters for this
potential are based on second virial coefficient
data (see Sec.2.3) which are not very sensitive
to the shape of the potential in the region of high
repulsion. It is possible that the modified potential
is indeed more accurate.

The primary integral, $q_n(T)_o$, now takes the
form of a configurational integral for a number of
hard spheres:

$$q_n(T)_o = q_{n,o} = \int_{\Delta_n} \exp\left(\frac{-E_1}{kT}\right) \, d(n)$$

where E_1 can only take two values, zero and infinity,
regardless of the temperature. Thus the integrand
is equal to either unity or zero and is temperature
independent. This last property makes the calculation
of the exact configurational integral at various
temperatures somewhat easier than might otherwise
be the case since they are all based on the same
primary integral.

The primary integral is found by using the
Simple Monte Carlo procedure. The configurational
space, Δ_n, can be divided into two parts. Δ_n'
is that part where the distance of none of the centres
of the sorbate molecules is greater than $(a - \sigma_{mw} \gamma)$
from the cavity centre, and Δ_n'' is the remainder of
the space volume. σ_{mw} is the Lennard-Jones σ para-

meter for the molecule wall potential, and a is the cavity radius. Thus

$$\Delta_n = \Delta'_n + \Delta''_n .$$

The primary integral for the hard core potentials is

$$q_{n,o} = \Delta'_n \alpha + \Delta''_n \beta$$

where α and β are the fractions of configurations in Δ'_n and Δ''_n which have $E_1 = 0$. Since, by the definition of Δ''_n, β is zero, the above equation simplifies to

$$q_{n,o} = \Delta'_n \alpha = (\tfrac{4}{3} (a - \sigma_{mw}\gamma)^3)^n \alpha$$

It is the evaluation of α which requires the Monte Carlo technique. Basically, n molecules are placed at random, a large number of times, in the space volume Δ'_n. α is the fraction of these configurations which have no distances between the n molecules less than $\sigma_{mm}\gamma$, where σ_{mm} is the σ parameter in the Lennard-Jones inter-sorbate potential. There are $\tfrac{1}{2}n(n - 1)$ such distances in each configuration.

It can be seen intuitively that for a set of trials a quantity like α will converge more rapidly if it has a final value of about one half. Its value in a given calculation will depend on the ratio of the effective sorbate diameter ($\sigma_{mm}\gamma$) to the effective cavity radius ($a - \sigma_{mm}\gamma$), as well as the number of interactions which can influence a

particular configuration $(\frac{1}{2}n(n + 1))$. For dilute
systems the simple procedure mentioned above can be
used directly.

For the more closely packed systems $(n \geqslant 7$ for
methane in Linde 5A) and a γ value of .9, the value
of α is very small. Clearly the system would become
less close packed and a cuncurrent increase in α
would result if γ was reduced in value. However,
as mentioned previously, this would make the 'inte-
gration over temperature' part of the calculation
more difficult due to the increased range of values
which would be allowed to E_2. Dr.N.G.Parsonage
has suggested a way of overcoming this problem.
In effect it splits the one small overall proba-
bility, α , into a product of probabilities,
p_1, p_2 ...., all of which will clearly be larger
than α . The method is best seen by examining
a definite example. Consider the case of 8 molecules
in a cavity. With $\gamma = .9$, the probability, α , of
randomly placing all the molecules in the cavity
without overlap is very small. With 5 molecules
however the probability is quite high. Therefore
with only a relatively small number of trials, a
value can be obtained of the probability, p_1, of
placing this number of molecules in the cavity.
Thus

$$q_{5,0} = \triangle \frac{1}{5} \; p_1 \qquad \bullet$$

Now one of these accepted trials is taken
and another set of say 100 trials is taken when
another, the sixth, molecule is added. The
probability of these new configurations having
zero potential energy is p_2.

The probability of randomly placing six molecules
in a cavity without overlap is equal to the
probability of randomly placing likewise five molecules
in a cavity (p_1) multiplied by the probability of
adding a sixth molecule (p_2) with no overlap.
Thus the configurational integral for six hard
spheres in the cavity is

$$q_{6,o} = \triangle_6^! \quad p_1 \; p_2 \qquad \cdot$$

This process can be repeated by adding a seventh,
and then an eighth, molecule and the probabilities
for performing each of these operations is denoted
by p_3 and p_4 respectively. The configurational
integral for eight molecules is then

$$q_{8,o} = \triangle_8^! \quad p_1 \; p_2 \; p_3 \; p_4 \qquad \cdot$$

The smallest of these probabilities will be
p_4. This is determined by the last set of trials,
any one of which is rejected if any one of the
eight new intermolecular distances created is too
small. If all eight molecules were being randomly
arranged during each trial, then a trial would be
rejected if any one of 36 distances were too small,
a much more severe condition.

The validity of this technique can be checked
by comparing, for example, the value obtained for the
configurational integral of six molecules in a cavity
by randomly placing all the molecules during each
trial with that obtained by the two stage process
as outlined above for six molecules. Both of these

computations are possible.

When, at the end of a set of trials, before
considering the addition of an extra molecule, a
particular configuration is accepted, what is actually
being done is a certain point in the new configu-
rational space is selected for detailed investigation.
Thus a small part of the final configurational
space is sampled in detail, but most of the space is
not sampled at all. By taking a different configu-
ration at the end of a set of trials for further
study, the same final probability should result if
the process is for all practical purposes ergodic.
Clearly it is not truly ergodic since in any one
programme execution all parts of configurational
space cannot be reached because only one molecule
is moved in all but the first set of trials.

3.4.5.   Effects of Hindered Rotation.

To obtain numerical results for the con-
figurational integrals formulated in the above sections,
it is necessary to assume that the sorbate-sorbent
interaction is spherically symmetric. This means
it can be expressed by the equation of Lennard-
Jones and Devonshire. It is known that this is an
approximation, since such a potential does not allow
sorbate molecules to migrate from one cavity to
another. The potential due to the sorbent is clearly
less homogeneous at a fixed distance from the cavity
centre in Linde 5A than in clathrates due to the
presence of mono- and di-valent cations. Thus at
low temperatures the sorbate molecule will tend
to become localized in the vicinity of these cations.
The above theory indicates that at these temperatures
the sorbate clusters itself in certain cavities,
so that the majority of cavities contain either near
the maximum allowed number of molecules or none at
all.   Both this close-packing of the sorbate and the
large electrostatic field gradients in the neighbour-
hood of the cations will cause the rotation of the
methane to be partially restricted or hindered.

It is reasonable to suppose that below the
temperature at which inter-cavity migration is possible,
the methane molecules will become localized on or
near the axes of the eight-membered rings of oxygen
atoms which are the positions of least energy in the
cavity (see Fig.2.2). These positions would also
cause these molecules to be near the cations. Thus
the potential energy well in which all or most of
these molecules in these close-packed systems find

themselves will be quite narrow, and there will be
an increased tendency for the methane molecules to
take up orientations either aligned to the cavity
wall or with respect to the cations.

A simple calculation shows that the ion-induced
dipole forces between a cation and a methane molecule
are sufficient to hinder the rotation of the latter
about two axes. But the above considerations also
have shown that the motion about all the three
rotational axes can be hindered as it is thought to
be the case for polyatomic molecules in uni-occupied
quinol cavities at low temperatures (Stepakoff and
Coulter 1963).

Using the assumption that the molecular polar-
isability is the sum of the bond polarisabilities
(Denbigh 1940) and the published interatomic C - H
distance in methane(Chem Soc.1958), the potential
barrier restricting rotation due to the cations
can be estimated as follows.

The average C - H bond polarisability, α ,
is given by

$$\alpha = \tfrac{1}{3}(b_1 + 2b_t)$$

where b_1 and b_t are the longitudinal and transverse
polarisabilities respectively. The values used
were 7.9×10^{-25} and 5.8×10^{-25} ml. With a C - H
bond distance of 1.0910A, the potential barrier
is about 225 cal/mole if the methane carbon atom is
3A from a sodium ion. The barrier is about 70 cal/mole
for a separation of 3.3 A. The barrier would be

93

four times larger if the sodium ion was replaced
by a calcium ion.   The inter-species separation
distance of about 3 A would seem reasonable since
the sum⁻ of half the collision diameter of methane
and the ionic radius of either of the two ions is
approximately 2.9 A.

  The barrier to rotation about the third axis,
that is the one joining the cation and the carbon
of the methane molecule, is difficult to estimate,
but is probably smaller than that calculated for
the other two axes since forces hindering this
rotation also acts on the other two.

  The statistical mechanical treatment of the
previous section has not allowed for any contribution
to the thermodynamic properties from the internal
motions of the sorbate molecules. If the molecules
rotated freely, then the contribution to the heat
capacity is given by classical statistical mechanics
as .5R for each rotational degree of freedom. For
hindered rotation there is an added term due to the
rotational potential energy which is then present,
since the motion is now more like an oscillator. The
corresponding contribution to the heat capacity for
this form of motion, as well as other thermodynamic
properties, is given in tables complied by Pitzer
and Gwinn (1942). At given temperatures the heat
capacity is given as a function of the potential
energy barrier and a function, Q_f, which is related
to the relevant moment of inertia. For methane
this last quantity is of the order $.2T^{\frac{1}{2}}$, where T
is the absolute temperature. Because of the very
small moment of inertia of methane about any axis

through the carbon, and hence low value of Q_f at
a given temperature, and above tables indicate
that the heat capacity for restricted rotation with
potential energy barriers of 225 and 900 cal/mole
are approximately as given below, in units of k,
the gas constant.

Temp. $^{\circ}K$	Barrier to rotation (cal/mole)	
	225	900
70		.7
100	.6	.9
150	.55	.96
270	.5	.8

It is seen that for molecules which have a barrier
restricting their rotation of about 225 cal/mole,
there is no appreciable addition to the heat capacity,
but that for a barrier of 900 cal/mole the heat
capacity is predicted as going through a maximum
at about 150°K. Clearly, if the actual potential
energy barrier is intermediate between the two given
above, then the heat capacity could rise above the
classical value for a free rotator at a temperature
below 150°K.

It can be seen from the above discussion
that it is not possible to predict with any precision
the contribution that restricted rotation makes to
the total heat capacity and other properties, especially
as the barriers to rotation caused by the atoms
which form the walls of the cavity and the neigh-
bouring sorbate cannot be accurately estimated and
will be temperature dependent. This latter point

will become particularly important when the molecules
can migrate from cavity to cavity because then the
system becomes less close-packed. It has been assumed
here that the sorbate molecules are localized near
the cations, or more exactly, that the residence
time for a sorbate molecule on a cation is much longer
than its period of rotation.

Stepakoff and Coulter (1963) in their treatment
of hindered rotation of carbon monoxide in the
β-quinol clathrate assumed, as the high temperature
approximation, the cell model theory as a description
of the movement of the centre of gravity of the
molecule within the cell and an approach similar
to that used above as a description of its internal
rotation. This is probably a valid procedure
because in their application the second of these
motions does not entail localization of the CO within
the cavity. In the case of zeolite sorption the use
of the Lennard-Jones and Devonshire potential in the
cell model approach specifically disregards any specific
interaction due to the cations, or localization of
the sorbate on them. It would be inconsistent to
combine this with a theory of restricted rotation
which assumed that the positions of the molecules
were largely determined by their distances from the
cations.

CHAPTER 4

THE SORPTION ISOTHERMS

4.1. Introduction.

Before engaging in the more complex heat
capacity studies of the sorbed state in zeolites,
equilibrium sorption isotherms were determined
volumetrically for methane, ethane, and krypton
in the temperature range 194 - 300°K. These results
were necessary for several reasons: to characterize
partially our sorbent sample, to enable the calculation
of the dose needed for each heat capacity run, and
to estimate various corrections to the experimental
heat capacity points due to desorption. Since the
Linde molecular sieve A is non-stoichiometric as
regards the aluminium to silicon ratio (ideally
unity), the cations present and the water content,
it is crucial that the heat capacity and isotherm
experiments should employ samples from the same
batch.

4.2. Apparatus and Procedure.

A conventional volumetric isotherm apparatus
was constructed with its associated high and low
vacuum pumping units (Fig.4.1). This apparatus
served also for dehydrating and dosing the sample
in the calorimeter vessel (Sec. 5.4.4).

Fig. 4.1   The Sorption Isotherm Glass-line
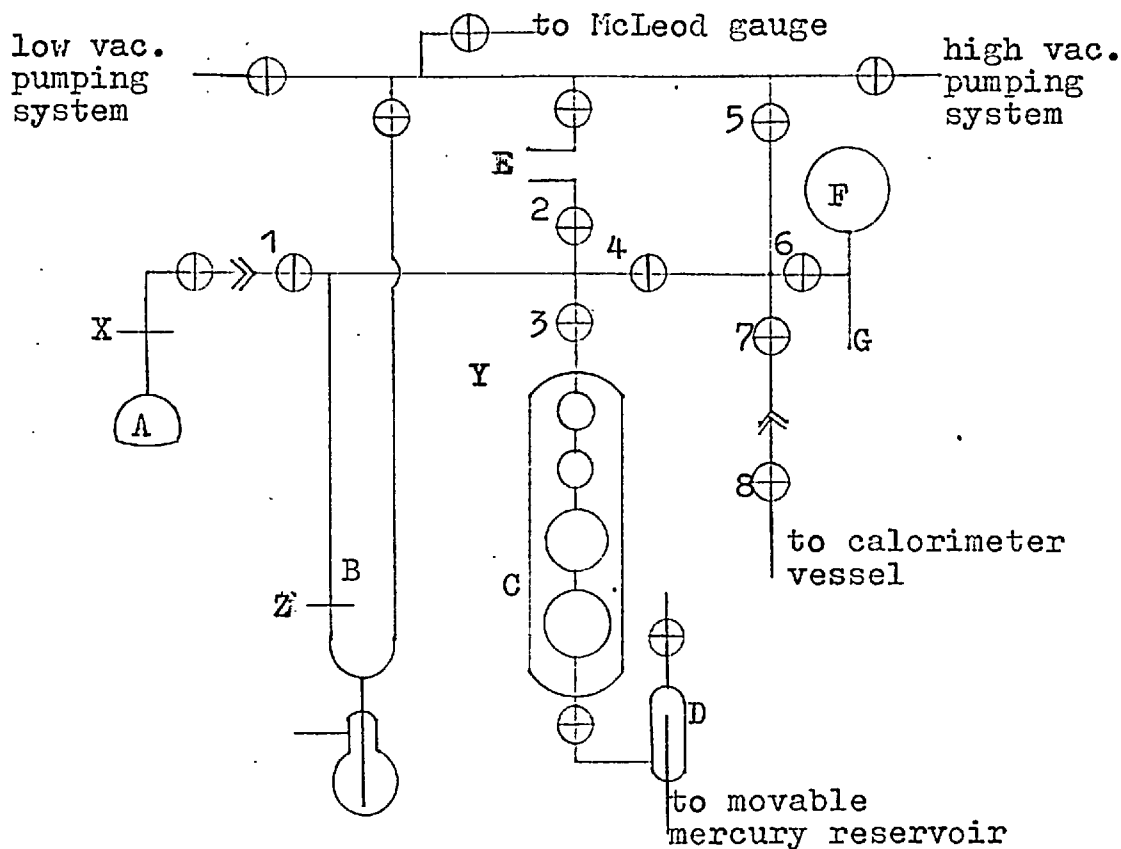
A   Zeolite sample   E   To gas storage line
B   Mercury manometer   F   Gas storage for
C   Gas burette   calorimeter loading
D   Bubble trap   G   Cold finger

The high vacuum pumping system is shown in Fig. 5.2.

X, Y, and Z are fixed marks referred to in the text.

The numbered taps are referred to on pages 98, 99 and 165.

The method is simple. Once the volumes of various parts of the measuring system are known, pressure and temperature measurements allow the quantity of gas contained in each part to be ascertained. When the zeolite sample is open to the system, any gas which cannot be accounted for by the above calculations is deemed to have been sorbed. The sorption system consists essentially of the sorption bulb joined to a gas burette and U-tube manometer with capillary tubing, so as to minimize the 'dead-space' volume. The manometer limbs are constructed from wide bore 'viridia' precision bore tubing (1 cm. I.D.) to counteract meniscus effects. Throughout the work no meniscus corrections were made. The mercury reservour of the manometer was lagged with asbestos tape to reduce thermal fluctuations, as was the capillary tubing. The temperature of the burette was well controlled by circulating water through its jacket from a large vigorously agitated thermostat. A small plug of glass-wool was held above the zeolite sample by a restriction in the capillary to avoid sucking sample from the sorption bulb during the initial evacuation. Mercury levels were measured to .001 cm. by using a cathetometer (Precision Tool and Instrument Co., 50 cm. scale). Before each isotherm experiment, the telescope was levelled in the usual way.

The volume of each of the four burette bulbs was accurately obtained by weighing the mercury required to fill them; otherwise volumes were determined by helium expansion. The sorption volume, the space above the sample to tap 1, was found at

each temperature at which isotherms were determined;
it being assumed there was no helium sorption in
this temperature range. The 'dead-space' volume,
enclosed by mark Y, tap 1, and the mercury meniscus
was kept nearly constant for all the experimental
points by always raising the mercury to just below
a fixed mark,$^{Z)}$ the position of which was read to
.001 cm , together with the two meniscus heads. The
burette volumes were approximately 15, 30, 50, and
100 ml, the smallest being at the top. The 'dead
space' was about 8 ml.

The constant isotherm temperatures were achieved
in various ways. Stirred ice-water and cardice-
acetone mixtures were used to obtain the ice point
and 194.65^{o}K respectively. The thermostat shown in
Fig.4.2. was used in the other experiments. A
Sunvic bi-metallic strip (type TS7) activated a
small hermetically sealed non-radiant fish-tank
heater by means of an electromagnetic relay. The
liquid level was maintained at the level of the
mark X on the capillary section of the sorption unit
so that the gas volume at the bath temperature was
constant. At temperatures above the ice-point,
the bath liquid was water with ice in the outer
dewar, whilst the cryostat for lower temperatures
contained 40/60 petroleum ether with cardice in
acetone as the refrigerant. Care must be exercised
with this system because of its high inflammability.
The pressure in the leaky dewar and the wattage of
the heater were chosen by trial and error to give
the optimum temperature control, which approached
$\pm$ .1°C. The heater power varied between 25 and 50
watts.

Fig. 4.2.   The Thermostat for Isotherm Studies
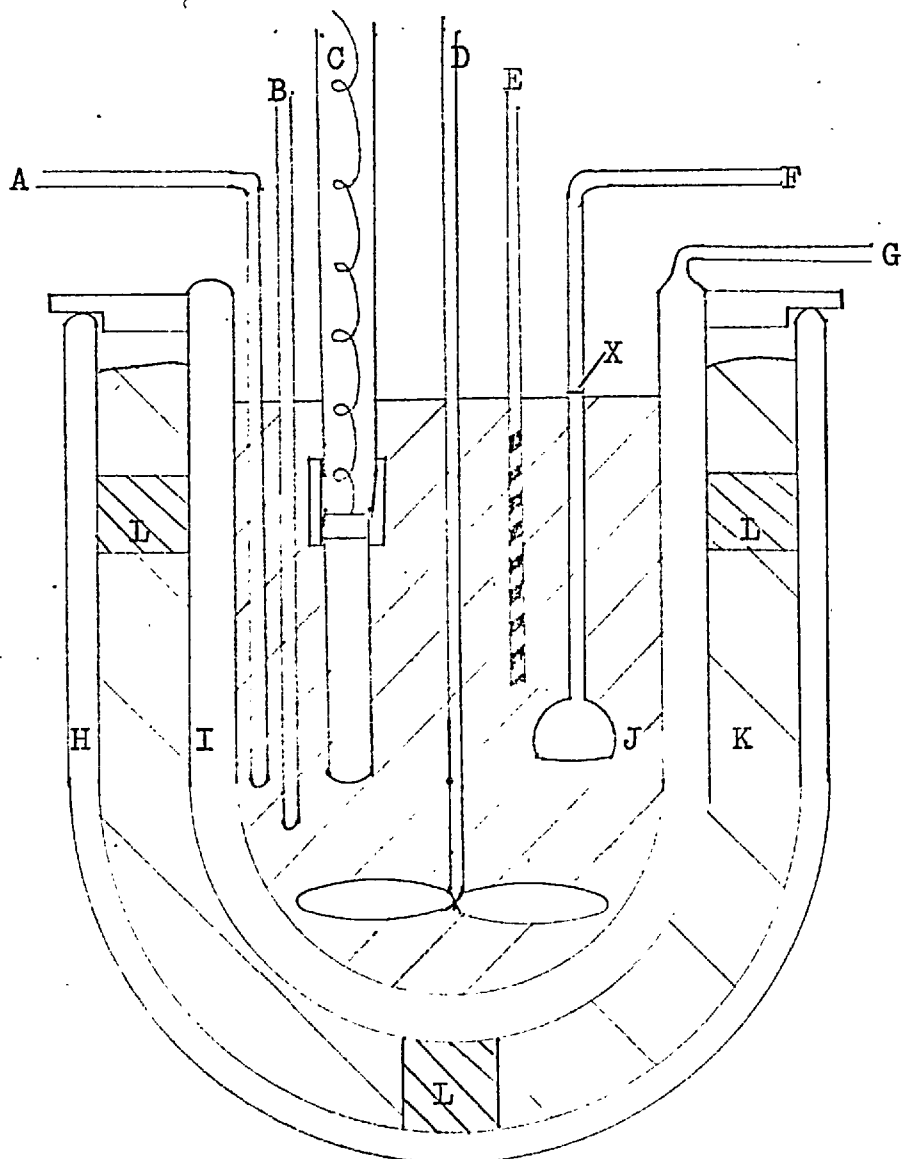
A	Gas thermometer	G	Leaky Dewar vessel outlet
B	Tube for thermocouple	H	Refrigerant Dewar
C	Fish-tank heater	I	Glass leaky dewar
D	Electric stirrer	J	Bath liquid
E	Bimetallic strip	K	Refrigerant
F	Sorbent holder	L	Rubber supports

The mark X on the sorption unit is referred to in the text

Temperature measurement was of means of a combination of liquid-in-glass (calibrated mercury or alcohol), thermocouple and vapour pressure thermometry, between which satisfactory agreement was generally observed. Above the ice point a works calibrated 0 - 50°C mercury-in-glass thermometer was used. The absolute temperature below the ice point was determined using a gas thermometer containing sulphur dioxide for the -20 and -40°C isotherms, or ammonia for the isotherms at -55 and -78.5°C. Published tables of vapour pressures were used (Handbook of Chemistry and Physics, 45th ed.). The constancy of these temperatures during experiments was observed by monitoring them with copper-constantan thermocouples. One junction of each was held at 0°C, and the total potential was measured on a potentiometer (H. Tinsley, type 4025) which read to $1 \mu V$. Thus a temperature variation of less than $.1°C$ could be easily seen.

The results were calculated by computer. Each pressure was corrected to the equivalent height of mercury at the ice point assuming a coefficient of expansion for mercury of .001819 $°C^{-1}$. For deviations from ideal gas behaviour, corrections were applied throughout by interpolating second virial coefficients, these being most significant for ethane. The behaviour of the gases in the temperature range under investigation was assumed to follow the equation

$$PV = nRT + nBP$$

where P is the pressure,

B is the second virial coefficient,

V and n are the volume and the number of
moles respectively of the gas at temperature T.

Thus

$$n = \frac{PV}{RT + BP}$$

The data for the second virial coefficient was
taken from the tables of Hirschfelder et al. (1954).
Values for each gas were calculated at $40^{\circ}C$ inter-
vals, from which the computer programme calculated
the value required for the above equation by linear
interpolation. At cardice temperatures the correct-
ions for ethane are as large as 2%.

Prior to sorption studies all volatile material,
mainly water, must be removed, and the same outgassing
procedure was used throughout. Under high vacuum
the sample temperature was increased slowly and
then held at $360^{\circ}C$ overnight. As much water as
possible should be removed at the lower temperatures
to avoid sample hydrolysis. Slight decolouration
of the zeolite was attributed to decomposition
of sorbed components of the tap grease.

4.3.   Materials.

As noted above, sorbent samples from the same
batch were used in the isotherms and calorimetric
measurements. This was a synthetic Linde molecular

sieve, 5A, of idealised stoichiometry

$$\tfrac{1}{3}Na_2O.\ \tfrac{2}{3}CaO.\ Al_2O_3.\ 2SiO_2.\ xH_2O\ .$$
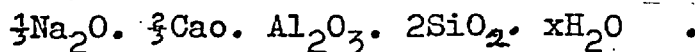
The sample used in this work was a gift from the Union Carbide Corporation (Linde Division, Tonawanda Laboratories). It was stated to be of high zeolite purity (greater than 95%), homogeneous, and to contain none of the binder material which is sometimes included to assist pellet formation. The fine white powder, Lot 5478, had the chemical composition

$$0.23Na_2O.\ 0.77CaO.\ Al_2O_3.\ 1.89SiO_2.\ xH_2O\ .$$
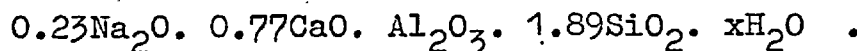
The significance of this formula has been discussed previously (Sec. 2.1). The material was used without further treatment, except that it was stored over a solution of saturated ammonium chloride in an open dish so as to be in an atmosphere of controlled water vapour pressure to ensure constant content of zeolite water. This resulted in a value of about 3.9 for x in the above formula.

Helium, krypton and sulphur dioxide were drawn from gas bulbs (B.O.C.) and were of 'grade X' purity; they were used without further purification. Ammonia and the hydrocarbons, methane and ethane, were taken from small metal cylinders (Matheson) and were graded 'chemically pure'. Samples were transferred, as required, to glass bulbs. Immediately prior to use, the gas was purified by pumping on solidified samples (surrounded by liquid nitrogen) and fractional distillation, the first and last

fractions not being kept for use.

4.4.   Results.

Both the sorption and desorption curves for
the sorption of methane, ethane, and krypton were
determined up to about 50 cm Hg pressure at regular
temperature intervals between 194 and 300°K.
The experimental results are presented in Tables 4.1
to 4.3.   They are also shown graphically (Fig. 4.3 to
4.5).   The amount of dehydrated sample used was always
about 1g.   In no case was there any signs, within the
experimental error, of sorption hysteresis.   All
the curves are if type I of the Brunauer classifi-
cation of physical adsorption isotherms (Brunauer
(1945).

At around room temperatures, the sorption
and desorption processes were always rapid and the
time between successive readings was mainly determined
by the period required for general thermal equilibration.
At the lowest temperatures used (about 200°K) the
rate of material equilibration was observably slower,
but was nevertheless complete in 10 - 15 minutes;
the period after altering the system and taking
measurements was always made at least twice this
time. The corresponding times for ethane were however
appreciably longer, and material equilibration was
very noticable and took up to 25 minutes.   The
apparatus used did not allow sorption kinetics to
be studied in any detail.

The theoretical points from Limcharoen's data for 300°K are shown thus ⊗ (see p236). For more recently calculated results, see p253.
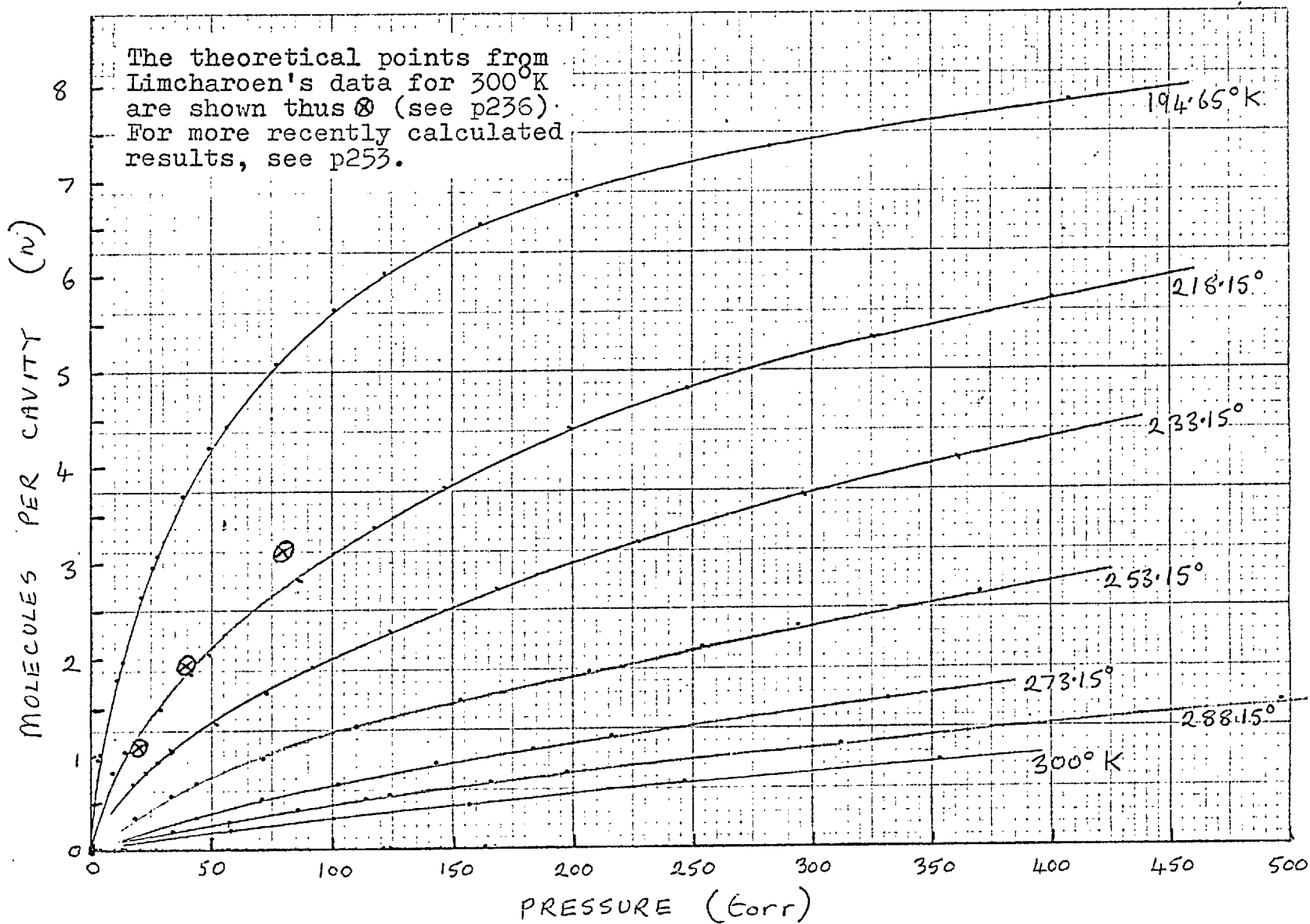
Fig. 4.3. Isotherms for Methane sorption in 5A.
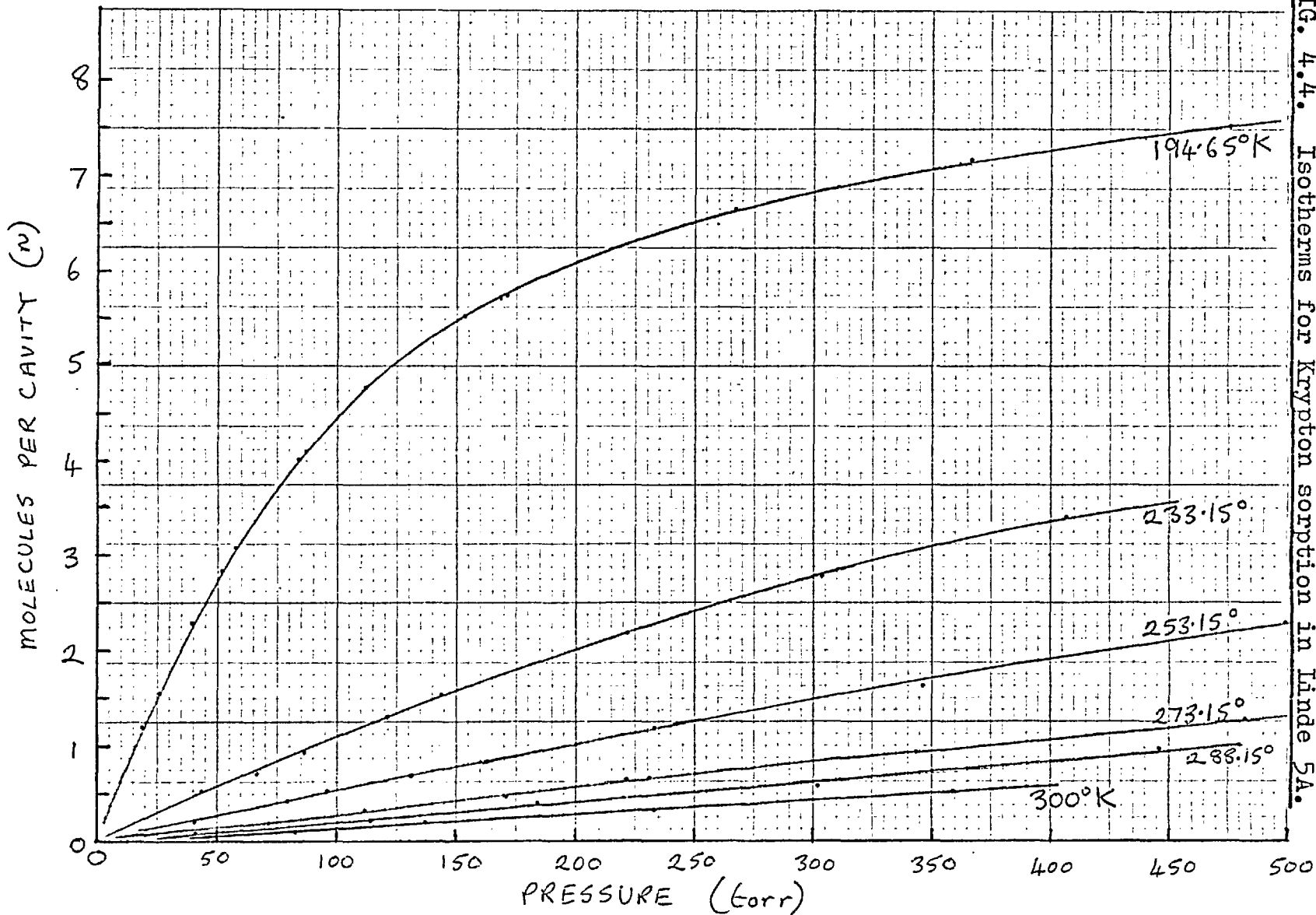
FIG. 4.4. Isotherms for Krypton sorption in Linde 5A.

194.65°K
233.15°
253.15°
273.15°
288.15°
300°K

MOLECULES PER CAVITY (ν)

PRESSURE (torr)

106
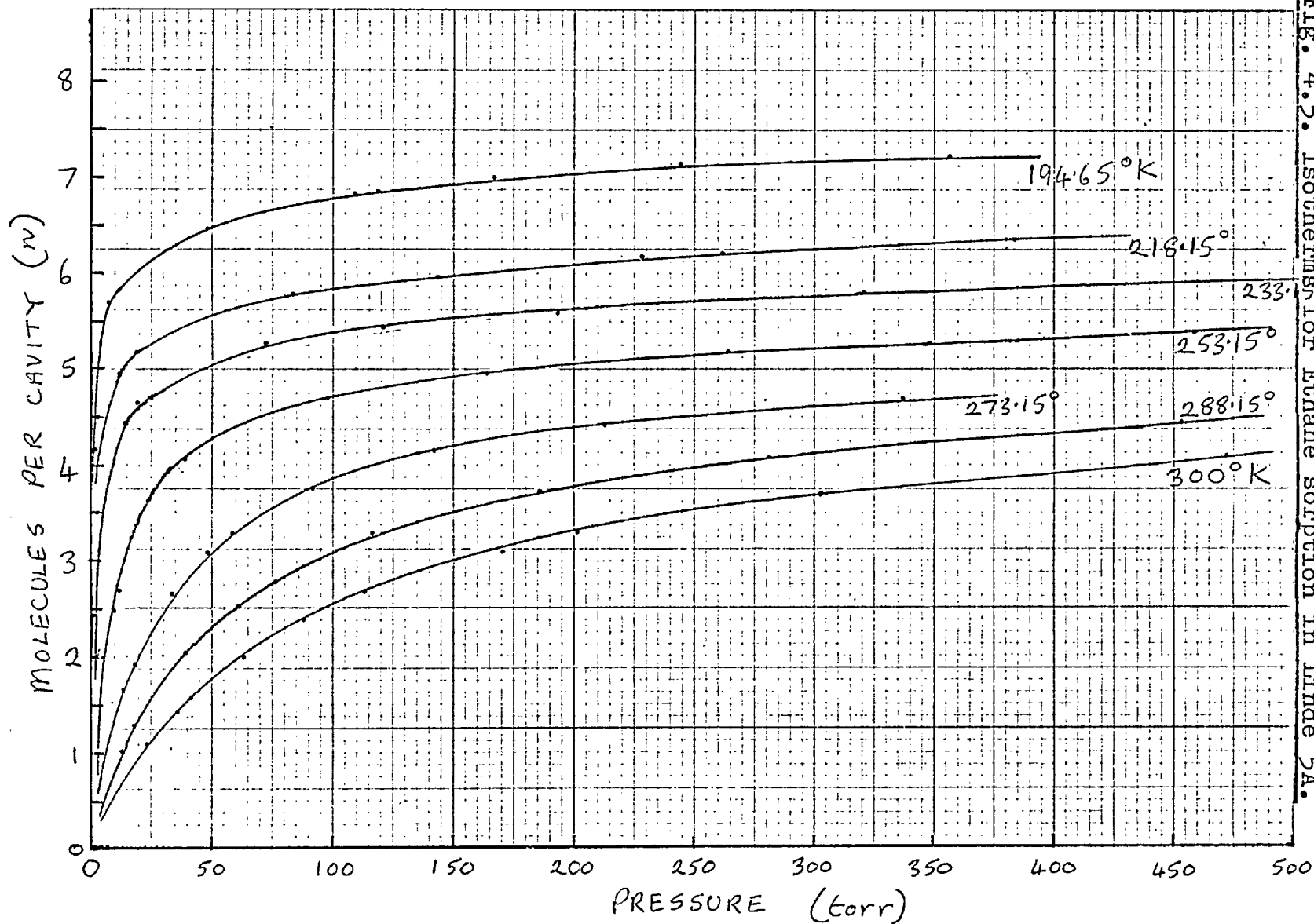
Fig. 4.5. Isotherms for Ethane sorption in Linde 5A.

From the results, plots of log P (pressure) against the reciprocal of the absolute temperature (isosteres) were drawn from which the isosteric heats of sorption could be calculated using the equations derived in section 3.3.2. When the average number of molecules per cavity sorbed was between .2 and 3, the isosteric heats for krypton and methane were found, within the experimental error, to be constant both with respect to composition and temperature. This is some assurance of the experimental accuracy, since it shows that each family of isotherms is internally consistent. The values for krypton and methane were 4245 and 5345 cal/mole respectively, both with an estimated error of about 50 cal/mole.

For ethane sorption the results from these calculations were more complex. The gradient of the isosteres progressively increased negatively as the amount sorbed increased, although for constant amount sorbed the isosteric heat was not observably temperature dependent. Thus between 230 and 280°K the isosteric heat is approximately 6020, 7020, 7705 and 8145 cal/mole for an average cavity filling of 1, 2, 3, and 4 molecules of ethane respectively. This range is much larger than the experimental error of about 50 - 100 cal/mole. The value for 5 molecules per cavity can be estimated to be consistent with that for 4 molecules per cavity, although the isostere can only be plotted for the lower part of the temperature range.

Normally an increase in the isosteric heat in this manner is attributed to increasing intersorbate attraction; such an explanation is probably quite valid here. The observed increase of 2100 cal/mole is slightly less than the heat of vaporisation of ethane at $253^{o}K$ (2661 cal/mole)(Gallant 1968). The average coordination of ethane in the zeolite cavities is probably lower than that which can be achieved in the liquid, and this would cause any effect in the sorbed phase due to intersorbate interaction to be less significant than in the bulk condensed phase.

A similar effect was observed for the higher n-paraffins (propane and above) on Linde 5A at slightly higher temperatures (Schirmer et al 1967) and for pentane in particular at room temperature (Kiselev and Lopatkin 1967). Rees and Williams (1964) reported an increase in isosteric heat with cavity filling for krypton on a large pore zeolite, Na X, which they attributed to the intersorbate attraction. In both of these last mentioned two works it was noted that the isosteric heat decreased again at higher fillings which was thought to be caused by the later sorption taking place on top of the first sorbed molecules and not in direct contact with the cavity walls. For the pentane sorption, Kiselev and Lopatkin found that the lowest value for the isosteric heat at high fillings was equal to the heat of vaporisation at that same temperature.

TABLE 4.1. - EQUILIBRIUM SORPTION ISOTHERMS OF
METHANE IN LINDE 5A.

p is the pressure in cm of mercury at the ice
point (273.15°K).
mm/g is the amount sorbed in millimoles per gram
of dehydrated zeolite.
 n is the average number of molecules per cavity.
An asterisk denotes desorption points.

194.65°K			194.65°K		
p	mm/g	n	p	mm/g	n
0.318	0.584	0.95	12.202	3.687	6.02
0.359	0.623	1.02	16.223	3.995	6.52
1.062	1.092	1.78	20.120	4.206	6.86
1.295	1.221	1.99	28.245	4.515	7.37
2.138	1.621	2.65	40.794	4.805	7.84
2.577	1.808	2.95	20.132*	4.206	6.86
2.758	1.880	3.07	10.806*	3.541	5.78
3.829	2.260	3.69	7.364*	3.076	5.02
4.982	2.581	4.21	5.550*	2.722	4.44
5.569	2.718	4.44	4.432*	2.437	3.98
7.695	3.126	5.10	3.652*	2.202	3.59
10.080	3.456	5.64			

TABLE 4.1. (continued)

218.15°K			233.15°K		
p	mm/g	n̄	p	mm/g	n̄
0.991	0.506	0.83	1.752	0.443	0.72
1.438	0.625	1.02	2.286	0.519	0.85
2.860	0.911	1.49	2.725	0.573	0.94
4.131	1.136	1.85	3.354	0.645	1.05
4.814	1.248	2.04	5.118	0.834	1.36
8.586	1.733	2.83	7.230	1.018	1.66
11.741	2.069	3.38	9.145	1.168	1.91
14.629	2.323	3.79	12.440	1.398	2.28
19.906	2.691	4.39	16.921	1.671	2.73
24.773	2.961	4.83	22.653	1.975	3.22
32.558	3.285	5.36	29.626	2.271	3.71
40.132	3.523	5.75	36.077	2.492	4.07
12.868*	2.187	3.57	22.693*	1.973	3.22
			11.319*	1.330	2.17
			9.344*	1.196	1.95
			6.243*	0.943	1.54
			4.606*	0.792	1.29
			2.817*	0.591	0.96
			1.485*	0.404	0.66

TABLE 4.1. (continued)

253.15°K			273.15°K		
p	mm/g	n	p	mm/g	n
1.865	0.227	0.37	4.441	0.221	0.36
3.300	0.351	0.57	7.112	0.322	0.53
4.404	0.435	0.71	10.232	0.424	0.69
7.123	0.592	0.97	14.401	0.540	0.88
11.043	0.780	1.27	18.432	0.639	1.04
15.401	0.957	1.56	21.607	0.712	1.16
20.732	1.148	1.87	33.162	0.939	1.53
25.484	1.301	2.12	21.609*	0.711	1.16
29.446	1.421	2.32	12.777*	0.498	0.81
37.064	1.628	2.66	10.839*	0.442	0.72
21.208*	1.172	1.91	6.449*	0.300	0.49
11.671*	0.808	1.32	2.922*	0.156	0.25
6.928*	0.589	0.96			
4.504*	0.444	0.72			
3.104*	0.343	0.56			
1.323*	0.178	0.29			

TABLE 4.1.   (continued)

288.15°K			300°K		
p	mm/g	n	p	mm/g	n
3.440	0.122	0.20	5.761	0.123	0.20
5.728	0.187	0.31	10.002	0.202	0.33
8.517	0.259	0.42	15.673	0.296	0.48
12.456	0.347	0.57	24.631	0.424	0.69
16.594	0.429	0.70	35.396	0.557	0.91
19.790	0.490	0.80	24.553*	0.426	0.70
31.176	0.671	1.09	15.625*	0.298	0.49
49.562	0.919	1.50	9.954*	0.205	0.33
11.440*	0.327	0.53	5.734*	0.127	0.21
9.365*	0.280	0.46	4.935*	0.110	0.18
5.099*	0.174	0.28	3.734*	0.086	0.14
2.113*	0.085	0.14	1.683*	0.041	0.07
1.820*	0.075	0.12	0.996*	0.024	0.04
0.783*	0.038	0.06			

TABLE 4.2. – EQUILIBRIUM SORPTION ISOTHERMS OF
ETHANE IN LINDE 5A.

p is the pressure in cm of mercury at the ice
point (273.15°K).

mm/g is the amount sorbed in millimoles per gram
of dehydrated zeolite.

n is the average number of molecules per cavity.
An asterisk denotes desorption points.

| | 194.65°K | | | 218.15°K | |
p	mm/g	n	p	mm/g	n
0.026	1.471	2.40	0.117	1.610	2.63
0.054	2.531	4.13	0.127	1.624	2.65
0.747	3.496	5.71	1.117	3.036	4.95
1.080	3.586	5.85	1.782	3.168	5.17
4.798	3.971	6.48	8.352	3.538	5.77
10.971	4.190	6.84	14.301	3.660	5.97
16.659	4.287	7.00	14.288	3.662	5.98
24.499	4.367	7.13	22.839	3.773	6.16
35.565	4.436	7.24	38.441	3.897	6.36
11.973*	4.210	6.87	26.196*	3.801	6.20
3.070*	3.851	6.28	4.886*	3.415	5.57
1.487*	3.665	5.98	1.892*	3.183	5.19
0.923*	3.547	5.79			

TABLE 4.2. (continued)

233.15°K			273.15°K		
p	mm/g	n	p	mm/g	n
0.355	1.787	2.92	1.390	1.004	1.64
1.462	2.714	4.43	1.802	1.173	1.91
1.917	2.837	4.63	3.362	1.623	2.65
2.249	2.888	4.71	4.832	1.889	3.08
7.159	3.221	5.26	5.825	2.018	3.29
12.067	3.343	5.45	9.112	2.298	3.75
19.337	3.435	5.61	14.227	2.533	4.13
32.021	3.559	5.81	21.227	2.708	4.42
52.441	3.667	5.98	33.725	2.877	4.69
7.147*	3.222	5.26	9.094*	2.300	3.75
2.480*	2.919	4.76	4.136*	1.781	2.91
1.509*	2.727	4.45	2.630*	1.445	2.36
1.126*	2.582	4.21	1.888*	1.203	1.96

253.15°K

0.958	1.521	2.48	45.842	3.295	5.38
1.103	1.639	2.67	16.349*	3.053	4.98
2.380	2.219	3.62	9.665*	2.894	4.72
3.260	2.413	3.94	8.453*	2.850	4.65
3.840	2.500	4.08	5.857*	2.708	4.42
9.711	2.888	4.71	3.545*	2.458	4.01
16.395	3.049	4.98	2.222*	2.175	3.55
26.417	3.170	5.17	1.655*	1.962	3.20

TABLE 4.2.   (continued)

	288.15°K			300°K	
p	mm/g	n	p	mm/g	n
1.273	0.619	1.01	2.419	0.679	1.11
1.796	0.773	1.26	3.530	0.869	1.42
3.969	1.240	2.02	4.166	0.964	1.57
6.054	1.540	2.51	6.310	1.227	2.00
7.536	1.699	2.77	8.844	1.460	2.38
11.659	2.003	3.27	11.384	1.638	2.67
18.545	2.281	3.72	17.019	1.914	3.12
28.040	2.496	4.07	20.137	2.023	3.30
45.315	2.706	4.42	30.254	2.266	3.70
11.672*	2.001	3.27	47.157	2.527	4.12
4.892*	1.389	2.27	20.115*	2.024	3.30
2.849*	1.026	1.67	8.979*	1.475	2.41
1.859*	0.788	1.29	5.439*	1.131	1.85
1.294*	0.622	1,02	2.869*	0.767	1.25
			1.729*	0.546	0.89
			1.127*	1.401	0.66

TABLE 4.3. – EQUILIBRIUM SORPTION ISOTHERMS OF KRYPTON IN LINDE 5A.

p is the pressure in cm of mercury at the ice point ($273.15°K$).

mm/g is the amount sorbed in millimoles per gram of dehydrated zeolite.

n is the average number of molecules per cavity. An asterisk denotes desorption points.

\-194.65°K			233.15°K		
p	mm/g	n	p	mm/g	n
1.881	0.728	1.19	4.485	0.310	0.51
2.547	0.955	1.56	6.623	0.451	0.74
3.994	1.404	2.29	8.634	0.579	0.95
5.181	1.739	2.84	12.152	0.792	1.29
5.733	1.882	3.07	14.443	0.934	1.52
8.693	2.523	4.12	22.153	1.330	2.17
11.132	2.915	4.76	30.414	1.698	2.77
15.339	3.389	5.53	40.596	2.084	3.40
16.878	3.519	5.74	30.251*	1.707	2.79
26.669	4.071	6.64	18.280*	1.128	1.84
36.531	4.384	7.15	5.903*	0.412	0.67
47.536	4.614	7.53	2.117*	0.152	0.25
26.709*	4.068	6.64			
17.048*	3.525	5.75			
8.443*	2.465	4.02			

TABLE 4.3. (continued)

	253.15°K			273.15°K	
p	mm/g	n	p	mm/g	n
4.063	0.139	0.23	4.125	0.075	0.12
9.530	0.319	0.52	7.183	0.130	0.21
13.140	0.431	0.70	11.204	0.200	0.33
16.287	0.527	0.86	17.168	0.301	0.49
23.347	0.731	1.19	23.543	0.405	0.66
34.534	1.026	1.67	34.421	0.574	0.94
49.944	1.392	2.27	48.274	0.776	1.27
23.332*	0.732	1.19	22.137*	0.383	0.63
7.956*	0.271	0.44	8.276*	0.149	0.24
2.886*	0.102	0.17	3.196*	0.057	0.09
1.086*	0.038	0.06	1.246*	0.022	0.04

	288.15°K			300.°K	
5.701	0.083	0.137	4.502	0.041	0.07
11.308	0.152	0.248	8.222	0.076	0.12
18.404	0.233	0.381	13.683	0.125	0.20
30.176	0.364	0.594	23.225	0.208	0.34
44.556	0.520	0.849	35.877	0.315	0.51
18.389*	0.234	0.382	13.638*	0.127	0.21
5.694*	0.083	0.136	3.677*	0.034	0.06
1.795*	0.035	0.057	1.003*	0.008	0.01
0.580*	0.019	0.032			

CHAPTER 5

CALORIMETRY

"Worse still, the measurement of heat capacity was the
most humdrum of measurements, well known and despised
by every schoolboy". (Birkenhead 1961)

5.1. Introduction.

It has been mentioned previously that when the
water has been removed from molecular sieve zeolites
by evacuation at high temperatures, the dehydrated
or 'activated' cationated framework remains as the
'host' lattice which is penetrated by regular micro-
porous channels capable of occluding a wide variety
of sorbed 'guest' molecules. Information on the
interactions and motions of these molecules in the
micro-cavities can be gained by observing the heat
capacity of the sorbed phase. Obviously this cannot
be detatched from the framework, hence the heat
capacity of the guest phase must be found as the diff-
erence in the heat capacities of the guest host
inclusion 'compound' and the empty framework. Since
the heat capacity required is the difference of two
much larger quantities, the experimental data must
be determined very precisely. The calorimeter system
described in this chapter was designed to yield such
data in the range 12 - 300°K. The calorimeter is
of the vacuum adiabatic type, following the general

design of Southard and Brickwedde (1933). The control
of the adiabatic shields was automated (Sec.5.3),
the same control network being used to operate with
the other calorimeter in the laboratory also (Cope
1967). Although the results given later are the
first to be quoted for this system, part of it was
built and used by Dr.P.Limcharoen.

Before describing the system in detail, note is
made of the nomenclature used throughout since there
is no established usage in the literature. The
calorimeter system consists of the measuring and
control circuits, a pumping line, and the cryostat,
within which is the calorimeter assembly enveloped by
an outer can. The container which holds the sample is
termed the calorimeter vessel or simply vessel.

5.2.1. The Complete Assembly.

The low temperature vacuum-type adiabatic calorimeter is shown diagramatically in Figure 5.1. During heat capacity determinations it is essential that the adiabaticity of the calorimeter vessel assembly (sealed vessel with greased thermometer and some wiring) is maintained continuously. In the main this is achieved by the control of the temperature of each of the three shields (top.side and bottom) (A,see Fig.5.1) to be the same as that of the vessel surface. No open hole is allowed in the shields so to avoid radiation losses to the outer can at the higher temperatures. A high vacuum within the outer can reduces thermal conduction and convection to a minimum. Wires to the differential thermocouple junctions and the calorimeter vessel (B) cicuits are brought to the temperature of the vessel by fixing them rigidly for several revolutions in helical grooves in the outer surface of the side shield.

The cylindrical stainless steel outer can (G) is soldered (indium-tin eutectic) to the top plate of the calorimeter assembly (D) which itself is supported by the monel steel tube (E) which passes through the cryostat brass top plate (F). To the top of the tube a wide glass tube with a side arm (G) is joined with picein wax. Into the cone which terminates this glass tube is inserted with picein wax a glass stopper (H), and between these two pass all the electrical wires to the calorimeter (24 copper 38SWG SSC enamelled and 6 Constantan 34SWG SSC). The side arm connects the space within the outer can via wide bore glass tubing to the glass-line shown in Figure 5.2.

Fig. 5.1.   The Calorimetric Apparatus
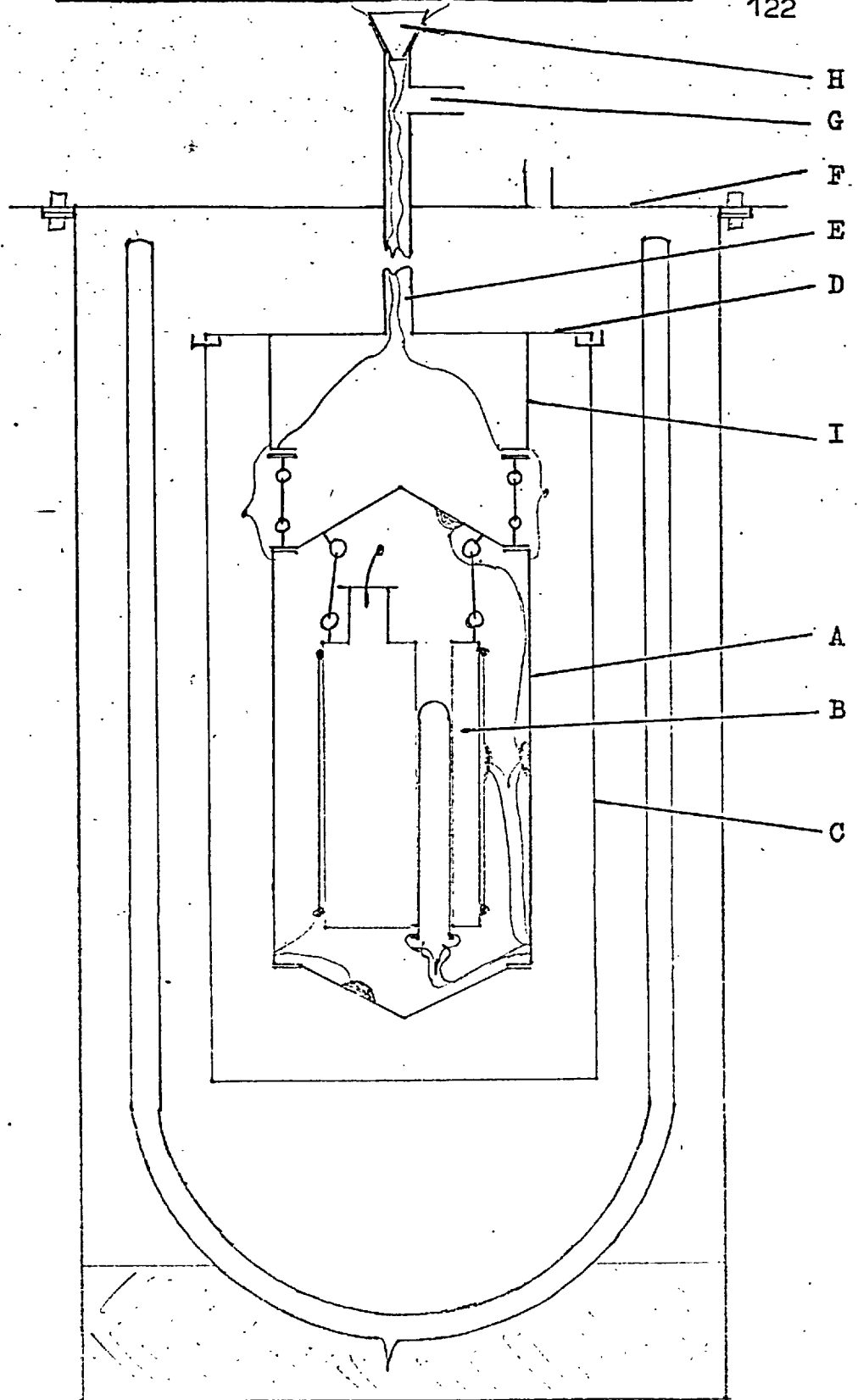
Fig. 5.2. The Calorimeter Glass-line
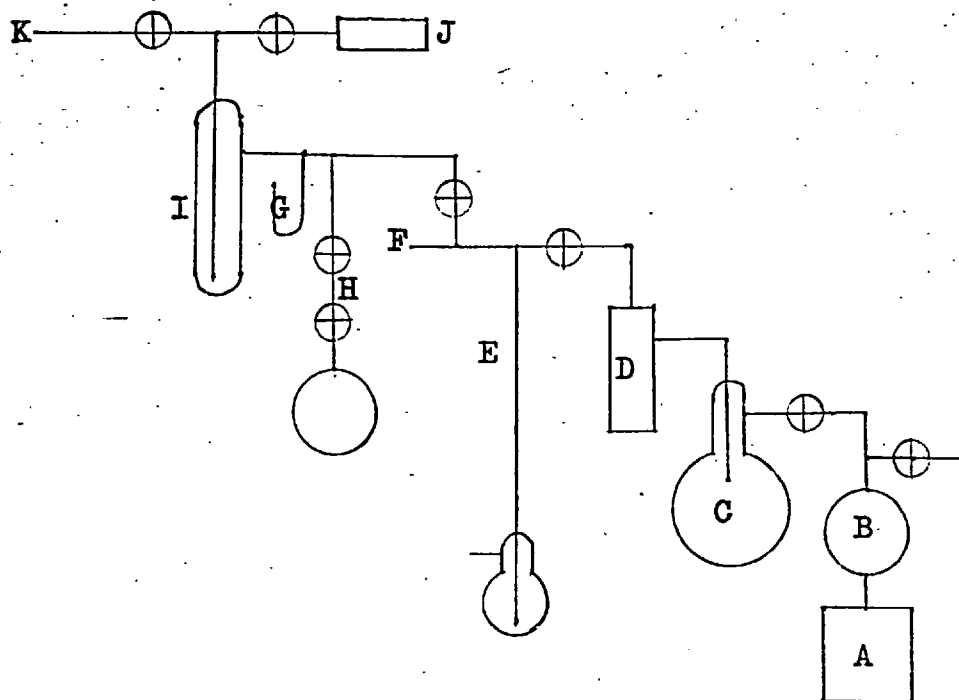
A	Oil rotary pump
B	Oil trap reservoir
C	Ballast Volume
D	Mercury diffusion pump
E	Mercury manometer
F	To general high vacuum line
H	Helium dosing system
I	Cold trap
J	Penning gauge head
K	To calorimeter system

A mercury diffusion pump backed by a oil rotary pump enables a high vacuum to be achieved within the outer can. The pressure can be ascertained by using the Penning or McCleod gauge, and a helium dosing facility is also included. The cold trap forbids entry of condensible vapours (water, mercury, etc.) to the calorimeter and Penning head.

After the electrical wires to the calorimeter enter the vacuum system as indicated above, they are brought together in a cable to descend through the monel tube (E) and the hollow cylinder (I) which is part of the top plate. This is a heat exchanger used to bring the wires to the temperature of the refrigerant by securing them with varnish for several revolutions around its outer surface. These windings are covered with aluminium foil to encourage thermal equilibration and to avoid burning the insulation when soldering on the outer can. The ends of these wires hang regularly spaced from the base of the cylinder and are coded with coloured cotton.

The outer can is cooled by refrigerant contained in a silvered dewar vessel. This is supported in a strong counterweighted cylindrical container which moves on two vertical runners. When at its uppermost position a neoprene gasket can be compressed to make an air-tight joint between the cylinder and the cryostat top plate. For experiments below $80^{o}K$, this volume is evacuated using a high capacity Kinney oil pump to solidify the refrigerant in the dewar: this being nitrogen or para-hydrogen for temperatures down to $50^{o}K$ and $10^{o}K$ respectively. Otherwise liquid nitrogen is the coolant.

5.2.2.   The Calorimeter Heater Circuit.

Thermal energy is added intermittantly to the
sample by passing a known ammount of electrical energy
through the calorimeter heater.   The construction of
the actual heater is described elsewhere (Sec. 5.4.1),
the complete cicuit is shown in Figure 5.3.

At the start of a day, with the heater series
resistance set approximately equal to the actual
heater resistance (R_H), the number of cells of the
battery used is chosen to give the required heater
current.   Further adjustments in this current through-
out the day are made by resetting the series resistance.
The battery is maintained under constant load conditions
by switching the current through an equivalent
resistance when not required for calorimeter heating.
Copperwire (38SWG DSC) connects the manganin heater
wire at the base of the calorimeter vessel to the inside
of the base of the side shield.   These heater leads
can cause problems in precise calorimetry (Ginnings
and West 1964).   Obviously at least two are required
to carry the current.   These wires must not be too thick
since then thermal conduction along them would be
a large source of errors, this becoming critical at
the lowest temperatures.   However their electrical
resistance must be very small compared with the heater
resistance because it is difficult to know how heat
developed in these wires is distributed between
the vessel and the shields.   Assuming equipartition,
we consider the wires to be identical and apportion
all the heat developed in one (ab in Fig.5.3) to the
calorimeter vessel, and that in the other to the
shields.   This is effected by the use of a third

Fig. 5.3.   The Calorimeter Heater Circuit.
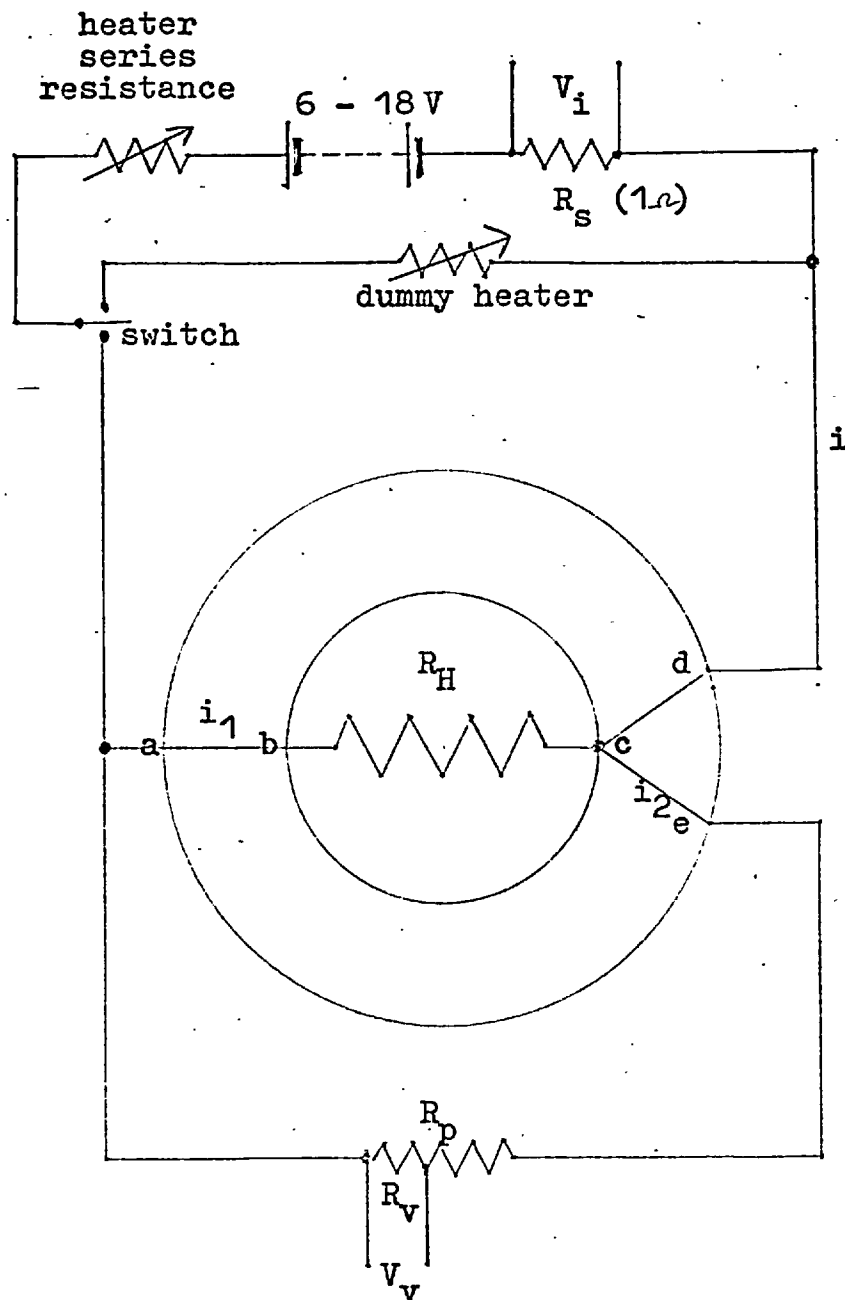
Potential difference between ac is V_H

heater lead and taking as the heater potential as
that which exists between the connections ac (Fig.5.3).

The electrical energy delivered to the heater
is measured by alternatively determining with a
vernier potentiometer the potential difference (V_H)
across it and that (V_i) across a standard resistance
$(R_s, \sim 1\Omega)$ in series with the battery. V_H is too
large to be measured directly so a 100:1 voltage
divider is used and the potential difference (V_v)
across the low voltage tapping is used to balance the
potentiometer. The resistances, R_v, R_p, R_s, had
been calibrated previously (Pemberton 1965), and are
kept in a draught-proof cabinet. The switch which
energizes the heater also activates a time period
counter which records on decatron tubes the number
of oscillations of a 10 kHz. crystal. The crystal
frequency was checked (May 1968) against a calibrated
frequency meter and found to be 10 kHz $\pm.2$ Hz. The
slowest tube indicated integral seconds. The integral
number of 10 sec. intervals was recorded on an add-
on register and independently checked by timing the
heating periods with a stop watch.

It is pertinent to add that some laboratories
only measure the current through the heater and
calculate the heating rate from a table of the
calorimeter heater resistance and temperature. This
method is not used here because the properties of
the heater could alter slightly run to run due to
the outgassing procedure (see Sec.5.4).

5.2.3. The Thermometer and its Circuits.

The temperature of the calorimeter vessel is
measured by a commercial four lead platinum resistance
thermometer (H. Tinsley, No. 177787). The coiled
filament of platinum wire is coiled on a former and is
held in a helium atmosphere within a platinum sheath
(5cm. long, 5mm. O.D.). To its end is joined a
glass seal through which emerge the four platinum leads.
These are tied with cotton to the seal and each is
soldered to a length of copper wire (38SWG DSC)
which could be connected to a lead at the side shield.
The thermometer was submitted to the National Physical
Laboratory (N.P.L.) for calibration.

Above $90^{\circ}K$ the temperature-resistance relationship
is of the form

$$t = \frac{R_t - R_o}{\propto R_o} + \delta(\frac{t}{100}-1)(\frac{t}{100}) + \beta(\frac{t}{100}-1)(\frac{t}{100})^3$$

where
t is the temperature ($^{\circ}C$) on the International
Practical Scale of temperature based on certain
reproducible fixed points of pure materials,
R_t is the resistance at temperature $t^{\circ}C$,
R_o is the ice point resistance ($0^{\circ}C$),
and $\propto$ and δ are constants determined by the N.P.L.
by measuring the resistance at the boiling point
of oxygen ($-182.97^{\circ}C$), the triple point of water
($.01^{\circ}C$), the steam point ($100^{\circ}C$) and the boiling
point of sulphur ($444.6^{\circ}C$). The constant β is calculated
to ensure that the equation gives a temperature
of $90^{\circ}K$ when the thermometer resistance is that
found for that temperature by interpolation from

the low temperature calibration (see below).

Below 0°C this is the Callendar-van Dusen equation; at 0°C and above the last term is dropped and it is termed the Callendar equation. The values determined are shown below:

α = 0.00392597
β = 0   t not less than 0°C
β = 0.1098 t below 0°C
γ = 1.4924
R_0= 25.0880 ohms (absolute).

Below 90°K, no such relationship has been established because of the increasing importance of impurity conduction at low temperatures. The calibration in the range 12 to 90°K was in terms of the Thermo-dynamic Temperature scale realized at the N.P.L. using a helium gas thermometer taking the boiling point of oxygen to be 90.18°K. The results were expressed as the difference (ΔW) at a number of temperatures (T) in the observed value of the ratio (W) of the resistance at that temperature to the ice point resistance (R) and values of W given in a table of W and T published by the N.P.L.; these are shown in Figure 5.4. The quoted accuracy was estimated to be $\pm0.02^\circ$K (12 to 20°K) improving to $\pm0.01^\circ$K (20 to 90°K). The above two temperature scales are related by 0°C equalling 273.15°K.

Fig. 5.4. The Deviation of the Platinum Resistance Thermometer from the Published N.P.L. Table 78/61.

W is the ratio of the thermomter resistance at a given temperature and the resistence at the ice point.

Thermometer No: 177787	
$W \times 10^6$	Correction $\Delta W \times 10^6$
1 000	+ 20
2 000	18
3 000	19
4 000	20
5 000	22
6 000	23
7 000	23
8 000	24
9 000	24
10 000	25
20 000	27
40 000	29
60 000	29
80 000	27
100 000	25
120 000	23
140 000	21
160 000	19
180 000	18
200 000	16
220 000	15
240 000	15

The Thermometer Circuit.

The thermometer resistance is determined by
passing a steady current through it; the vernier
potentiometer is used to measure the potential
difference both across the thermometer and across a
standard resistance ($\sim 10\Omega$) in series with it (Fig 5.5).
To eliminate the effect of switch contact and other
parasitic potentials, each potential is determined
with the current passing in each direction and the
average value taken (see Sec5.2.4.). Clearly the
thermometer and potentiometer currents must be reversed
concurrently. The battery consists of five six
volt car accummulators stored in a draught-proof
cupboard; they are always kept well charged. At
all thermometer temperatures, a current of about
3 mA was chosen, so a resistance ($10k\Omega$) is in-
corporated in the circuit. This resistance, together
with the 10Ω resistance, which had been calibrated
previously (Pemberton 1965), is kept in a draught-
proof cabinet. When the thermometer is not in use,
the battery was kept under constant load conditions
by switching the current through a decade box which
could be adjusted to the thermometer resistance.

5.2.4.   The Potentiometer and Associated Circuitry.

Both the thermometer resistance and the rate of
heat input to the calorimeter vessel are measured using
a vernier potentiometer. The heat capacity measurements
for the empty calorimeter and benzoic acid were
determined using the measuring circuits described
in detail previously (Pemberton 1965). This was
centred around a vernier potentiometer (H. Tinsley

Fig. 5.5.   Circuit for the Platinum Resistance
            Thermometer.
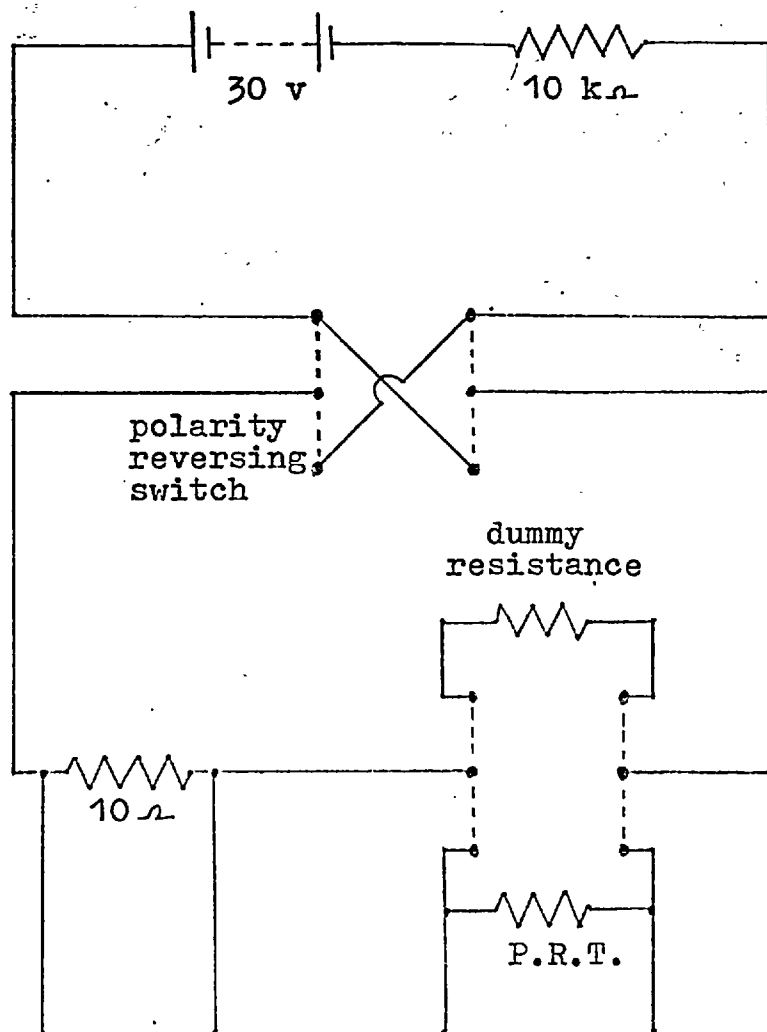
to vernier potentiometer

type 4363) which measured in steps of $1\mu V$, together
with a mirror galvanometer (H. Tinsley type 4500L)
of over two metres path length. Each of the switches
was of the two-pole throw-over type (Leeds and
Northrup) with copper-beryllium blades contacting
in copper pinches. These had to be thoroughly
cleaned and lubricated with contact oil regularly.

The performance of the thermometer circuit
switching is critical if reliable results are to
be obtained: this is especially true of the polarity
reversers (thermometer and potentiometer supply
currents). Unfortunately the former of these is
particularly vulnerable to produce spurious e.m.fs.
because the switching potential is 30 V which gives,
during the reversing process, high instantaneous current
densities at the contacts and concurrent electrolysis
of surface contaminants. This is probably aggravated
by inhomogeneity of the structure of the Cu-Be alloy.
Moreover these potentials are not corrected for by
averaging the forward and backward values.

Therefore for all the subsequent heat capacity
studies the circuits were modified. A new potentiometer
(H. Tinsley type 5590B) which read to $0.1\mu V$ was incorp-
orated and all the Leeds and Northrup switches were
replaced by one switch (Pye type 6001) having nine
poles and four way selection. This switch was of
the break-before-make variety (Sterret et al. 1965)
and the thermal e.m.f. per pole was specified as less
than $0.2 \mu V$ for $1^{\circ}C$ across the contacts with switch
resistance variation of less than $\pm 50\mu\Omega$ over at
least 10^7 operations. The current carrying parts
are made of copper which are clad with silver at the
contacts. The switch is enclosed in a metal box

to reduce dust and other contamination and has been
found to require no servicing.

A standard Weston cell contained in a draught-
proof cabinet is used to standardize the potentiometer
to read absolute volts. An accummulator (2V) kept in
the battery cupboard is used to power the potentiometer.

5.2.5. The Adiabatic Shield Assembly.

The shields (top, side, and bottom) completely
encase the calorimeter vessel which is suspended with
three lengths of button-cotton from the top shield.
The top shield itself is supported by three nylon
cords from hooks on a metal annulus which is attached
to the base of the calorimeter top plate cylinder with
three screws (Fig.5.1). Fine adjustment of these allow
the side shield to be set hanging vertically. The
side shield (13cm. long, 4.5 cm. O.D.) is a thin
walled hollow cylinder to which is joined an annular
section at each end for the attachment of an end
shield. Eighteen helical grooves were made in its
external surface extending from the very top to
the small holes near the base. After varnishing
this outer surface, insulated wires (14 Cu 38SWG,
4 constantan 34SWG) which terminated just inside the
shield were taken each through a hole and secured
with varnish in a groove. At the top a few centi-
metres of wire are left free, to be soldered on
assembly of the calorimeter to the wires from the heat
exchanger (see Sec.5.4.1). The wires are colour
coded at each end to facilitate their identification.
The wires are covered with varnished cigarette paper.
The side shield heater (Manganin wire 36SWG,~400Ω)

was then wound non-inductively and fixed with
varnish.

The end shields are of conical section with
small flanges through which pass screws to secure
them to the side shield. Their outer surfaces are
covered with varnished cigarette paper and a small
heater (Manganin wire 34 SWG, ~ 50Ω) is wound on
each in the same manner as the side shield. Each
shield is finally provided with an outer covering
of aluminium foil to minimize thermal transfer with
the outer can.

5.2.6.   The Differential Thermocouple Circuits.

Differential thermocouples are used to sense
the small temperature differences between the side
shield and the surface of the calorimeter vessel
(the side shield thermocouple) and between the two
end shields and the side shield (the top and bottom
shield thermocouples). The wiring arrangement is
shown in Figure 5.6., the cables lead to the shield
automatic control system (Sec.5.3). The constantan
(Cn) leads which come from the calorimeter have to
be joined to these copper leads. Since Cu-Cn junctions
are very sensitive at ambient temperature (40μV/^{o}C)
the two such junctions of each differential thermo-
couple system must be at the same temperature.
Thus the joints of all the Cn leads to the apparatus
(6) and the Cu leads are placed in wells placed
in the base of a large varnished brass block (3"X
1.5" square) and the leads are well equilibrated by
wrapping them around the block. The block is well
lagged with expanded polystyrene. The constantan

Fig. 5.6.   The Differential Thermocouple
             Circuits (diagrammatic).
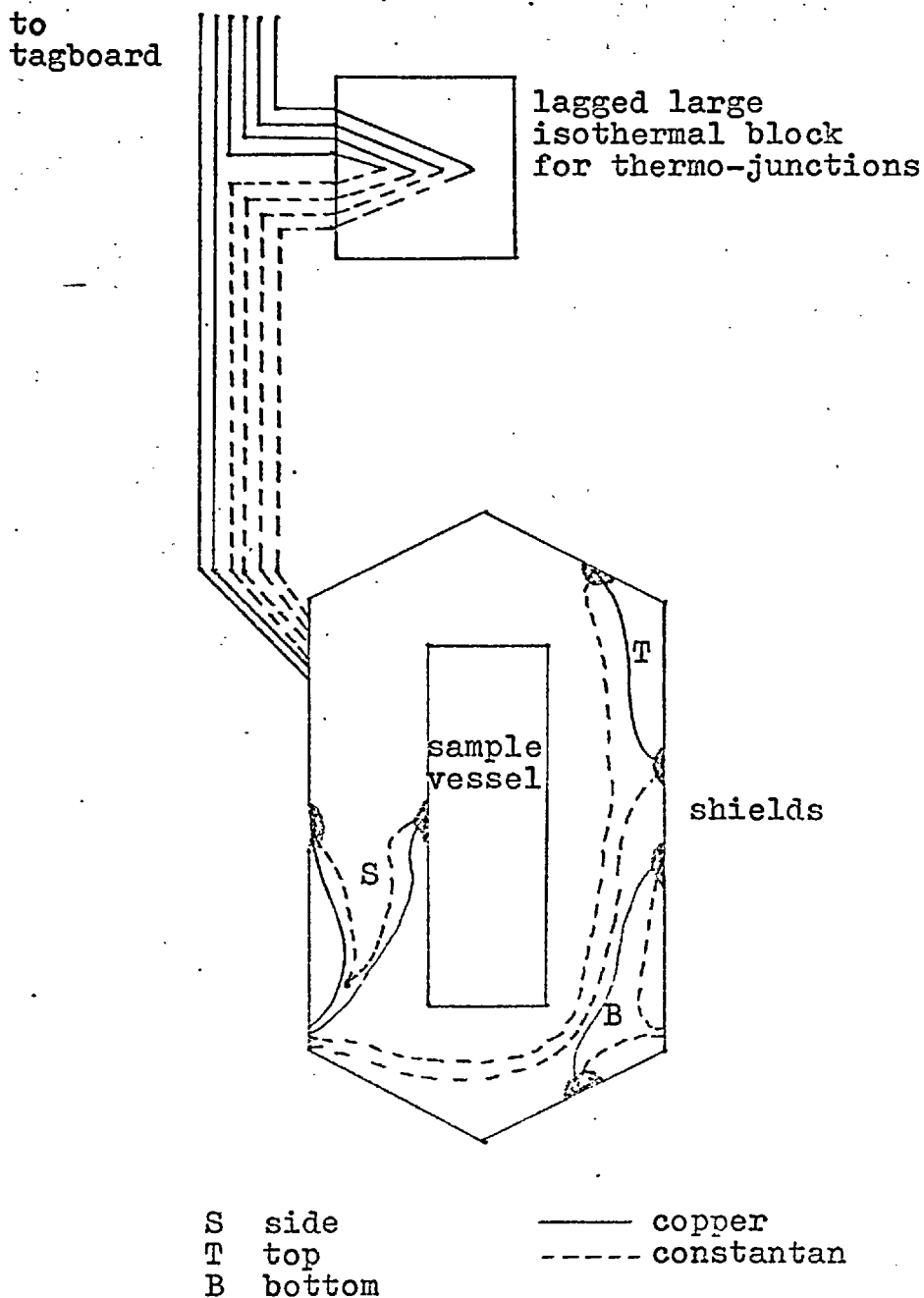
wire to the calorimeter was checked for inhomo-
geneity of the alloy composition. This was done
be connecting each length to a sensitive galvano-
meter; if a current flowed when part of the wire
was in liquid nitrogen it was discarded. All the
thermocouple joints are soldered directly to the
shields and calorimeter vessel to ensure optimum
thermal response although potentially this can cause
electrical problems in automatic shield control
(see later) when all the thermocouple circuits are
used simultaneously. A constantan lead must come
from the side shield thermocouple joint for each
of the top and bottom shield thermocouples because
the lead resistance is appreciable ($\sim 30\Omega$). If
only one lead is used (Pemberton 1965) the current
resulting from one non-isothermal differential thermocouple
would cause in this lead an 'IR drop' which would
be evident in the other circuit and vice-versa.
Note that the copper connection for the two end
thermocouples is also made through the metal of
the shield itself.

5.3. Automatic Shield Control.

5.3.1. Introduction.

Heat capacities can be measured by adding an accurately measured amount of heat to the calorimeter vessel assembly (Sec.5.2.1) and measuring the rise in temperature produced, again as accurately as possible. Naturally there must be no energy transfer between the vessel and its surroundings: the calorimeter shields. As mentioned this is achieved by having the calorimeter vessel and the shields highly polished to minimize radiation and by evacuation of the space within the outer can to reduce heat exchange by conduction and convection. However in high precision calorimetry to reduce this heat transfer to a tolerable degree it is necessary to maintain the temperature of the shields equal to that of the calorimeter. This is achieved by immersing the whole apparatus in a refrigerant and heating the shields electrically as required. The first such adiabatic vacuum calorimeter with an electrically controlled shield was described by Lange (1924). Since then the only significant advance in design was to supersede the one shield heater by top, side and bottom shield heaters as in the apparatus described in this thesis, thus obtaining more accurate 'shield control'.

Formerly these shields were controlled manually. When measurements were being taken one observer continuously controlled the shields whilst another used the potentiometer to measure the heat input and the corresponding temperature rise. By constructing

an automatic shield control system, the number of
operators would be reduced to one and an improvement
in precision would be expected since the concentration
of the shield control operator would fall due to sheer
fatigue during the long duration (up to 14 hours)
of the experimental runs.

The main problem in the implimentation of an
automatic control system is the requirememt to meet
sudden changes in the amount of shield heating due
to turning on and off the vessel heater. Note that
in less precise calorimeters where the vessel is heated
continuously this problem does not arise. It means
that the primitive type of automatic control where
the heating current is stepped from a low value
to a high value when the shield is cold (with
respect to some reference point) will rarely be very
satisfactory, although the early automatic systems
were based on this technique (e.g. Stull 1957,
Zabetakis et al. 1957, Southard and Andrews 1930,
Suga and Seki 1964) using various servo-mechanisms
to operate the switching. Later control systems
(West and Ginnings 1957, Cooper et al. 1959, Gayle
and Berg 1966) employed electronic controllers
which allow the operator to programme the magnitude
of the heating current as a complex function of the
temperature difference which it is attempting to
reduce, so achieving more accurate control; the
controllers are readily available and well-proven
since they have many industrial applications.

Gayle and Berg's system differed from the first
two in having transistor circuitry in the last stage
of amplification and in requiring no 'crash' control

to increase the heater current at the beginning of
the heating period. The system described in the
next section is of similar design, although the
performance of our system had to be rather superior
because it has to control the calorimeters in the
range 12 - 300°K, as opposed to 2 - 20°K, the shield
control becoming more critical at higher temperatures
because of radiative transfer.

The systems mentioned above consist of just
one control channel producing one output current
which either activates just one heater or is apport-
ioned with rheostats among heaters on each of the
three shields. The latter system is obviously an
improvement but not entirely satisfactory since
the proportion of the total current required by each
heater is different during drifts and heating periods.
The heat transfer coefficient alone determines the
drift current whereas the heat capacity of each
shield is an added factor during vessel heating.
The system adopted here therefore consists of three
separate channels for controlling each of the shields
independently. In principle, such a system is no more
complex than a one channel one if the two therm-
ocouple junctions required for each channel are
electrically insulated from the other couples and
the shields, as is done in another three channel
system (Sterrett et al. 1965). However, since good
electrical insulators are poor thermal conductors,
with this arrangement it is possible to have un-
measurable errors due to the thermal lags which
will exist; this is clearly of particular importance
in intermittently heated calorimeter systems. In a
slightly different context, the performance of these

insulated juctions has been investigated (Stansbury
et al. 1965) where their response time was shown to be
appreciable. These workers suggested it was better
to use a directly soldered junction with a therm-
ocouple comparator circuit (Dauphinee 1953), although
this creates further problems in sensistivity, noise
and amplifier stability. With the thermocouple circuits
described earlier (Sec.5.2.6) our three channel
control operates with the thermocouple junctions
soldered directly to the shields and the vessel,
so minimizing these thermal lags.

Before describing the system in detail, a brief
indication is given of the principles of operation
of the temperature controllers, since this must be
understood in order to arrange the settings of the
controls for optimum performance. Each controller
acts as a simple on-line analogue computer which
gives a 'control' signal, i, which is related to
the difference of temperature, θ, by the following
equations:

$$i = P(\theta + R\int \theta \, dt + D \frac{d\theta}{dt}) = PM, \qquad M_{max} \geqslant M \geqslant 0$$

$$i = 0, \quad M < 0; \qquad i = i_{max}, \quad M > M_{max} \quad .$$

The coefficients, P, R, and D, are each chosen
to give optimum control by varying resistances in
the controller circuit. The first term represents
straightforward proportional control which is
augmented by automatic reset and rate controls.
The former continuously acts to reduce the time-
average of the temperature difference to zero, it
is the control faculty with the controller senses
which

the zero base line. Proportional control alone
cannot do this since for any control situation
i and θ would then tend to come to steady state
values, θ would settle at some value which was not
necessarily zero. The rate control mode effects the
control current by an amount proportional to the
rate of change of the temperature difference, and is
used to give a reasonable speed of response and to
reduce 'hunting' or sustained oscillations about the
zero base line.

These settings, or the amount of each control
mode used, are found empirically and are altered only
a little for different temperature ranges, but quite
significantly for the two calorimeters on which the
system is used. Adjustment can easily be made on the
final power amplifier to relate the 'control' current
to the final heater current, this gain factor is
guadually increased with increasing temperature.

5.3.2. Implimentation.

Basically each of the three control systems
is identical; Fig.5.7 is a block diagram of the
system. The thermoelectric potential developed across
the differential couples causes the heater at the other
end of the circuit to be energised. The potential
from the copper-constantan thermocouple is amplified
and displayed on a chart recorder. A control unit
produces a 'control' current which is a function
of the above temperature difference. This current
causes the transistor unit to output a 'process'
current which passes through the shield heater.
Screened cable is used throughout to join the various

Fig. 5.7.   Block Diagram of an Automatic
Control System.
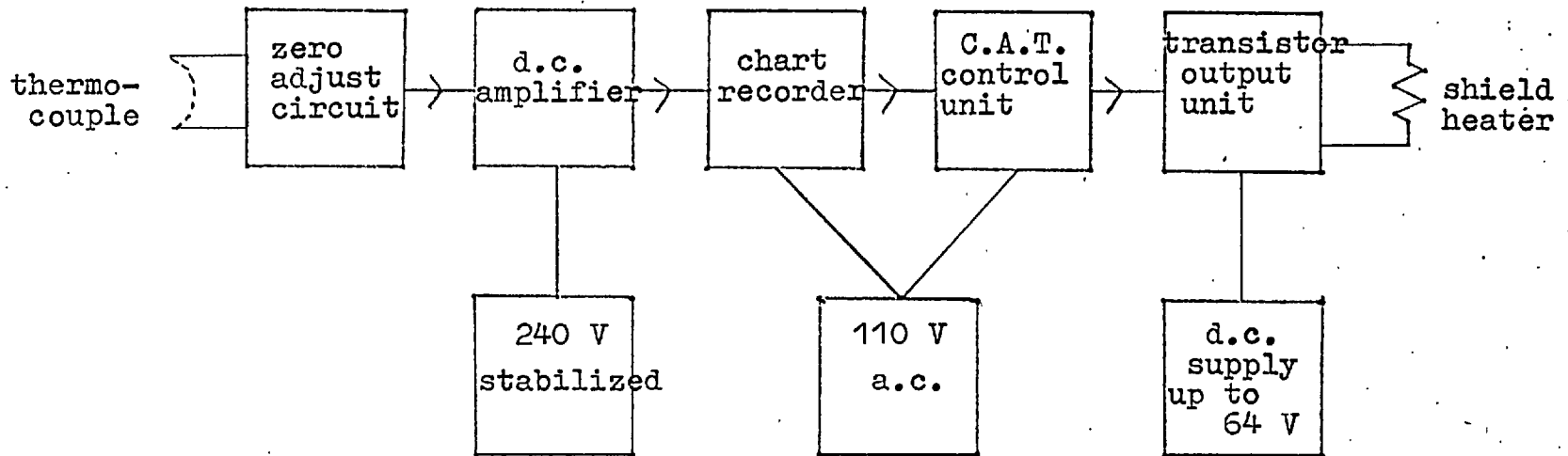
arrows indicate flow of information.

units.

The thermocouple circuits have been described elsewhere (Sec.5.2.6.). Each is coupled to a D.C. amplifier using the circuit shown in Fig.5.8. which allows fine adjustment of the amplifier zero; a coarse adjustment being incorporated on the amplifier. The circuit generates a potential of several micro-volts and the accumulator is kept well-charged in the battery cupboard. Since, due to its feed-back arrangements, the amplifier zero depends on the input resistance if it is below about 30 ohms (found by experiment) a series resistance of a greater value is always in circuit. To zero the amplifier the switch is closed to short circuit the thermocouple, one rotary thermal-e.m.f.-free switch (Croydon Instrument Co.) is used for all the thermocouples. Originally a circuit (Fig.5.9.) with higher input sensistivity was used, but this was abandoned as the switch, being on circuit all the time, itself led to drifts of the zero, especially overnight. All the resistors are wound with manganin wire which has negligible thermal-e.m.f. against copper. The D.C. amplifiers used are Pye microvoltmeters (type 11340/S) which are powered from a constant voltage transformer. The output resistance of each is increased from 700 ohms to 4000 ohms by short-circuiting the 'phase advance circuit' in the instrument as described in the Pye manual. Each galvanometer modulator unit of the amplifiers is placed on a vibtation-free mounting (lead slab on foam rubber) in a draught-proof cabinet. During runs the amplifiers are used on their most sensitive range.

Fig. 5.8. The Circuit for the Fine Zero Adjustment of the d.c. Amplifiers.

thermo-couple

zero switch

d.c. amplifier

1Ω 50Ω

1kΩ

250Ω

10 kΩ

2 v

Switch is thermal-e.m.f.-free type.

All resistances are wound with manganin wire.
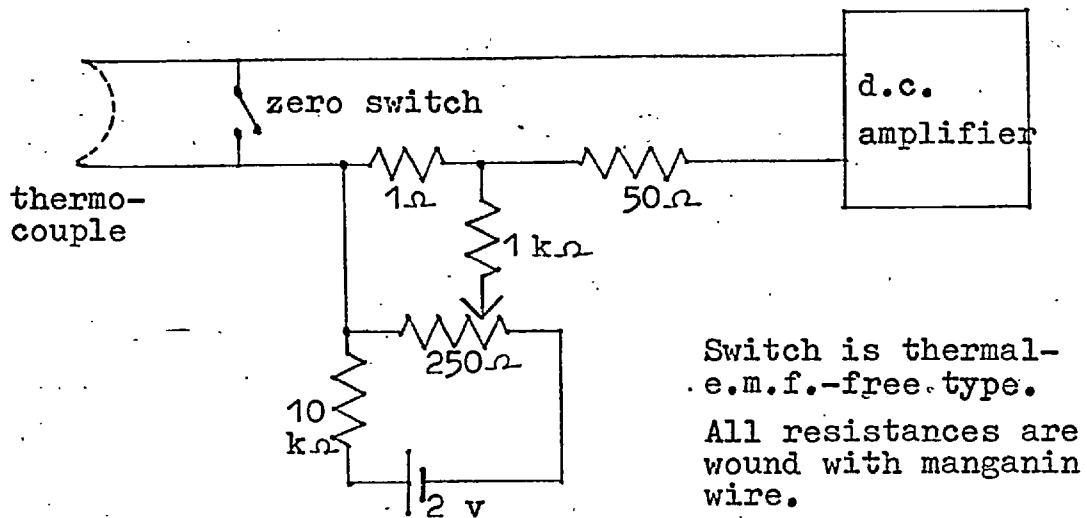
Fig. 5.9. The Former Zero Adjustment Circuit (used for manual control).

d.c. amplifier

25Ω

say 5Ω

30Ω

1Ω

230Ω

250Ω

10kΩ

2 V
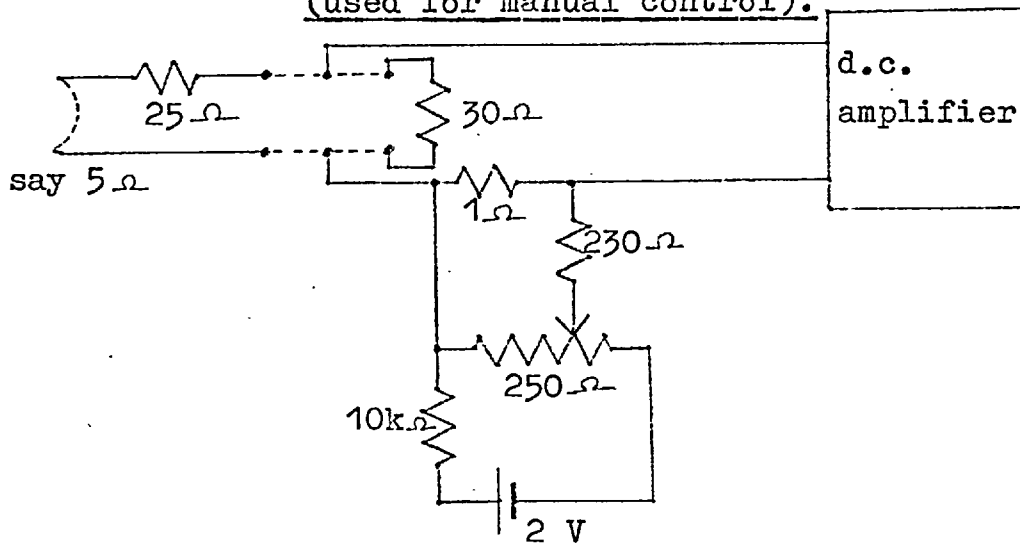
A resistance-capacitance network is employed
to couple the amplifiers to the recorders. The
circuit (Fig.5.10.) has a resistance of about 4000
ohms. Since the polarity of the input potential
changes continuously, non-polar solid tantalum
capacitors (Union Carbide) are used. Moreover these
are superior to other paper or electrolytic capacitors
in being very small; this enables the whole unit to
be constructed in a small tin to reduce induction
effects. The output resistance of 100 ohms means
that a thermocouple signal of $1 \mu V$ produces a de-
flection of 1 mV on the chart recorder. This is the
highest value which can be used without having an
unsatisfactory zero drift and signal-to-noise ratio.

Leeds and Northrup Speedomax H recorders are used
with response times of 5 seconds full scale (-5/0/+5 mV).
Each of these is powered from a seperate 120V trans-
former. The shaft which moves the recorder pen and
pointer also activates three switches and a contact
along a slide-wire; these are used to operate the
control unit. The control units used are of the series
60 (Leeds and Northrup) current adjusting type (C.A.T.).
These are integrally built with the recorders. There
must be no more than one common point in the output
circuits of the three control units, which is the
positive line of the 60V supply. This required the
earthing arrangements on both these recorders and
control units to be modified to avoid mutual inter-
ference between the three systems by ungrounding
the high tension negative of each unit. After initial
calibration, all these units were found to operate
quite satisfactory.

Fig. 5.10. The Coupling Circuit for Chart Recorder Input.
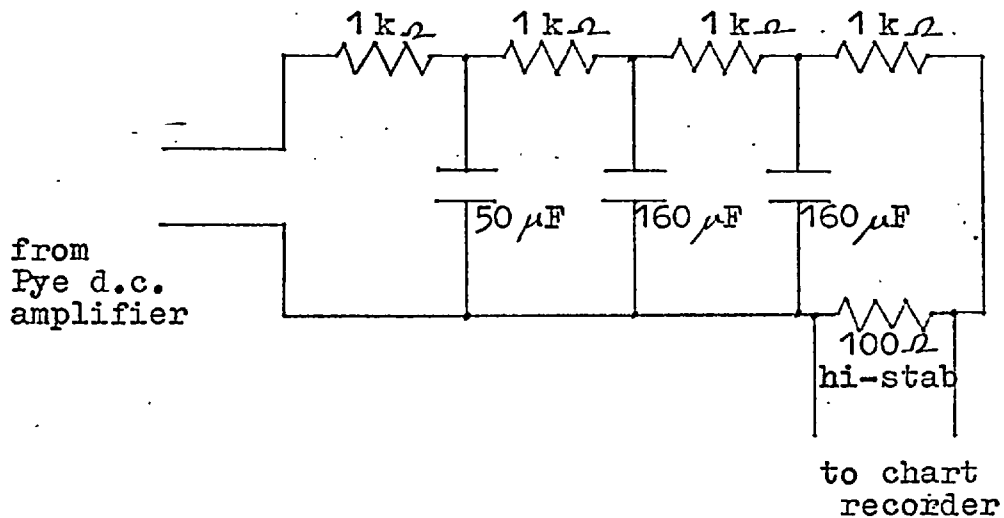
The whole circuit is constructed in a metal box.

Capacitors are Kemet N-series non-polar solid
tantalum types (Union Carbide Co.).

| 50 | F type | K50N2ONS | 20v rating |
| 160 | F type | K160N6NS | 6v rating |

Each of these units produce a 'control' current
which is delivered to a 5000 ohm potentiometer
connected between terminals FH and FL. Since the
dummy resistance incorporated in the control unit
can be set to this value, control can be switched
from automatic to manual very smoothly; also the
control slide-wire can be recalibrated very easily
(for details see the Manufacturer's handbook).
A current, tapped from the above potentiometer,
serves as the input signal for the transistor power
amplifier (Fig.5.11.). The Mullard transistors have
their base connection joined to their metal envelope
so they cannot be provided with the conventional
chassis heat shunt. They must not be allowed to become
hot since then an output leak current remains after
they have been passing a large current and ultimately
they would be damaged. Therefore a small fan is
placed under the units which cools the insulated
metal foil wrapped around each transistor.

Each heater circuit was modified to include a control
switch in the recorder so that there could be no heating
if its shield is more than $0.4\,\mu V$ hotter than its re-
ference point. This is a safeguard against the leak
currents mentioned above particularly. Due to the
low resistance of the top and bottom shield heaters
(ca. 50 ohms) a small leak current (ca 5 mA) was
always evident until current limiting resistors
(ca. 200 ohms) were placed in series with these
heaters. The transistors units are powered by the
unit shown in Fig.5.12. The vari ac is adjusted
to obtain about 60 volts across the ballast resistor
when all the 'process' currents are zero. The voltage
from this unit decreases with increasing load re-
quirements. This can be tolerated when only one

Fig. 5.11.   The Transistor Output Unit.
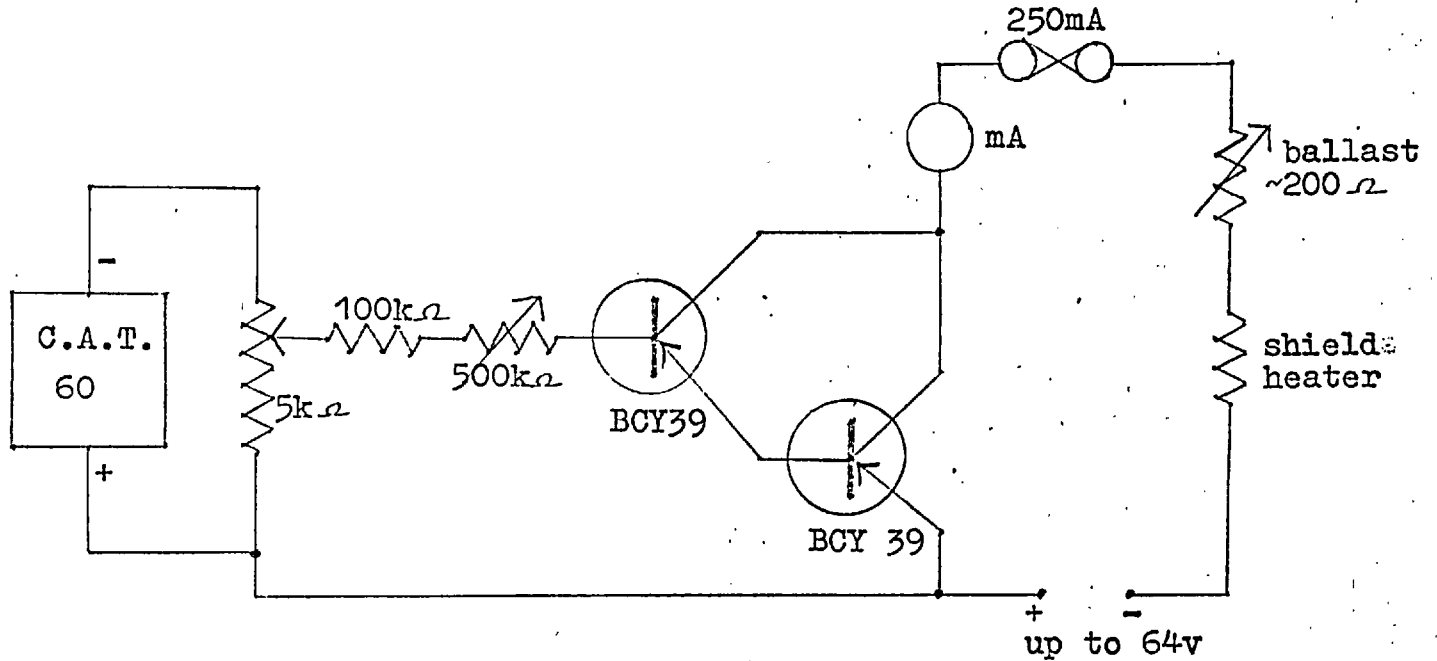
Shield heater resistances

top and bottom ~50Ω
side   ~400Ω

There is no ballast resistor
in the side shield circuit.

Fig. 5.12.   The Transistor D.C. Supply Circuit.
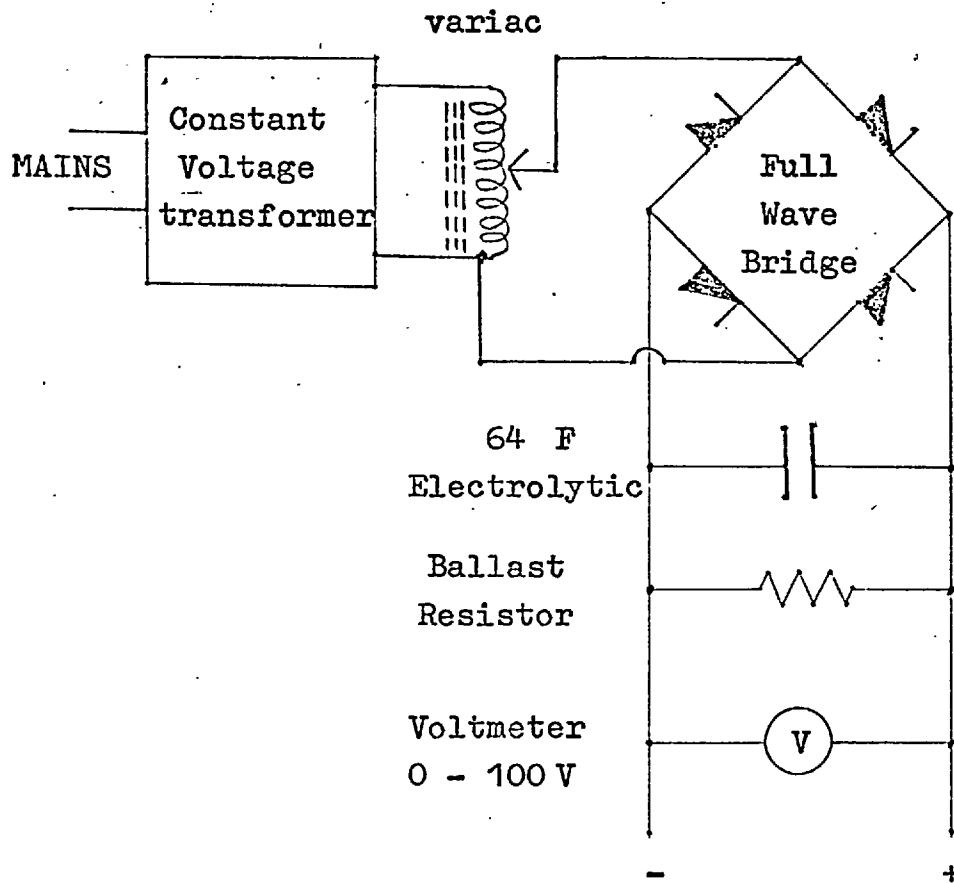
The metal rectifiers are STC type RM4, rated at 250V
and 250mA. Hence the total current which can be
drawn at 250V is 500mA.

shield is being controlled. When two or more shields
are on control, the fall in current supplied to one
shield causes the current in the other shields to
increase resulting in these shields overheating;
that is 'hunting' occurs. Therefore the ballast
resistor was incorporated. Since this consumed a
continuous current, the fractional change in total
current supplied with varying demands for the heaters
is much smaller resulting in the voltage change and
hunting being much reduced.

5.3.3. Operation and Performance.

Excellent control has been obtained with the
automatic control system described above, the temperature
differences being normally no more than a few thousandths
of a degree during drift or heating periods. The
network is very easy to use. The design of the first
stage amplifiers and the use of smoothed direct
current for the output process current mean that no
interferring signals are propagated to the measuring
circuits in the long wires of the calorimeter assembly.
Generally, once the positions of the various control
settings have been determined by trial and error,
the only further attention required is to recheck
the zero setting of the Pye amplifiers. This is done
at least once for every point and more often when the
equilibration times are long (see Ch. 8). The procedure
is first to set the C.A.T. controller to its manual
position to hold the process current at its steady
value momentarily and then to set the microvoltmeter
zero in the method described in the previous section;
the drift was rarely more than a fraction of a micro-
volt if the amplifier had warmed up. For the first

few points of the hydrogen and nitrogen pumping
runs the shields are manually controlled to avoid
any possible errors due to overheating because the
cold sink is very small, as there is no means to
cool the shields again.

The system is used with two calorimeter systems.
The control is better with the calorimeter described
above than in the older system (Pemberton 1965) because
the much smaller and lighter shields required smaller
currents and had shorter response times. This is
reflected in the different control settings needed
for each calorimeter. These, and the quality of the
control, are shown in Figs. 5.13-15, where it is
seen that the control off-balance at the beginning
and ending of a heating period is much more pronounced
for the older calorimeter.

Because of the continuous drift of its zero,
the Pye microvoltmeter is not perfectly suited for
use as a null detector in an automatic control net-
work. Investigation indicated that the drift is due
to small temperature changes altering the torsional
characteristics of the suspension of the galvanometer
modulator. These were reduced but not eliminated by
placing these units in enclosed cabinets. Null detectors
not using this method of carrier modulation would
eliminate this problem completely and so dispense
with the zero adjustment circuit.

Automatic shield control is beneficial in heat
capacity work with samples which achieve thermal
equilibrium rapidly; for the samples used in the
work described in this thesis it is virtually essential

TSEquilibration time ~45 min

Temperature rise 6·757°C

Equilibration time ~45 min

TS
−3   −2

Temperature rise 6·849°C

Chart speed 4"/hour

BOTTOM   SIDE   TOP

−1μV   1μV   −1μV   1μV ?   −1μV   1μV

OFF   OFF   OFF

A87   A87   A87

ON   ON   ON

Thermocouple sensitivity ~ 37μV/°C

−1μV OFF   1μV   −1μV OFF   1μV ?   −1μVOFF   1μV

A86   A86   A86

ON   ON   ON

BOTTOM   SIDE   TOP

Fig. 5.13. Automatic Shield Control for the Calorimeter described in this Thesis. Details of Run A are given in Chapter 7.

153
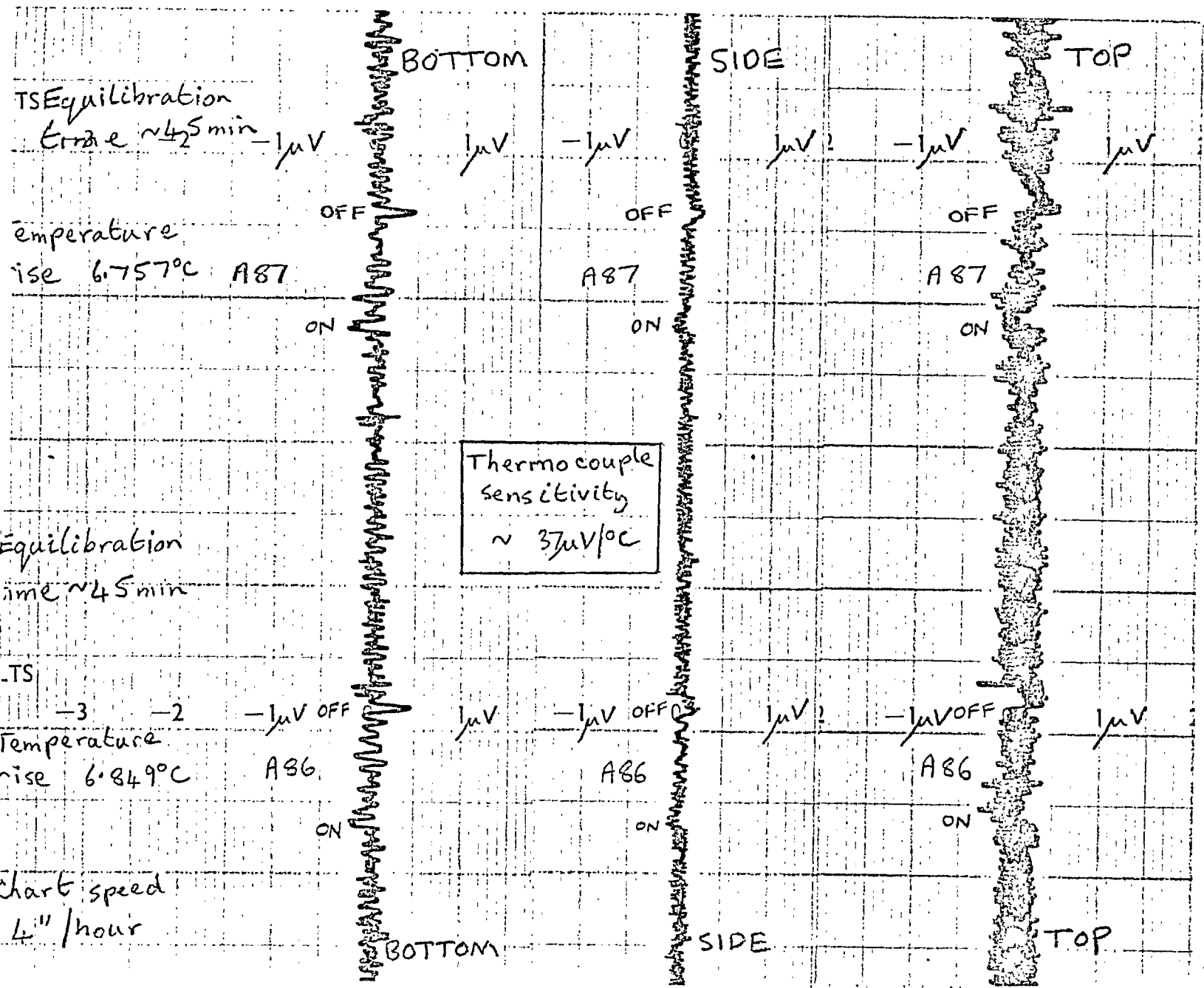
Fig. 5.14. Automatic Shield Control for the Calorimeter described in this Thesis. Details of Run B are given in Chapter 7.
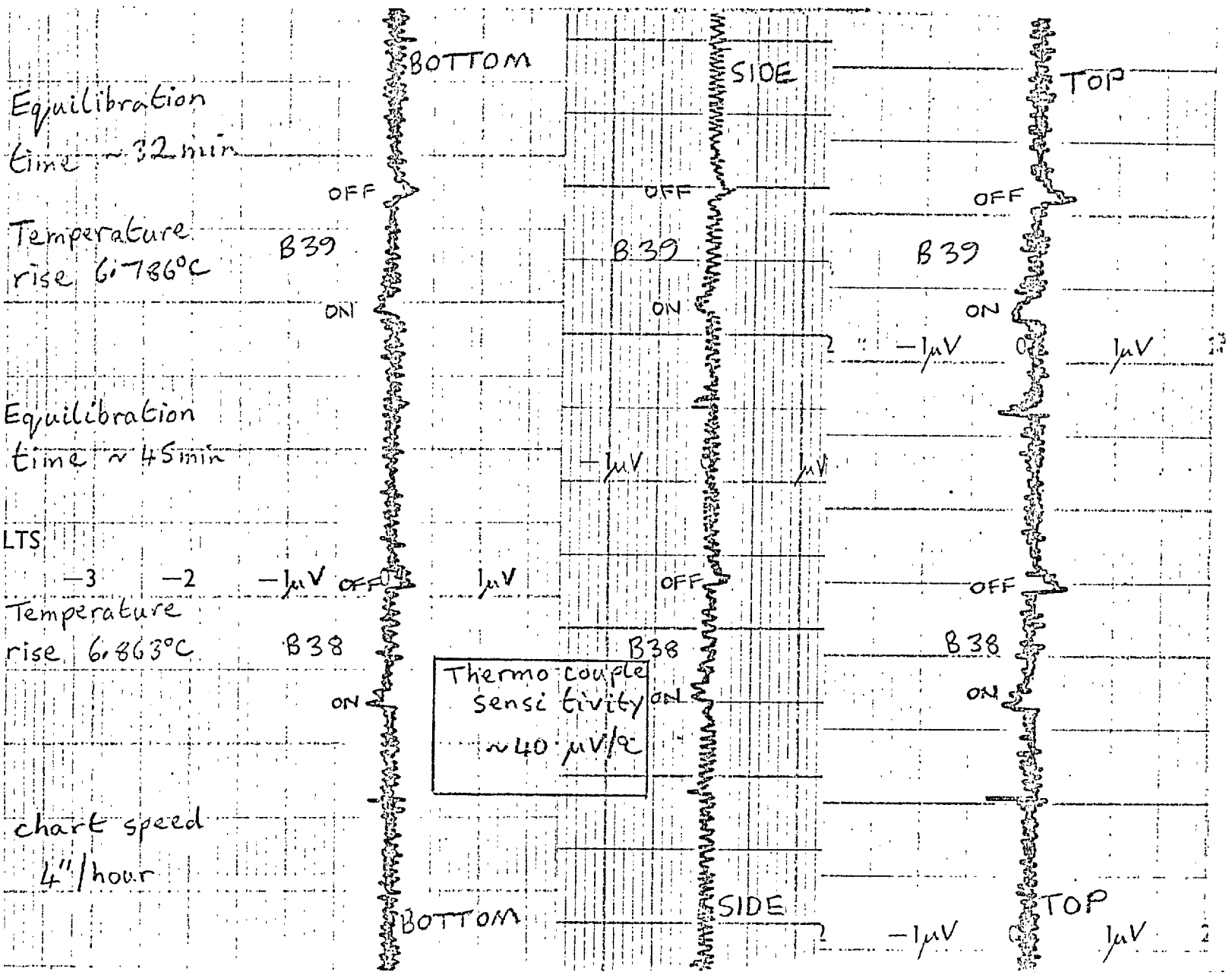
Fig. 5.15

AUTOMATIC SHIELD CONTROL

for

Runs H87, H88, H89.
Thiourea – 2,2. D.M.B.

CONTROL SETTINGS
(Proportional, Rate, Reset)

Thermocouple Sensitivity.
~ 28 µV °K⁻¹

BOTTOM

H89 $\bar{T}$ = 192.3°K
CONTROL SETTING
(6 , 0.06, 3)

H88 $\bar{T}$ = 185.0°K
(6, 0.06, 3)
0.55µV (0.02°K)

H87 $\bar{T}$ = 177.5°K
I_{max} increased
(6, 0.06, 3)

SIDE

H89 $\bar{T}$ = 192.3°K
CONTROL SETTING
(30, 0.4, 3)

H88 $\bar{T}$ = 185.0°K
(30, 0.4, 3)
0.6µV (0.02°K)

H87 $\bar{T}$ = 177.5°K
(30, 0.4, 2)

TOP

H89 $\bar{T}$ = 192.3°K
CONTROL SETTING
(15, 0.08, 6)

H88 $\bar{T}$ = 185.0°K
(15, 0.08, 6)
0.3µV (0.01°K)

H87 $\bar{T}$ = 177.5°K
(15, 0.08, 6)

VOLTS
-3 µV -2 µV -1 µV 1 µV 2 µV
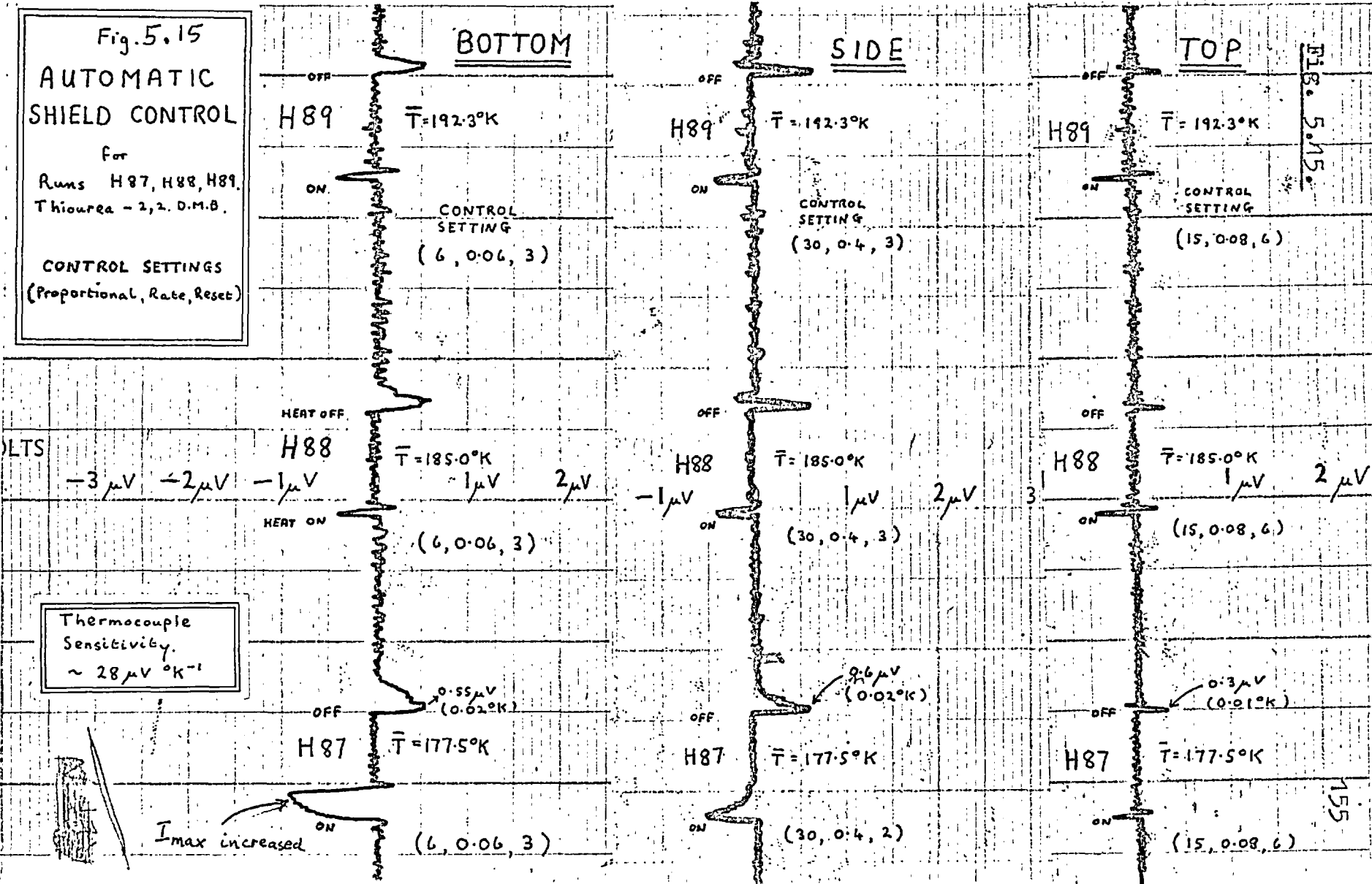
since the drift periods are very long, often over
an hour, thus continually demanding the highest
quality of shield control.

5.4. The Calorimeter Vessel and Its Loading.

5.4.1. Construction.

The calorimeter vessel is made of 10% iridium-
platinum alloy by Johnson-Matthey Ltd. An outer
cylinder (9cm. X 3.3 cm. O.D.) has gold soldered
at its extreme inner surfaces two end plates. The
base plate contained a redundant re-entrant heater
cavity and a tube (5mm. I.D.) extending to the top
plate which accommodated the platinum resistance
thermometer; the sample capacity is about 64 ml.
From the top plate also emerged a tube (8 mm. X
8 mm. O.D.) through which the vessel is filled.

A circular platinum plate is soldered (see below)
over the top of this tube to seal the vessel. A small
hole in this plate allowed a silver tube to pass
through. To avoid excessive heating of the sample
during vessel sealing, the filling tube is often
made of a very poor conductor like german silver
(Pemberton 1965), but here Pt-10%Ir alloy was used
throughout so that the zeolite powder could be
removed by dissolving it in hydrofluoric acid. The
chemical resistance of platinum alloys does recommend
them for use in calorimeter vessels, but their poor
thermal conductivity compared with copper or silver
can cause appreciable thermal gradients in the vessel
surfaces, which are a major source of calorimetry
errors. This problem is obviously most evident

during heat input, in this platinum calorimeter
the effect was minimized by heating a large area
directly by winding the heater over much of the outer
surface as opposed to having a capsulated heater
in a small heater cavity in the base plate (Cope 1967).

The heater used had to be of rather special
design. Since it is rigidly attached to the vessel,
it cannot be removed between runs. Nor would such
removal of the heater be desirable since it might
change its thermal characteristics. However in the
particular studies reported here it was necessary
to heat the zeolite in the vessel to above 300°C
before each run. Conventional wire insulation and
varnishes begin to decompose above 200°C. Many wire
and varnish combinations were tested at 300°C. both
in air and in a nitrogen atmosphere. "Insuglass"
glass-lapped thermocouple quality wire (IGL)
(Soxonia Electric Wire Co,) was found satisfactory
if it was well covered with varnish to save the
glass fibres unwrapping. The varnish selected was
"Pyre ML" (Du Pont de Nemours) which was used, as
supplied, in a xylene/N-methylpyrrolidone solvent
(Product R.C.675).

The curing of this product is achieved in two
stages. Firstly all the solvent must be removed,
followed by polymer conversion at $200-250^\circ$C. The
thermally stable end-product is a polyimide believed
to be based on pyromellitic anhydride and 4,4'-diamino-
diphenyl ether (Flavell and Yarsley 1967). The
stability of these polymers depends on ensuring
a very low hydrogen content and having all aromatic
units; in nitrogen or vacuo their degradation is

much reduced (Marvel 1965).

The heater was constructed as follows. First
a copper wire (22 SWG), silver coated to prevent
oxidation, was silver-soldered around the calorimeter
vessel a few millimeters from each end of the vessel
to hold the outer radiation shield from touching
the wire. A small gap (2mm) was left between the
ends of the bottom wire. Previously these parts
of the vessel were slightly roughened and thinly
covered with a layer of silver solder. "Easy-Flo"
solder (m.p.630°C.) and flux were used throughout
(Johnson Matthey Ltd.). Several coatings of varnish
were then applied to the curved vessel surface to
within 1cm. of the wires. The vessel was heated
to 150°C. for 30min. after each coat, and finally
baked at 240°C. for 12 hours. Complete electrical
insulation resulted.

The glass covered manganin heater wire (40 SWG
IGL, ∼410Ω) was then wound non-inductively over the
varnish from about 1.5cm of the top. The wire was
wound on in short sections, each being secured by
applying varnish and drying it under an I.R. lamp.
The winding was completed 1.5cm. from the bottom,
and the two end leads were passed through the gap
in the bottom wire and terminated. On completion
of this the whole heater was varnished over, baked
at 130°C. overnight and then at 200°C. for 24 hours.
The heater was covered with a radiation shield
(.005"Cu plated with .00004" gold on both sides,
Johnson matthey Ltd.). This foil was silver-soldered
to the two copper rings. Care was needed to avoid
damaging the heater. The heater end leads were then

revarnished to the side of the vessel with a little
of each end left bare. The connection to these wires
is explained elsewhere (Sec.5.2.2).

On heating the calorimeter vessel to 300°C. in
air the radiation shield tended to tarnish, probably
due to the gold first diffusing into the copper.
Thin platinum foil would be preferred for future
vessels to avoid this problem, although its poor
thermal conductivity would cause problems in the
actual calorimeter runs due to thermal gradients.
Therefore whenever this vessel was heated above
150°C., it was maintained in a atmosphere of nitrogen
to protect not only the foil, but also the varnish
(see above). The vessel was so heated at 300°C. until
it came to constant weight (loss on final heating
was .002% total weight). A small area mid way up
the radiation shield was tinned to which could be
soldered the Cu-Cn junctions of the calorimeter
thermocouple (Sec.5.2.6).

5.4.2   Calorimeter Sealing.

The calorimeter vessel is sealed by joining
a platinum plate over the end of the filling tube.
This plate had a hole at its centre through which
was joined a capillary silver tube (.5mm.I.D.)
which allowed the vessel to be connected to a glass-
line. The sample space could then be evacuated and
filled with gas, the final sealing being achieved by
cutting and sealing the silver tube. For the runs
on the empty calorimeter and benzoic acid, the
silver tube was simply joined (Picein Wax) to the
glassline, evacuated to below 1.10^{-5}mm.Hg, and dosed

with dry helium (about 2cm. $\overset{Hg}{\downarrow}$). The helium is used
to promote heat distribution within the calorimeter
at all temperatures. The tube was then firmly pinch-
sealed, cut about 5mm. from the platinum plate and
immediately sealed with soft solder. When it contained
zeolite, before the final sealing the vessel had to
be heated to 300°C. Therefore the two joints on the
platinum plate had to be either capable of sustaining
this temperature without cleavage or, during this
process, to be cooled to a lower temperature. Much
work was done by a previous worker in the laboratory
(P.Limcharoen) on the first method but it was not
found to be satisfactory. A wide range of silver
solders with heating both by flame and radio frequency
induction methods were attempted but the seal could
not be guaranteed vacuum-tight, although good mechanically,
partly due to the lead content of some of these solders
forming porous alloys with platinum at the high temp-
eratures used. Also the very potent fluxes required
attacked the platinum which limited drastically
the number of times the process can be performed,
and consequently each time the properties of the
vessel alter slightly.

It was found that an excellent joint could be
obtained between platinum surfaces using a soft
solder (Grade K, m.p. 185°C., Sn 60% Pb 40%) provided
that a powerful flux was used (Baker's fluid). This
technique contradicts the popular notion that platinum
cannot be soft-soldered successfully. Use of this
method meant that when the bulk of the calorimeter
vessel was heated the filling tube of the vessel
had to be cooled whilst the whole calorimeter was
in an inert atmosphere. The apparatus and procedure

for this is described in the next section.

5.4.3.   The Hot-box Assembly.

For runs with zeolites, the calorimeter vessel
had to be heated to a known temperature ($300^{o}C$)
in an inert atmosphere whilst its top part is kept
below $100-150^{o}C$. and the silver tube is connected
to the galassline described earlier (Sec.4.2.).
It had to be possible to seal the silver tube when
required and also to cool the vessel to $77^{o}K$ when
dosing with methane (Sec.5.4.4.). The apparatus
is shown in Fig.5.16. The perspex hot-box ($12^{"}$ X
12" X 8") had an opening in one side (9" X 6");
this could be sealed by a greased rubber gasket
which was compressed around the opening by a large
perspex plate. Various small holes in the box allowed
air-tight connections to be made for the following:
   1) two electrical connections for the heating element,
   2) two pipes for water for the vessel top cooler,
   3) a tube through which passed nitrogen,
   4) a length of copper tubing ($3/16^{"}$ O.D.) through
which passed the silver tubing from the vessel.
Various thermocouple wires passed between the rubber
gasket and its perspex mating surface.

The calorimeter vessel was prepared for heating
as follows. The copper leads from the vessel heater
and the calorimeter thermocouple were unsoldered
and preserved. The long silver tube was passed
through a tube in the cooling tank and the copper tube
in the top of the box. The vessel sealing plate was
then pressed against the tank using the brass holder,
the insert (Fig.5.16.) shows the arrangement at the

Fig. 5.16.   The Hot Box Assembly
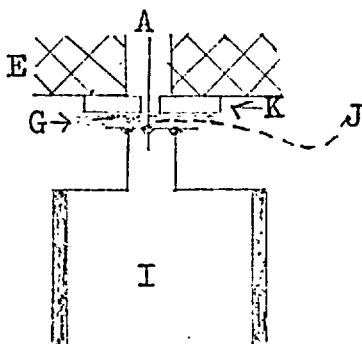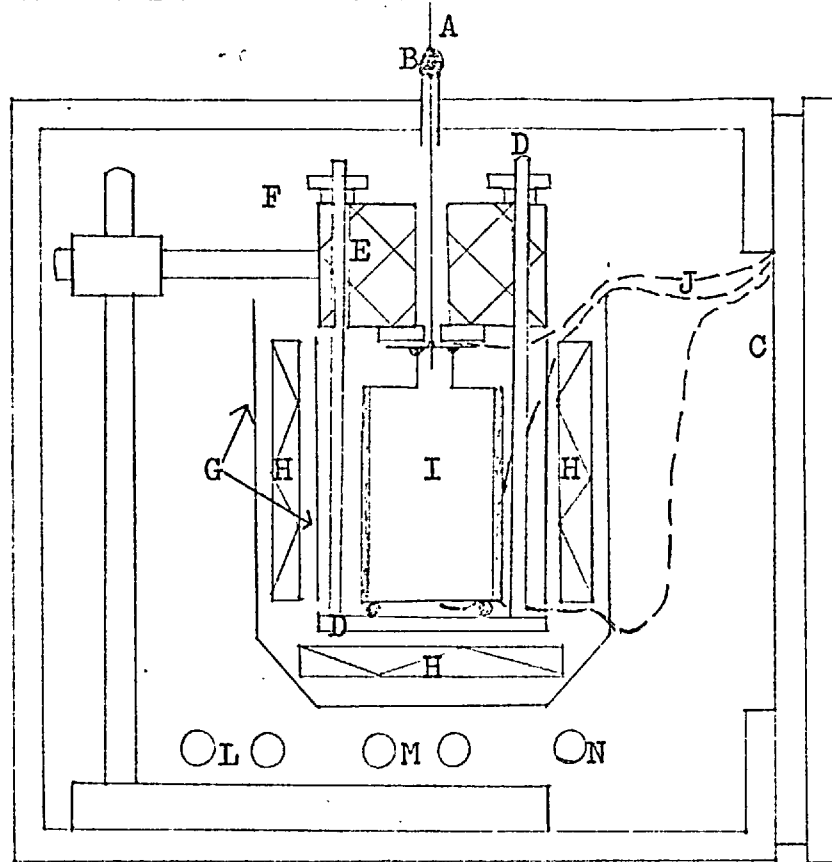
Method of ensuring
efficient heat
transfer from
vessel top seal

A   Silver tube (to tap 8, Fig.4.1)
B   Picein wax to copper tube
C   Greased rubber gasket
D   Calorimeter vessel clamp
E   Water heat exchanger
F   Nuts above rubber washers
G   Aluminium foil
H   Heating tape
I   Calorimeter vessel
J   Thermocouples
K   Machined copper washer brazed
     to cooling tank
L   Airtight terminals for H
M   Water connections for E
N   Inlet nitrogen tube
L, M, and N are sealed in backplate

plate. Folded aluminium foil kept the bottom of the
holder, which tended to tarnish at 300°C., from the base
of the vessel; foil was also wrapped around the wires
of the monitoring thermocouples (Cu-Cn) for the
same reason. An "Electrothermal" heating tape was
wrapped tightly around the holder, and this was
finally covered with aluminium foil. The box was
then sealed; picein wax sealed the opening between
the silver and copper tubes. All the leads from the
box were brought together, where the opening of a
large polythene bag which enclosed the box was closed
as tightly as possible. Whenever the vessel temperature
was above 150°C., nitrogen was passed into the box.
That which escaped from the box filled the bag before
escaping to the atmosphere. The heating tape was
supplied from a vari-ac, and the rate of water flow
through the tank was regulated to keep the platinum
plate at about 100°C. The thermocouples around the
vessel indicated that the temperature was reasonably
uniform although the top was cooled.

5.4.4. Zeolite Dehydrating and Dosing.

In the heat capacity runs with a zeolite sample,
whether it contained a sorbed gas or not, all the
water which the sorbent holds so tenaciously must be
removed before the vessel is dosed or sealed. Once
the zeolite was in the vessel the platinum top plate
was attached and not removed again for the subsequent
runs. Instead it was necessary to cut and to remove
the little silver tube used in the preceding run and
to install a new length (at least 20cm.) of new tube.
A small soldering iron was used with Baker's fluid
flux but only the very minimum of new solder was used.

Since platinum is a poor conductor the solder at the centre of the plate could easily be melted without disturbing the joint at its edge. This process ensured that very nearly the same amount of solder was used in all the zeolite runs.

The vessel with long silver tube was fitted in the hot-box as described previously. The silver tube was joined (picein wax) to a glassline (Fig.4.1.), and the vessel evacuated. When the pressure was below 1.10^{-3}mm.Hg., the temperature of the vessel was raised over 24 hours to 300°C. Some zeolite hydrolysis would occur if the bulk of the sorbed water was not removed at near room temperature. Pumping was then continued until a pressure approaching 1.10^{-6}mm.Hg. was attained, after which the heating was discontinued and the hot-box opened. For the empty zeolite run (i.e. no methane added) the precedure was to add helium and seal the silver tube as described for the benzoic acid run (Sec.5.4.2.). Otherwise the vessel was then cooled by placing it in a metal can surrounded by liquid nitrogen. A small polythene bag immediately surrounded the vessel into which was passed nitrogen which came through a heat exchanger dipped in liquid nitrogen; this prevented water saturating the calorimeter heater which would cause the pump-down time of the outer can to be excessive. The temperature of the vessel, monitored by a thermocouple, was about 85°K during the following operations; this was to ensure that all the methane added to the vessel would be sorbed.

Somewhat more than the calculated dose was measured in the known calorimeter dosing volume (Fig.4.1.). This dose was then opened to the calorimeter vessel until the manometer indicated that sufficient methane had been sorbed. Tap 8 was then closed and the amount of the original dose not transferred to the calorimeter vessel determined. The amount sorbed could then be calculated. Time was allowed for all the methane to be sorbed, during which a dose of helium at about 6cm.Hg, was trapped between Taps 7 and 8. Thus on opening Tap 8 helium was admitted to the vessel without the loss of any methane. Since the vessel must be maintained at a low temperature whilst being sealed, this was completed in two stages. Initially the silver tube was sealed outside the box by pinching, cutting and immediately soldering it. The vessel with about 15cm. of silver tubing was removed from the box, and, whilst still being cooled and kept dry, the tube was sealed as described above about 5mm. from the platinum plate.

5.5. The Determination of Heat Capacities.

5.5.1. Assembly of Apparatus.

The calorimeter vessel must first be prepared.
After the silver tube has been sealed (Sec.5.4.2. or
Sec.5.4.4.) the external wires are soldered into
position, that is if they had been previously removed
to allow the vessel to be heated. These wires are
the Cu-Cn thermocouple junction to the soldered
joint in the radiation shield and the heater wires.
The three latter wires are joined as described in
Section 5.2.2. Lastly the thermometer is placed
in its tube with a little grease (Apeizon T).
A record is kept through all the above processes
of the weight of the calorimeter and its components,
so for each run the quantity of Apeizon T grease,
silver, solder, and sample are known. When the
concern is in the heat capacity difference between
two separate runs a correction in the observed
difference can be applied for different amounts of
grease, silver, and solder present.

The vessel is hung vertically to the top shield
and the side shield fitted, guarding that the same
relative orientation is always used for these three
units. The same precaution is taken with the bottom
shield which can be attached once all the electrical
connections between the vessel and side shield have
been soldered and checked. These wires lead to the
top of the side shield where they are soldered to
wires hanging from the heat exchanger, as are the
wires from the shield heaters. The circuits are then
completed as far as the tagboard where the connections

are made to the control room. After a series of
obvious insulation and continuity tests, the outer
can is affixed (Sn - In eutectic solder) using zinc
chloride flux. A water jacket around the can prevents
unreasonable heating of its contents. The system is
evacuated continuously until the ensuing pressure is of
the order of 1.10^{-5} mm Hg. or better.

5.5.2.   The Actual Measurements;

Basically to find heat capacities, the temperature
rise of the calorimeter vessel assembly caused by the
input of a known amount of heat is measured.
Difficulties arise in the measurement of the initial
and final temperatures due to incessant heat leaks to
and from the vessel; that is perfect adiabaticity of the
vessel can rarely be achieved. Further to this the
current through the thermometer will always tend to
heat the vessel, this becoming much more pronounced at
higher temperatures. The practice therefore is to
measure the drift in the temperature of the vessel both
before and after the heat input which, by extrapolation
of each drift to the mid-point of the heating period,
gives the required temperature rise. For these extra-
polations to be valid, the heat leak must be held
constant, which is the purpose of the shield control
(Sec.5.3), and preferably small.

Once the vacuum in the outer can is satisfactory
and the batteries, especially that for the thermometer,
have been on circuit for several days so as to give
steady currents, the outer can is placed in coolant.
The calorimeter vessel is brought to the required
temperature either by dosing helium into the outer
can or by just relying on radiative and conductive

cooling. The latter method, which is very time
consuming, is only used when zeolite-methane samples
are under study (see Ch.8). The first method is
always used when the coolant is solid nitrogen or
hydrogen.

When the system has thermally equilibrated
and the shield control is satisfactory, the first
'fore' drift can be commenced. The thermometer
current and potential are each determined with the
current passing in both directions, a drift consists
of this set of four readings being taken five or six
times. With each reading the time to within five
seconds is recorded. Heat is then supplied to the
calorimeter vessel, the exact amount of which is
estimated by measuring not only the period of heating
but also alternately during this period the heater
potential and current, each recorded with the time
to within five seconds.

Excluding the points at hydrogen temperatures
(below $25^{\circ}K$) the heating rate is chosen to give a
heating period of greater than about ten minutes
but such that the shield control can cope adequately
with the increased demand in the heater currents.
The resultant temperature rise is chosen such that
the heat capacity can be assumed to vary linearly
in the region, making curvature corrections negligible.
This was about $1^{\circ}C$ at $15^{\circ}K$ rising to $7^{\circ}C$ at $300^{\circ}K$.
Time is allowed after the heating period for the
system to become thermally equilibrated again before
the 'after' drift is measured in a like manner to
the fore drift. This drift can then serve as the fore
drift for the next point.

5.5.3.   Calculation of Heat Capacities.

A computer programme was written to calculate the gross heat capacity in absolute Joules $^\circ C^{-1}$. The elements of the calculation are as follows.

Calorimeter Vessel Temperature

For each drift (Sec.5.5.2) the variations in the thermometer potential and current were fitted by the method of least squares to straight lines. Extrapolation gave the values at the mid-point of the heating period, the ratio of these gave the thermometer resistance in terms of the standard resistance. Above $90^\circ K$, the corresponding temperature was ascertained by an iterative procedure using the equation given earlier (Sec.5.2.3.), otherwise the temperature was linearly interpolated from a table of 360 temperature: resistance pairs.

Energy Input.

The rate of energy input to the calorimeter vessel is given by (Sec.5.2.2., and Fig.5.3.).

$$E = V_H i_1 + i_2^2 r$$

where r is the resistance of the leads like ab, cd, ce. Also

$$i_1 = i - i_2 = \frac{V_i}{R_s} - \frac{V_v}{R_v} .$$

The current, i_2, in the circuit aec (see Fig.5.3.) gives potential differences related by the following equation:

$$i_2 = \frac{V_v}{R_v} = \frac{V_H}{(R_p + R_1 + r)}$$

or

$$V_H = \frac{V_v}{R_v}(R_p + R_1 + r)$$

where R_1 is the resistance of the copper leads between the shield and the measurements room.

So

$$E = V_v\left(\frac{R_p}{R_v^2} + \frac{r+R_1}{R_v}\right)\left(\frac{V_i}{R_s} - \frac{V_v}{R_v}\right) + i_2 r .$$

Since R_p, R_1, r are 10000, 4, 0.1 ohms respectively, and i_2 is about $4\% i_1$, it is clear that the second term is insignificant compared with the first and the equation can be simplified to

$$E = V_v\left(\frac{R_p}{R_v^2} + \frac{R_1}{R_v}\right)\left(\frac{V_i}{R_s} - \frac{V_v}{R_v}\right) .$$

This is the instantaneous rate of heating. The integral of this with respect to time over the whole heating period gives the total heat input. V_v and V_i change throughout the heating period due to the temperature dependence of the heater resistance and battery decay. From the values recorded of these two potentials, the above integral is computed numerically.

Conclusion.

The resultant heat capacities were plotted on large scale graphs and a smooth curve drawn. In the temperature range 25-250°K, this particular apparatus gave very acceptable results (see details later) which were generally within ±0.1% of the smooth curve. At higher temperatures the points deviated rather more from the smooth curve due to the increasing significance of radiative transfer (Stefan's fourth power law) which leads to excessive heat leaks for

a given temperature difference. These large heat leaks existed between the calorimeter and shields even though the shield control was good. This was due to two causes; firstly any small residual e.m.fs. in the differential thermocouples would cause non-zero temperature differences to be maintained between the shields and the vessel. Secondly, but of most consequence, the shields and vessel develope non-isothermal surfaces. The large cooling drifts showed that these were mainly on the shields because the vessel would only have large surface temperature gradients during the heating periods. The low thermal conductivity of metals at these temperatures, compared with that at liquid hydrogen temperatures, aggrevates this problem. especially as a large amount of heat has to be delivered to the shields constantly. Shields of low heat capacity would decrease the heat needed to control them and so the tendency to create non-isothermal surfaces, but this would have to be balanced with the other purpose of the side shield of equilibrating the leads to the calorimeter vessel. It is noteworthy that calorimeters designed specifically to work at high temperatures have extra shields around the adiabatic shield, but maintained just a little colder, in order to reduce the heat sink to a much lower value than in this calorimeter. Additionally the leads from the heat exchanger could be heated to avoid conduction along the wires to the shields, as in the 'floating ring' arrangement used by (Stull 1957)

At temperatures below $25^{\circ}K$, the problem was large and uncontrollable heating drifts, due to heat descending the wires to the shields. At these low

temperatures the thermal conductivity of metals is
very large. The heat exchanger (Fig.5.1.) should
have brought all the incoming leads to solid hydrogen
temperatures, but this was inefficient because
excessive varnish, of poor thermal conductivity,
was used to guard against electrical shorts.
If this was remedied the apparatus should work well
in this temperature range as the mass of the outer
can and its contents is relatively small and excess
para-hydrogen can be placed around it. Of course at
these temperatures there are natural limitations
in the precision which can be achieved due to the much
decreased thermometer sensitivity and the small value
of the heat capacities.

CHAPTER 6

HEAT CAPACITY OF THE EMPTY CALOR-IMETER VESSEL AND THE ACCURACY OF THE SYSTEM.

6.1. The Empty Calorimeter Vessel.

The heat capacity of the empty calorimeter vessel was found between 16° and $304^{\circ}K$. The vessel had first been heated at $300^{\circ}C$ in a nitrogen atmosphere until its weight was constant, and then it was sealed containing helium at a few centimetres of mercury pressure. The actual results are given in Table 6.1. The rise in temperature for each point was chosen so as to make corrections for curvature very small. A large scale graph of the values was plotted and a smooth curve drawn, from which were obtained the heat capacity at one degree intervals between 16° and $304^{\circ}K$. These values are suitable for linear interpolation and are given in Table 6.2. The deviation of the experimental data from the smooth curve was calculated (Fig.6.1). The points are generally within .1% of the smooth curve, the results are discussed later.

6.2. The Heat Capacity of a Standard Substance.

The absolute precision of the system was determined by measuring the heat capacity over the working range of the calorimeter of a standard substance. The heat capacity of thermochemical standard benzoic acid was measured; this had

Fig. 6.1. Deviations of the Experimental heat capacity from Smoothed Values for the Empty Calorimeter Vessel
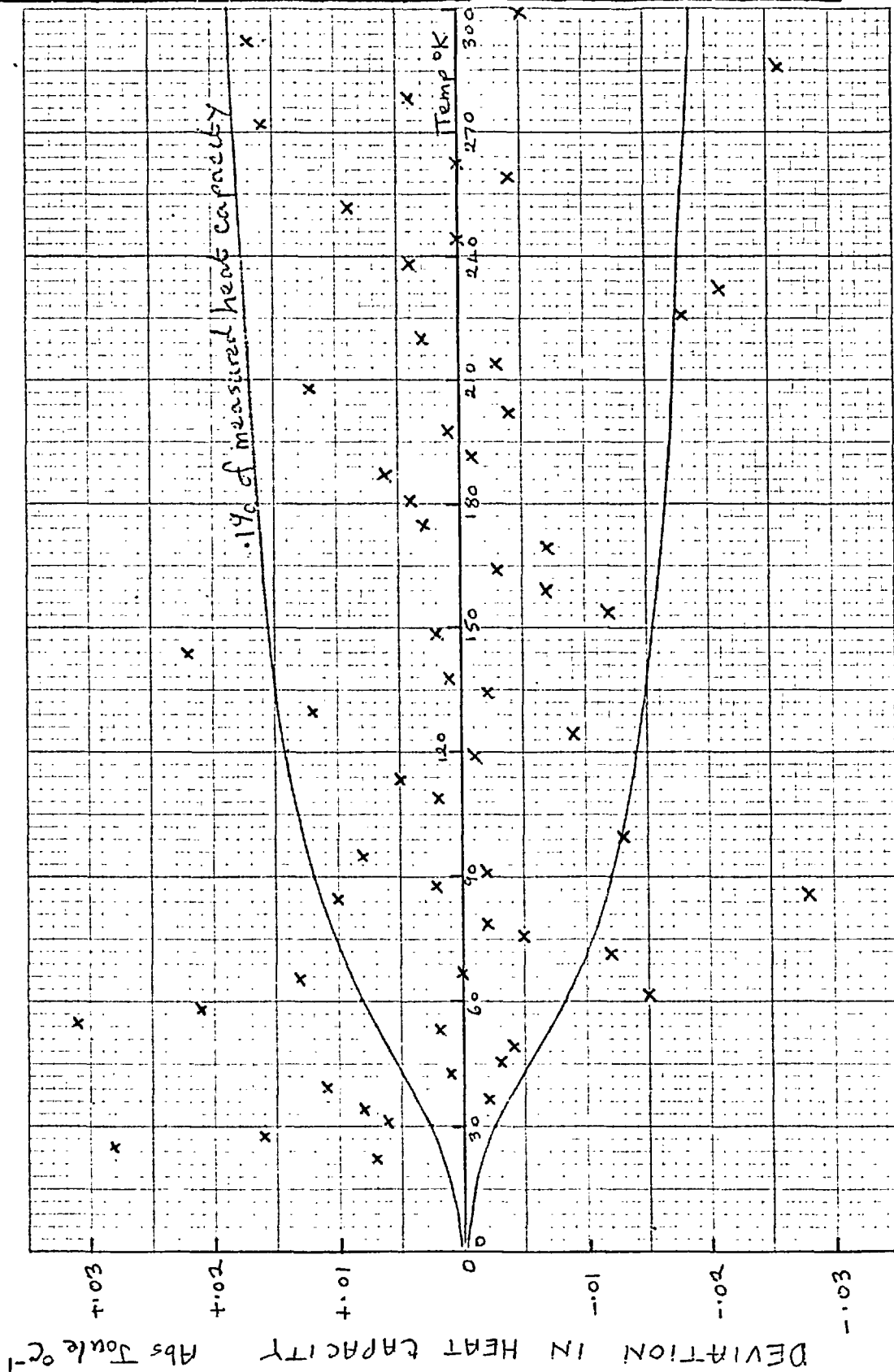
previously been determined by other workers in the laboratory, and also elsewhere (Furukawa et al. 1951, Osborne et al. 1955, Cole et al 1960, Busey ~~et al.~~ 1956). The deviation of previous results from those obtained at the National Bureau of Standards (Washington) is shown (Fig.6.2) and for the present results (Fig.6.3). The actual results are presented in Table 6.3. The contribution from the benzoic acid to the bulk heat capacity was 77% at $21^{\circ}K$, 60% at $91^{\circ}K$, and 70% at $290^{\circ}K$.

The three heat capacity calorimetry standards used are benzoic acid, α-aluminium oxide, and n-heptane (Ginnings and Furukawa 1953). Since zeolites are closely related to alumina, it could be argued that this would have been a better standard to have used. This is relevant because the heat exchange during calorimeter vessel heating could depend on vessel filling and the nature of the sample, indeed some vessels are specifically designed to minimize these effects by using a vessel with several skins so that the sample is not in direct contact with the outer radiating surface (West and Ginnings 1957). However for the precision required here, a sample of benzoic acid was used.

α-Alumina has a very high Debye temperature, like most hard crystalline solids. Thus its heat capacity below $100^{\circ}K$ is much lower than benzoic acid both on a weight and volume basis. From this point of view, it would therefore be a poor standard to use when testing a calorimeter system at these temperatures. It is, of course, an excellent standard at very high temperatures (above $400^{\circ}K$) because of

Fig. 6.2. Deviation of the Heat Capacity of Benzoic Acid Previously Reported and the N.B.S. Values

N.B.S values taken from
Furukawa et al.(1951)
    □ Busey(1956)
    + Cole et al.(1960)
    ○ Pemberton(1966) } this
    • Cope(1967)   } laboratory

PERCENTAGE DEVIATION
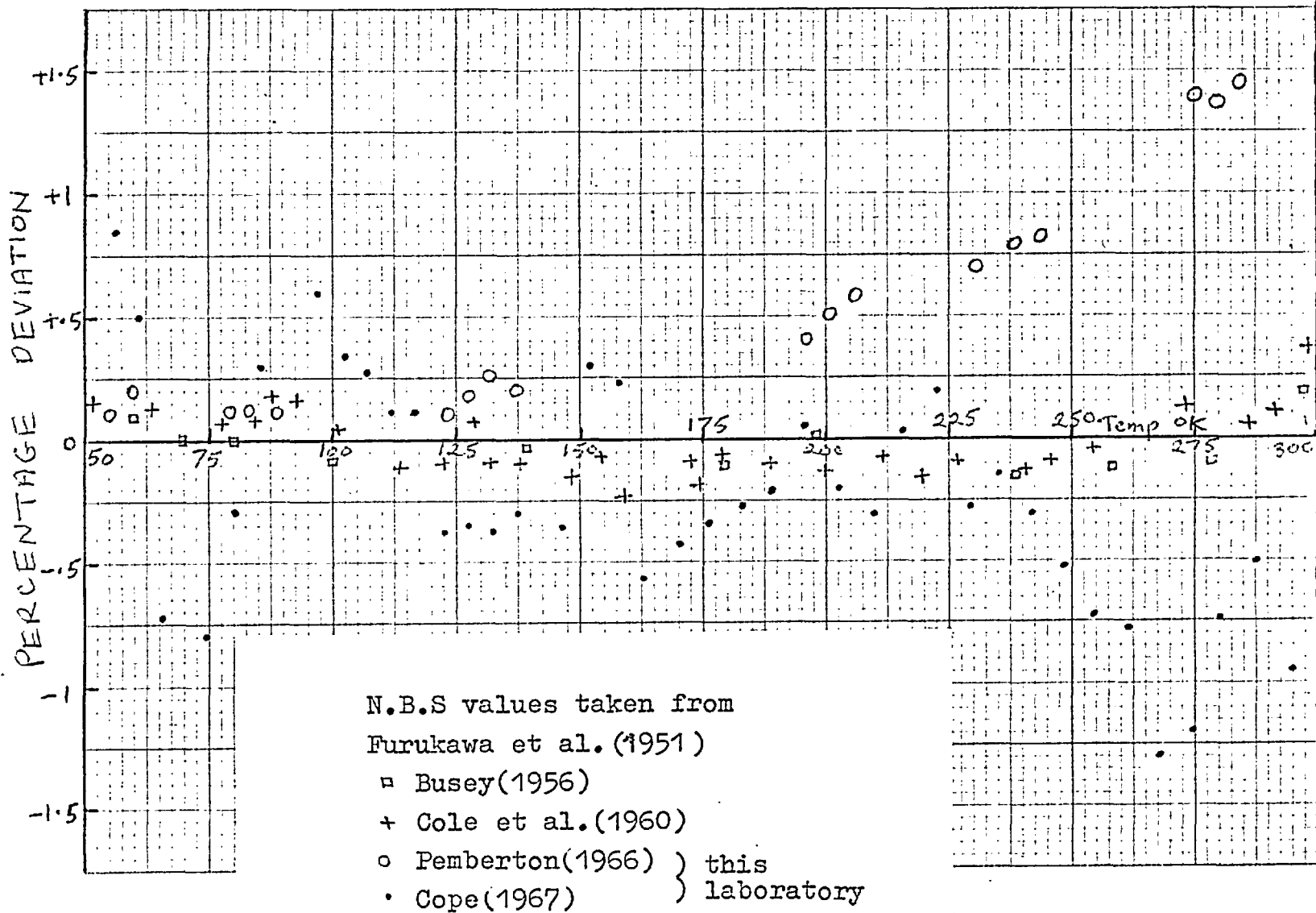
Fig. 6.3. Deviation of the Heat Capacity of
Benzoic Acid Reported Here and the N.B.S. Values
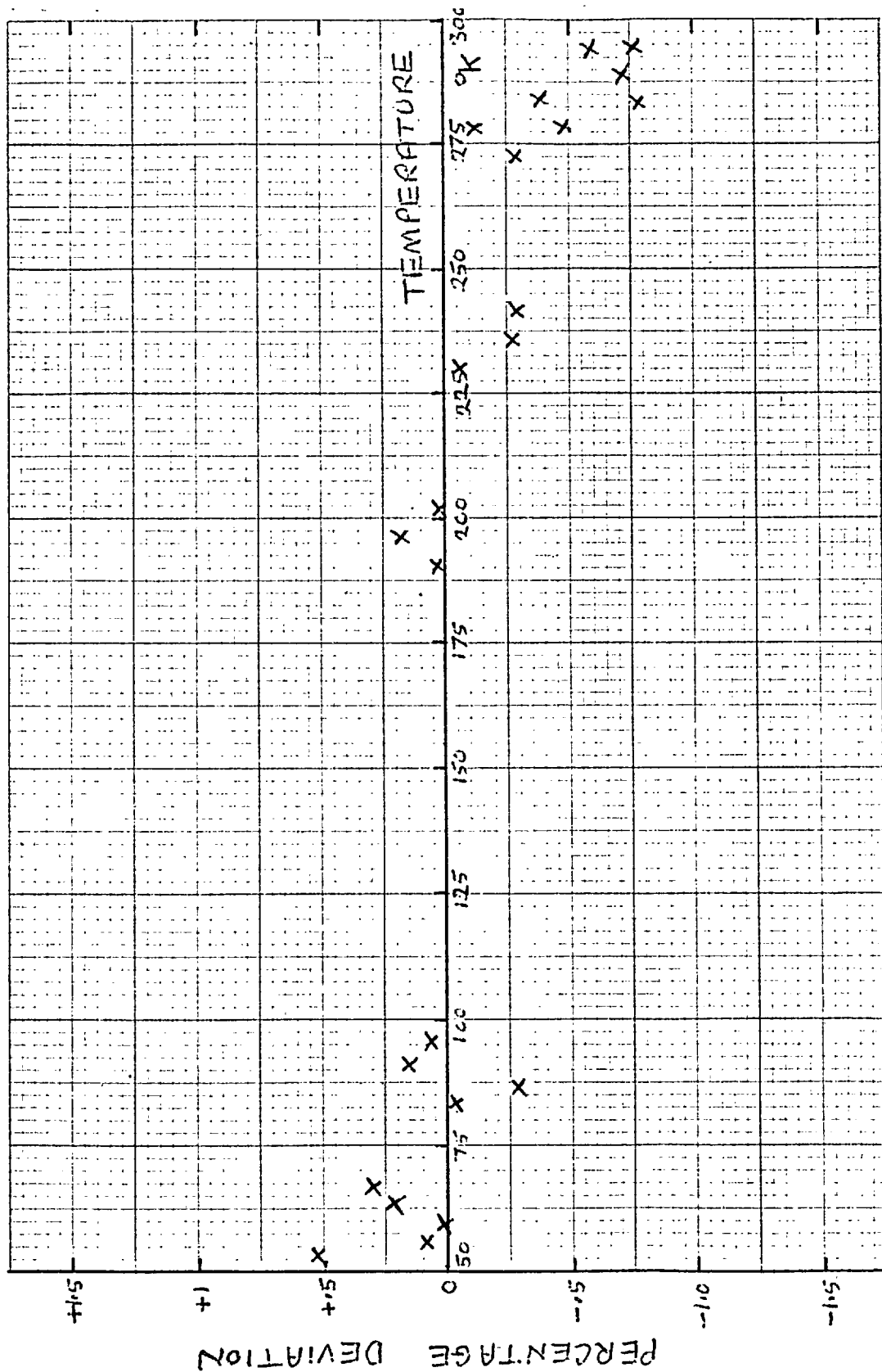
its high thermal stability.

6.3.   The Accuracy of the Calorimeter.

There are many factors which govern the ultimate
accuracy of heat capacity measurements.   The errors
result from imperfections in the calorimeter design,
the measuring circuits, the shield control and the
method of calculating the results.   These are some-
what interdependent, but for the accuracy required
here it is thought that the last two factors are
relatively unimportant, especially when automatic
shield control is in operation.   This is not to say
that the control is perfect, but that the errors due
to temperature differences at the commencement and
completion of vessel heating and otherwise are small,
and anyway cancel one another within experimental
error.   The errors arising from the system's design
have been discussed elsewhere (Sec.5.5.3).   In the
main they cause non-adiabaticity of the vessel and
are serious at the ends of the working range of the
system;   the effect of such heat exchange has been dis-
cussed in detail by West (1963).   This leaves errors
due to the measuring circuits, which have in the
past been generally overlooked.

The measurements made for each point include
the amount of heat input and the temperature drift
both before and after this input.   The first is based
on an average of several products of two measured
potentials and also a time period, all determined
to 1 in 10^5.   Thus, assuming that the potentiometer
is reasonably accurately standardized, the error
in finding the heat input should be far less than

1 in 10^4, that is .1%.

The error in measuring the drift is rather
more critical. Given that the values of the various
standard resistances are known accurately (say, to
±.01%), and that the drifts are in fact linear, then
the final error is due to the inprecision in measuring
the drift. The effect of this on the final heat
capacity can be readily calculated. Take, for example,
a heat capacity measurement at a temperature (T)
around 130^oK, where the drifts are effectively
zero and the thermometer resistance is about 10 ohms.
The current through the thermometer (I) is about
3mA producing a potential difference across it (V)
of about 30mV. Since V and I can be measured to
1.10^{-7}volts and 1.10^{-8}amps respectively and the drifts
in V and I are taken over 10 minutes, it follows
that if the true drift in each is zero, the measured
drift could be as large as 2.10^{-8}volt/min and 2.10^{-9}
amp/min respectively. As the thermometer sensitivity
is about 10^oC/ohm, the following relationships can
be formulated:

$$R \text{ (ohms)} = \frac{V \text{ (volt)}}{I \text{ (amp)}} \quad , \qquad \frac{dT}{dR} = 10^o\text{C/ohm} \quad ,$$

$$\frac{dV}{dt} = 2.10^{-8}\text{volt/min} \quad , \qquad \frac{dI}{dt} = 2.10^{-9} \text{ amp/min} \quad .$$

$$\frac{dT}{dt} = 10\, \frac{dR}{dt} = 10\, \frac{\left| I\, \frac{dV}{dt} \right| + \left| V\, \frac{dI}{dt} \right|}{I^2}$$

$$= 1.33.\ 10^{-4}\ ^o\text{C/min.}$$

Since the time required for a complete set of
measurements (fore drift, heating, after drift)

is about one hour, the uncertainty in the temperature
rise is about 8×10^{-3} °C. The fractional error
introduced into the total temperature rise of about
5°C is about .16%. Presumably much the same error
will exist if the actual drifts are non-zero.
An added factor here is that the difference between
the potentials measured with the current flowing
in each direction is seldom constant, and this effect
can lead also to apparent drifts of about the same
order as those above. It can be seen therefore that
the bulk heat capacity will have an error of at least
±.1 - .2%. This will be proportionately larger
for those runs which take much longer (see Chapter 8)
due to slow thermal equilibration.

Although heat exchange between the vessel and
the shields is allowed for by taking drifts, if these
are large it is usually found that the scatter of
the points from a smooth curve is large also. This
is due to errors arising in measuring the drifts,
and in their non-linearity. Some workers alter the
shield control to reduce the drift to measurable
proportions by maintaining a seemingly constant
temperature difference between vessel and shields.
This does not of course improve the non-linearity
of the drifts. Since the size of the drifts vary
from one sample in the vessel to another, this may
be good practice since it would make the results
more readily comparable. It is a means of allowing
for changes in the residual e.m.fs. in the differential
thermocouples which undoubtedly occur each time
the joints in their circuits are resoldered.
During experiments with a zeolite sample, the vessel
has to be heated to 300°C before each set of

measurements. Despite the precautions taken (Sec. 5.4.4.) there was slight tarnishing of the outer surface of the vessel during this process which must have altered its emissive power. The errors resulting from this could be minimized by reducing the heat transfer in the way suggested above.

In fact, for all the measurements taken the temperature difference between the vessel and the shields was kept to zero, and large negative drifts were obtained when the vessel was near room temperature. The size of typical drifts is shown in Table 6.4.

The root mean squared percentage deviation of the points for the empty calorimeter was .3 (25 - 70°K) improving to .09 (70 - 300°K). Below 25°K, it was difficult to draw the smooth curve; the points were probably in error by up to 10%. For benzoic acid, the results deviate from those given by the National Bureau of Standards generally by no more than .3% between 35 - 250°K, but are progressively lower by up to .8% between 250 - 300°K. Since other workers have reported discrepancies of similar size and in view of the magnitude of errors which can arise in heat capacity calorimetry, the performance of the current system is thought to be acceptable.

TABLE 6.1. - EXPERIMENTAL VALUES OF THE EMPTY
             CALORIMETER HEAT CAPACITY in Abs.
             Joules Deg^{-1}.

$0^{o}C$ = $273.15^{o}K.$

Run No.	Temp.^{o}K	ΔT	Cp.
1	86.30	4.125	11.611
2	90.60	4.458	12.043
3	94.99	4.327	12.435
4	99.50	4.673	12.770
5	104.10	4.531	13.185
6	108.59	4.436	13.467
7	113.71	5.792	13.824
8	119.30	5.362	14.165
9	124.47	4.980	14.440
10	129.41	4.883	14.717
11	134.27	4.833	14.939
12	137.68	5.497	15.099
13	143.13	5.399	— 15.356
14	148.50	5.328	15.553
15	153.78	5.259	15.741
16	159.00	5.194	15.925
17	164.17	5.135	16.093
18	169.27	5.085	16.243
19	174.61	5.591	16.406
20	180.42	6.042	16.559
21	186.27	5.674	16.699
22	191.90	5.625	16.825
23	197.48	5.580	16.952

TABLE 6.1. (continued)

Run No.	Temp.°K	ΔT	Cp.
24	201.91	5.715	17.045
25	207.58	5.664	17.171
26	213.20	5.619	17.289
27	219.35	6.746	17.422
28	225.85	6.331	17.522
29	232.11	6.285	17.630
30	238.30	6.224	17.762
31	244.63	6.556	17.875
32	251.45	7.226	18.004
33	258.60	7.181	18.107
34	265.67	7.129	18.226
35	271.60	7.059	18.337
36	278.52	7.013	18.433
37	285.40	6.980	18.504
38	292.30	7.091	18.645
39	299.23	7.062	18.711
p40	54.22	4.091	7.269
p41	58.21	3.739	7.938
p42	61.89	3.474	8.477
p43	65.58	3.819	9.043
h44	18.54	1.840	0.713
h45	20.19	2.053	0.851
h46	22.49	2.828	1.236
h47	24.97	2.184	1.602
h48	27.85	3.533	2.062
h49	30.99	2.777	2.624
h50	33.78	2.759	3.167
h51	36.31	2.377	3.677

TABLE 6.1. (continued)

Run No.	Temp.°K	ΔT	C_p.
h52	39.03	3.090	4.238
h53	42.11	3.002	4.853
h54	45.68	4.146	5.570
h55	49.58	3.635	6.351
h56	53.19	3.600	7.058
p57	67.01	4.731	9.233
p58	71.46	4.145	9.834
p59	75.48	3.902	10.386
p60	79.30	3.718	10.875
p61	84.30	3.482	11.445
p62	87.85	3.592	11.791

In this and all subsequent tables of heat capacities, the refrigerant used is denoted as follows:

 no letter preceding run number = liquid nitrogen

 p before run number = solid nitrogen

 h before run number = para-hydrogen (pumped)

The letter t denotes that the point is a 'transition point' where the temperature rise is reduced below the normal value used at that temperature.

TABLE 6.2. – SMOOTHED VALUES OF THE HEAT CAPACITY
OF THE EMPTY CALORIMETER VESSEL FROM
16 TO 304°K in abs J. $°C^{-1}$.

$0°C = 273.15°K$.

Temp.°K	Cp.	Temp.°K	Cp.	Temp.°K	Cp.
16	0.544	41	4.624	66	9.089
17	0.624	42	4.830	67	9.232
18	0.714	43	5.031	68	9.369
19	0.814	44	5.232	69	9.510
20	0.916	45	5.435	70	9.647
21	1.038	46	5.638	71	9.783
22	1.165	47	5.839	72	9.920
23	1.296	48	6.040	73	10.055
24	1.433	49	6.240	74	10.192
25	1.578	50	6.438	75	10.327
26	1.732	51	6.631	76	10.460
27	1.900	52	6.830	77	10.595
28	2.072	53	7.023	78	10.722
29	2.249	54	7.198	79	10.842
30	2.431	55	7.382	80	10.960
31	2.620	56	7.551	81	11.074
32	2.811	57	7.720	82	11.190
33	3.009	58	7.883	83	11.299
34	3.201	59	8.046	84	11.404
35	3.412	60	8.203	85	11.507
36	3.616	61	8.356	86	11.609
37	3.819	62	8.509	87	11.710
38	4.020	63	8.656	88	11.803
39	4.221	64	8.802	89	11.896
40	4.422	65	8.948	90	11.990

TABLE.6.2. (continued)

Temp.$^\circ$K	Cp.	Temp.$^\circ$K	Cp.	Temp.$^\circ$K	Cp.
91	12.082	120	14.203	149	15.570
92	12.171	121	14.261	150	15.609
93	12.359	122	14.317	151	15.648
94	12.342	123	14.372	152	15.686
95	12.428	124	14.424	153	15.723
96	12.511	125	14.478	154	15.761
97	12.591	126	14.531	155	15.796
98	12.670	127	14.582	156	15.830
99	12.746	128	14.634	157	15.865
100	12.819	129	14.684	158	15.900
101	12.896	130	14.734	159	15.932
102	12.972	131	14.784	160	15.964
103	13.048	132	14.833	161	15.997
104	13.122	133	14.882	162	16.029
105	13.198	134	14.929	163	16.060
106	13.271	135	14.974	164	16.091
107	13.347	136	15.022	165	16.122
108	13.421	137	15.067	166	16.153
109	13.495	138	15.113	167	16.184
110	13.564	139	15.158	168	16.213
111	13.633	140	15.201	169	16.242
112	13.704	141	15.244	170	16.271
113	13.772	142	15.288	171	16.300
114	13.838	143	15.329	172	16.329
115	13.903	144	15.371	173	16.358
116	13.967	145	15.411	174	16.385
117	14.031	146	15.452	175	16.414
118	14.092	147	15.492	176	16.442
119	14.150	148	15.531	177	16.469

TABLE 6.2. (continued)

Temp. °K	Cp.	Temp. °K	Cp.	Temp. °K	Cp.
178	16.496	206	17.138	234	17.683
179	16.521	207	17.159	235	17.701
180	16.545	208	17.180	236	17.718
181	16.568	209	17.201	237	17.735
182	16.591	210	17.222	238	17.752
183	16.616	211	17.244	239	17.771
184	16.639	212	17.266	240	17.791
185	16.663	213	17.288	241	17.809
186	16.687	214	17.309	242	17.828
187	16.711	215	17.329	243	17.847
188	16.734	216	17.350	244	17.864
189	16.758	217	17.371	245	17.882
190	16.781	218	17.391	246	17.900
191	16.803	219	17.412	247	17.918
192	16.828	220	17.431	248	17.934
193	16.850	221	17.450	249	17.952
194	16.873	222	17.469	250	17.970
195	16.896	223	17.489	251	17.987
196	16.919	224	17.507	252	18.004
197	16.940	225	17.526	253	18.021
198	16.962	226	17.543	254	18.037
199	16.984	227	17.561	255	18.053
200	17.008	228	17.579	256	18.070
201	17.029	229	17.598	257	18.086
202	17.051	230	17.614	258	18.101
203	17.073	231	17.631	259	18.118
204	17.095	232	17.649	260	18.134
205	17.117	233	17.667	261	18.151

TABLE 6.2. (continued)

Temp. °K	Cp.	Temp. °K	Cp.	Temp. °K	Cp.
262	18.167	277	18.406	291	18.610
263	18.183	278	18.421	292	18.624
264	18.199	279	18.436	293	18.638
265	18.216	280	18.451	294	18.650
266	18.231	281	18.466	295	18.663
267	18.248	282	18.481	296	18.676
268	18.264	283	18.496	297	18.689
269	18.279	284	18.510	298	18.701
270	18.297	285	18.524	299	18.713
271	18.311	286	18.539	300	18.727
272	18.328	287	18.554	301	18.739
273	18.343	288	18.568	302	18.752
274	18.259	289	18.582	303	18.764
275	18.374	290	18.596	304	18.776
276	18.391				

TABLE 6.3. — EXPERIMENTAL VALUES OF THE HEAT CAPACITY OF BENZOIC ACID.

Wt. of Benzoic Acid in calorimeter = 37.0074g. (in vacuo)
Molecular wt. of Benzoic Acid = 122.18.
No. of moles of Benzoic Acid in calorimeter = 0.30305
Heat Capacity, Cp, in Abs. Joules $°C^{-1}$.

Run No.	Temp.$°K$	ΔT	Cp.	Cp/mole
1	83.31	3.224	28.701	57.325
2	86.93	3.993	29.495	58.727
3	91.01	4.147	30.446	60.611
4	95.12	4.042	31.252	62.132
5	190.40	6.050	46.770	98.952
6	196.39	5.929	47.700	101.565
7	202.27	5.825	48.529	103.875
8	230.01	6.062	52.680	115.705
9	236.02	5.966	53.515	118.121
10	241.91	5.863	54.406	120.711
11	277.61	5.568	59.962	137.138
12	283.28	5.820	60.558	138.824
13	289.01	5.730	61.464	141.543
14	272.58	5.698	59.119	134.610
15	278.21	5.616	59.894	136.887
16	289.53	5.469	61.559	141.830
17	283.91	5.841	60.852	139.764
18	289.53	5.469	61.675	142.186
p19	52.56	3.467	19.484	41.406
p20	56.09	3.583	20.752	43.521
p21	59.74	3.688	22.013	45.716

TABLE 6.3. (continued)

Run No.	Temp.$^{\circ}$K	ΔT	Cp.	Cp/mole
p22	63.34	3.502	23.199	47.834
p23	66.92	3.624	24.307	49.794
h24	16.29	0.801	2.814	7.415
h25	17.77	1.078	3.585	9.543
h26	19.54	2.122	4.355	10.412
h27	21.62	2.047	4.941	12.622
h28	23.97	2.722	6.176	15.668
h29	27.54	4.396	7.871	19.400
h30	31.49	3.511	9.877	23.640
h31	35.22	3.951	11.709	27.233
h32	39.32	4.225	13.699	71.071
h33	43.83	4.784	15.740	34.793
h34	48.66	4.875	17.844	38.509

TABLE 6.4. TYPICAL DRIFTS AFTER THERMAL EQUILIBRATION.

Temperature	$^{\circ}$C.min^{-1} x 10^5
12	+1600
15	+3900
20	+110
30	+28
50	+5.4
100	+12
200	+4.2
250	−23
300	−100

CHAPTER 7

HEAT CAPACITY OF DEHYDRATED
ZEOLITE LINDE TYPE 5A

The heat capacity due to the sorbed phase in zeolites can be found as the difference between that of the sorption complex and the dehydrated 'empty' zeolite. It is clearly essential to prepare the sorbent in an exactly analoguous manner before each run so that its heat capacity is consistent throughout.

The calorimeter vessel was loaded with Linde molecular sieve type 5A from the laboratory's stock which is kept at constant humidity (Sec.4.3). The covering plate with silver tube was soldered onto the vessel and the zeolite outgassed as described in Section 5.4.4. After outgassing the vessel was cooled, helium added, and finally the silver tube was pinched sealed, cut and immediately its top was soldered over. The weight in vacuo of the dehydrated zeolite in the vessel was 23.4338g, the corresponding weight before outgassing was 29.7057g. This corresponds to a water content of 21.1% of the initial weight. The calorimeter system was assembled and heat capacities were determined in the range 20 - 304°K. The amount of non-sorbed helium was always sufficient to effect efficient heat transfer within the calorimeter vessel.

The root mean squared percentage deviation from the smoothed curve was calculated as .15 ($30-70^{\circ}$K) and .11 ($70-300^{\circ}$K). The heat capacity determinations below 30°K are in much doubt since they are higher than those for one of the sorption compexes. Values are given for the observed heat capacities (Table 7.1). From the smoothed curve the heat capacity of the vessel plus sorbent was found at 1°C intervals in the range 20 - 304°K; the values are suitable for linear interpolation and are given in Table 7.2. Since these synthetic dehydrated zeolites are non-stoichiometric as regards the aluminium to silicon ratio and the cations present, the heat capacities determined apply strictly only to our sample. Nevertheless, for general interest, the heat capacity per gram is given (Table 7.3) over the temperature range of the measurements.

TABLE 7.1. – EXPERIMENTAL VALUES OF THE HEAT CAPACITY
OF THE CALORIMETER VESSEL CONTAINING
DEHYDRATED LINDE 5A. in Abs. Joules $^{o}C^{-1}$.

Wt. of dehydrated zeolite = 23.4338g.
$0^{o}C = 273.15^{o}K$.

Run No.	Temp.^{o}K	ΔT	Cᴅ.
1	86.11	4.834	17.836
2	90.82	4.597	18.726
3	95.54	4.832	19.559
4	100.39	4.841	20.367
5	105.24	4.852	21.156
6	110.11	4.869	21.910
7	115.00	4.892	22.628
8	119.97	4.900	23.043
9	125.06	5.274	24.000
10	130.26	5.118	24.665
11	135.31	4.979	25.288
12	140.42	5.228	25.867
13	145.90	5.743	26.431
14	151.54	5.586	27.100
15	157.16	5.668	27.731
16	162.86	5.749	28.290
17	168.54	5.618	28.843
18	174.08	5.782	29.352
19	179.89	5.885	29.847
20	185.79	5.981	30.357
21	191.78	6.066	30.856
22	197.79	6.026	31.332

TABLE 7.1. (continued)

Run No.	Temp. °K	ΔT	Cp.
23	203.77	6.053	31.794
24	209.77	6.058	32.267
25	215.81	6.130	32.690
26	221.84	6.056	33.155
p27	51.60	5.718	9.788
p28	56.96	4.971	1.123
p29	61.86	4.742	1.249
p30	66.65	4.837	1.366
p31	71.39	4.620	1.474
p32	76.05	4.665	1.581
p33	80.87	4.928	1.681
h34	13.61	0.990	0.408
h35	16.46	0.653	1.007
h36	18.10	1.136	1.245
h37	19.73	2.186	1.227
h38	21.79	1.965	1.496
h39	23.60	1.979	1.884
h40	25.58	2.220	2.392
h41	28.24	3.097	3.060
h42	31.26	2.924	3.875
h43	34.94	4.357	4.946
h44	38.93	3.511	6.089
h45	43.37	5.313	7.385
h46	48.40	4.694	8.828
h47	53.26	4.984	10.221
48	221.46	8.977	33.119
49	231.09	10.392	33.756
50	240.65	8.895	34.404
51	249.38	8.745	34.990
52	257.98	8.625	35.494

TABLE 7.1. (continued)

Run No.	Temp. ^{o}K	$\triangle T$	Cp.
53	266.42	8.504	35.996
54	270.35	8.180	36.263
55	278.47	8.334	36.674
56	286.59	8.222	37.173
57	294.74	8.398	37.504
58	302.86	8.314	37.889
p59	53.46	5.558	10.298
p60	58.80	5.111	11.702
p61	63.82	4.904	12.979
p62	68.80	5.035	14.135
p63	73.89	5.148	15.290

TABLE 7.2. – SMOOTHED VALUES OF THE HEAT CAPACITY
OF THE CALORIMETER VESSEL PLUS DE-
HYDRATED LINDE MOLECULAR SIEVE 5A
FROM 20 TO 304°K in abs. J. $°C^{-1}$.

Weight of dehydrated zeolite is 23.4338g.
$0°C = 273.15°K$.

Temp.°K	Cp.	Temp.°K	Cp.	Temp.°K	Cp.
20	1.256	43	7.272	66	13.497
21	1.398	44	7.558	67	13.732
22	1.549	45	7.845	68	13.963
23	1.775	46	8.131	69	14.194
24	2.022	47	8.415	70	14.419
25	2.267	48	8.695	71	14.646
26	2.516	49	8.994	72	14.871
27	2.775	50	9.289	73	15.092
28	3.032	51	9.583	74	15.312
29	3.391	52	9.878	75	15.531
30	3.555	53	10.161	76	15.753
31	3.825	54	10.440	77	15.968
32	4.095	55	10.717	78	16.182
33	4.369	56	10.990	79	16.395
34	4.647	57	11.262	80	16.607
35	4.929	58	11.525	81	16.812
36	5.219	59	11.785	82	17.018
37	5.519	60	12.042	83	17.218
38	5.811	61	12.292	84	17.416
39	6.110	62	12.535	85	17.614
40	6.400	63	12.776	86	17.811
41	6.695	64	13.016	87	18.006
42	6.985	65	13.257	88	18.197

TABLE 7.2. (continued)

Temp.°K	Cp.	Temp.°K	Cp.	Temp.°K	Cp.
89	18.383	118	23.048	147	26.613
90	18.571	119	23.188	148	26.724
91	18.753	120	23.323	149	26.833
92	18.933	121	23.461	150	26.943
93	19.112	122	23.594	151	27.052
94	19.284	123	23.726	152	27.161
95	19.458	124	23.858	153	27.269
96	19.632	125	23.988	154	27.375
97	19.802	126	24.119	155	27.482
98	19.968	127	24.248	156	27.588
99	20.136	128	24.377	157	27.692
100	20.301	129	24.502	158	27.795
101	20.465	130	24.628	159	27.898
102	20.629	131	24.753	160	28.000
103	20.791	132	24.876	161	28.101
104	20.952	133	24.998	162	28.201
105	21.110	134	25.118	163	28.301
106	21.268	135	25.238	164	28.400
107	21.423	136	25.354	165	28.499
108	21.581	137	25.472	166	28.596
109	21.733	138	25.588	167	28.692
110	21.886	139	25.701	168	28.788
111	22.036	140	25.818	169	28.883
112	22.183	141	25.932	170	28.978
113	22.333	142	26.048	171	29.072
114	22.478	143	26.162	172	29.166
115	22.622	144	26.274	173	29.257
116	22.765	145	26.388	174	29.344
117	22.907	146	26.501	175	29.432

TABLE 7.2. (continued)

Temp.°K	Cp.	Temp.°K	Cp.	Temp.°K	Cp.
176	29.521	206	31.964	236	34.093
177	29.609	207	32.040	237	34.161
178	29.699	208	32.115	238	34.228
179	29.784	209	32.190	239	34.296
180	29.867	210	32.263	240	34.361
181	29.953	211	32.339	241	34.428
182	30.037	212	32.412	242	34.493
183	30.122	213	32.485	243	34.561
184	30.307	214	32.559	244	34.627
185	30.290	215	32.631	245	34.692
186	30.369	216	32.703	246	34.760
187	30.451	217	32.776	247	34.824
188	30.536	218	32.848	248	34.890
189	30.619	219	32.919	249	34.953
190	30.702	220	32.988	250	35.019
191	30.785	221	33.059	251	35.082
192	30.869	222	33.143	252	35.148
193	30.949	223	33.214	253	35.210
194	31.028	224	33.281	254	35.271
195	31.108	225	33.349	255	35.332
196	31.188	226	33.418	256	35.395
197	31.267	227	33.485	257	35.453
198	31.344	228	33.558	258	35.512
199	31.423	229	33.624	259	35.572
200	31.501	230	33.691	260	35.633
201	31.580	231	33.758	261	35.691
202	31.659	232	33.825	262	35.753
203	31.735	233	33.892	263	35.812
204	31.811	234	33.959	264	35.870
205	31.888	235	34.028	265	35.927

TABLE 7.2. (continued)

Temp. °K	Cp.	Temp. °K	Cp.	Temp. °K	Cp.
266	35.983	279	36.701	292	37.370
267	36.041	280	36.753	293	37.419
268	36.099	281	36.808	294	37.468
269	36.153	282	36.859	295	37.518
270	36.211	283	36.911	296	37.564
271	36.267	284	36.962	297	37.612
272	36.321	285	37.014	298	37.661
273	36.376	286	37.067	299	37.709
274	36.430	287	37.119	300	37.758
275	36.484	288	37.169	301	37.802
276	36.541	289	37.219	302	37.849
277	36.593	290	37.270	303	37.898
278	36.648	291	37.320	304	37.943

TABLE 7.3. — HEAT CAPACITY OF DEHYDRATED
ZEOLITE LINDE 5A.

The heat capacity is given in absolute joules
per degree Celsius per gram of dehydrated
Linde 5A, and applies only to the sample used
in this experiment.

Temp. $^{\circ}$K	Cp per gram
20	0.0145
30	0.0480
40	0.0844
50	0.1217
60	0.1638
70	0.2036
80	0.2410
90	0.2808
100	0.3193
120	0.3892
140	0.4531
160	0.5136
180	0.5685
200	0.6185
220	0.6639
240	0.7071
260	0.7467
280	0.7810
300	0.8121

CHAPTER 8

HEAT CAPACITY OF METHANE IN LINDE 5A

8.1.   Introduction.

The heat capacity of dehydrated Linde 5A con-
taining two different doses of methane was determined.
For each run the calorimeter was joined to the glass-
line, so that the sorbent could be outgassed and
dosed according to the procedure described previously
(Sec. 5.4.4.). From the time the zeolite was first
placed in the calorimeter vessel the platinum sealing
plate was not unsoldered nor the amount of sorbent
changed. Thus the amount of Grade K solder was
virtually constant throughout. The heat capacity
of the methane was the difference between the heat
capacities of the vessel with and without methane
plus a correction for the change in weight of thermo-
meter grease and silver tubing present in the two
runs.

To obtain the heat capacity of the sorbed phase,
C_{vs}, corrections then have to be applied according
to the equation given in section 3.3.3. These
corrections are for the heat capacity of the methane
which is in the gaseous phase and for the energy
which has to be supplied to desorb methane in order
to maintain thermodynamic equilibrium after the
temperature increase. These corrections only become
significant in the region of $170^{\circ}K$ and above.

The two runs with methane sorbed will be
denoted A and B. The experimental observations will
be given for the runs and then these results will
be discussed together (Sec.8.4).

8.2.   Methane in Linde 5A: Run A.

For run A the vessel contained .025966 moles
of methane, which is equivalent to an average of
1.808 molecules per zeolite cavity. In all 94 heat
capacity experiments were carried out on the sample.
The results are given in Table 8.1.

Initially the system was cooled very rapidly
by filling the space within the outer can (Fig.5.1)
with helium as a heat exchanger whilst this can was
surrounded by liquid nitrogen. Measurements were
taken from $84^{\circ}K$, and are reported as runs numbered
1 to 7 (marked with an asterisk in the above table).
At first the thermometer drifts were only very
slightly warming and the system equilibrated in about
30 minutes. Above $98^{\circ}K$ (after drift of run 4) the
drifts became warming and very large, being equal
to about $.0015^{\circ}C/min$. Coincident with this the time
required for thermal equilibration became much longer,
and at $112.6^{\circ}K$ the equilibration was followed for
over two hours without the large drift rate decreasing.
This was the after drift of run 6, and run 6a, b, and
c correspond to the apparent heat capacity determined
from after drifts taken 30, 70 and 100 minutes after
the end of the heating period.

The heat capacities found from runs 1 to 7
were higher than the curve of equilibrium heat

capacities found later. The equilibration times and
drift rates were normal in this temperature range
when the vessel was cooled slowly. Clearly the quick
cooling had caused the sorbate to become frozen
in a meta-stable state. Similar effects are known
in glasses and other polymers where the activation
energy for molecular rearrangement is large compared
with the available thermal energy. In this case,
as the vessel was subsequently heated the sorbate
was able, due to the inceased thermal excitations
of both itself and the sorbent, to transform into
a more stable equilibrium configuration. The heat
liberated during this process was the cause of the
warming drifts.

Knowing the size of these drifts and the heat
capacity of the loaded calorimeter vessel, the amount
of heat involved can be estimated if the period of
time for which the drift lasts is known. This type
of calculation shows that the heat involved is about
335t calories per mole of methane if the period of
time for which the drift lasts is t hours. This time
interval is known to be of the order of 3 to 5
hours. This excess energy was also estimated by a
direct calorimetric method. The vessel was cooled
quickly as before to below the region where the
warming drifts commenced and then heat was added
to raise the temperature such that small drifts were
again attainable. In fact the temperature rise
was from 96.6 to 123.9°K. A comparison of the
resulting heat capacity and the heat capacity
determined in this region with slow cooling gave
a value of 1290 cal/mole methane for the extra heat.
This is in accord with the previous estimate.

For all subsequent experiments the vessel was
cooled from room temperature as slowly as possible.
by maintaining a high vacuum in the outer can.
For the runs using solid hydrogen or nitrogen as
refrigerant, the system was cooled in the above
manner to about $80°K$, but during and after the pumping
of the coolant helium was added within the outer
can to assist heat exchange because of the short time
these refrigerants last.

The thermal equilibration time varied with
temperature in a non-typical way, even for these runs
where the sample was cooled slowly. For normal
samples (crystalline solids, etc.) the equilibration
is very quick at both very low temperatures and at
the higher temperatures ($250 - 300°K$) but goes
through a maximum at about $70 - 100°K$. For this
system the equilibration times were short at
temperatures below about $26°K$, but became much larger
above this temperature. They were largest at about
$30°K$ where the equilibration time was about $50 -60$
minutes, this phenomenon being accompanied by cooling
drifts. The behaviour of the system became normal
again at about $45°K$.

The equilibration time followed the usual
pattern through the $100 - 120°K$ region and the drifts
were always small and slightly cooling as opposed
to the behaviour described above for this region
when the sample was cooled quickly. However large
warming drifts with an associated increase in
equilibration time appeared at about $155°K$. The
equilibration time was about 50 minutes in the
temperature region $165 - 200°K$. It can be seen from

an inspection of Table 8.1 that many heat capacity
experiments were performed in this region but the
points were subject to a large scatter of up to
.4% of the total heat capacity about the smooth curve.
Normally the scatter in this region is very small.
The large scatter is thought to be due to two causes.
Firstly the long equilibration times make the ex-
trapolation of the drifts less reliable (see Sec. 6.3)
and secondly it is thought that the heat capacity
might be dependent on the thermal history of the
sample in this region. For example, some of these
experiments were done immediately the sample had been
slowly cooled to 170°K, whilst others in this region
were done after the sample had been held at these
temperatures overnight. Above 200°K the equilibration
times became shorter and the thermal behaviour was
normal up to the highest temperatures used.

The contribution of the sorbate to the total
heat capacity was 7.7% at 50°K, 5.6% at 100°K, 5.47%
at 150°K, 5.4% at 190°K and only 4.74% at 250°K.

The graphical method described in section
3.3.4 was used to find the pressure in the calorimeter
vessel at each temperature. This is illustrated in
Fig. 8.1, from which it can be seen that the partial
pressure of methane is negligible below 165°K.
From these calculations the corrections to the
methane heat capacity mentioned previously were
made. The heat capacity of the sorbed methane that
was thus obtained is presented in Table 8.2 and
Fig. 8.2. It has a broad maximum in the region
185 - 190°K. There also seems to be an extra
contribution to the heat capacity in the range

Fig. 8.1.   The Partial Pressure of Methane in the Calorimeter Vessel: Run A
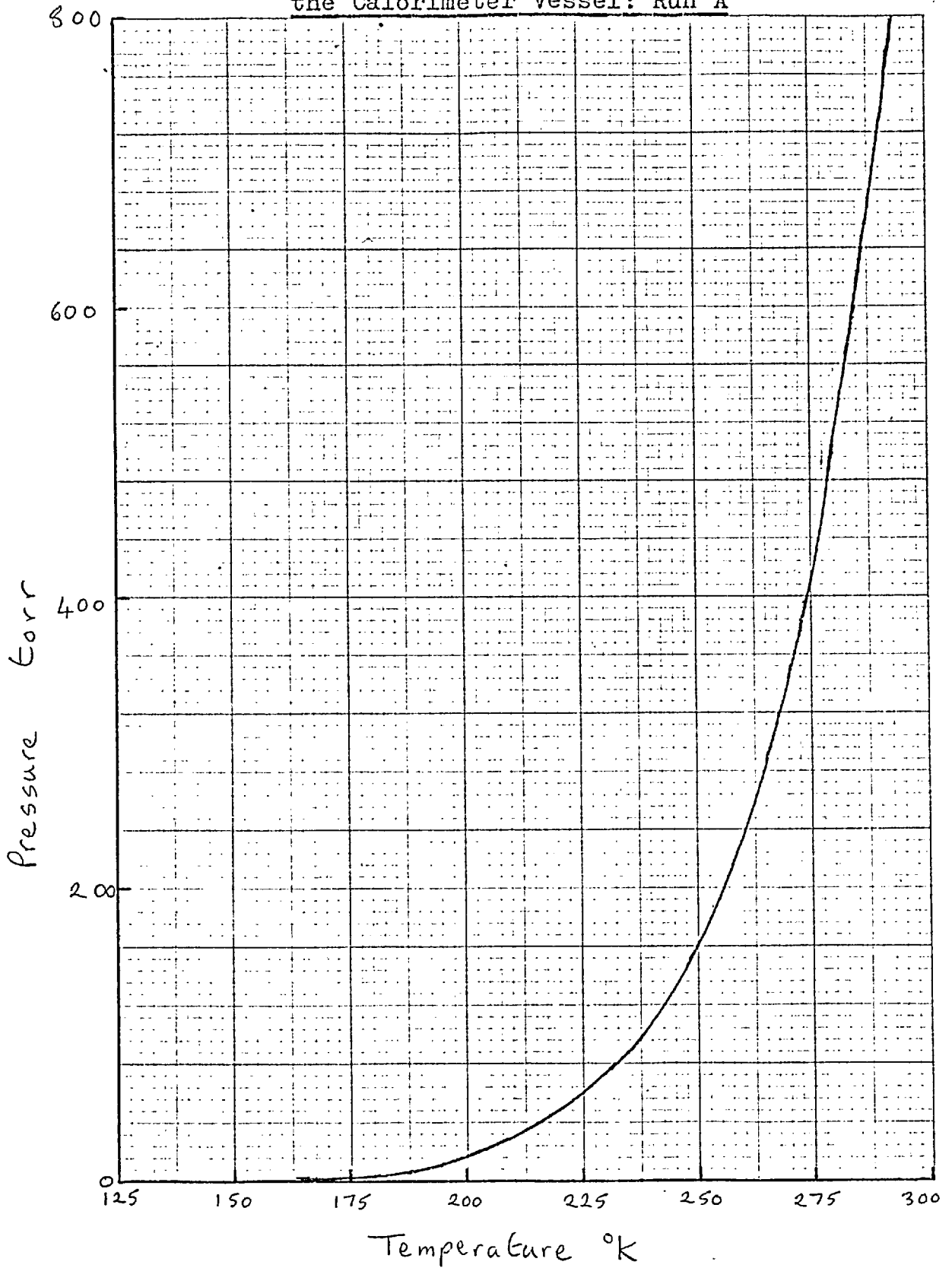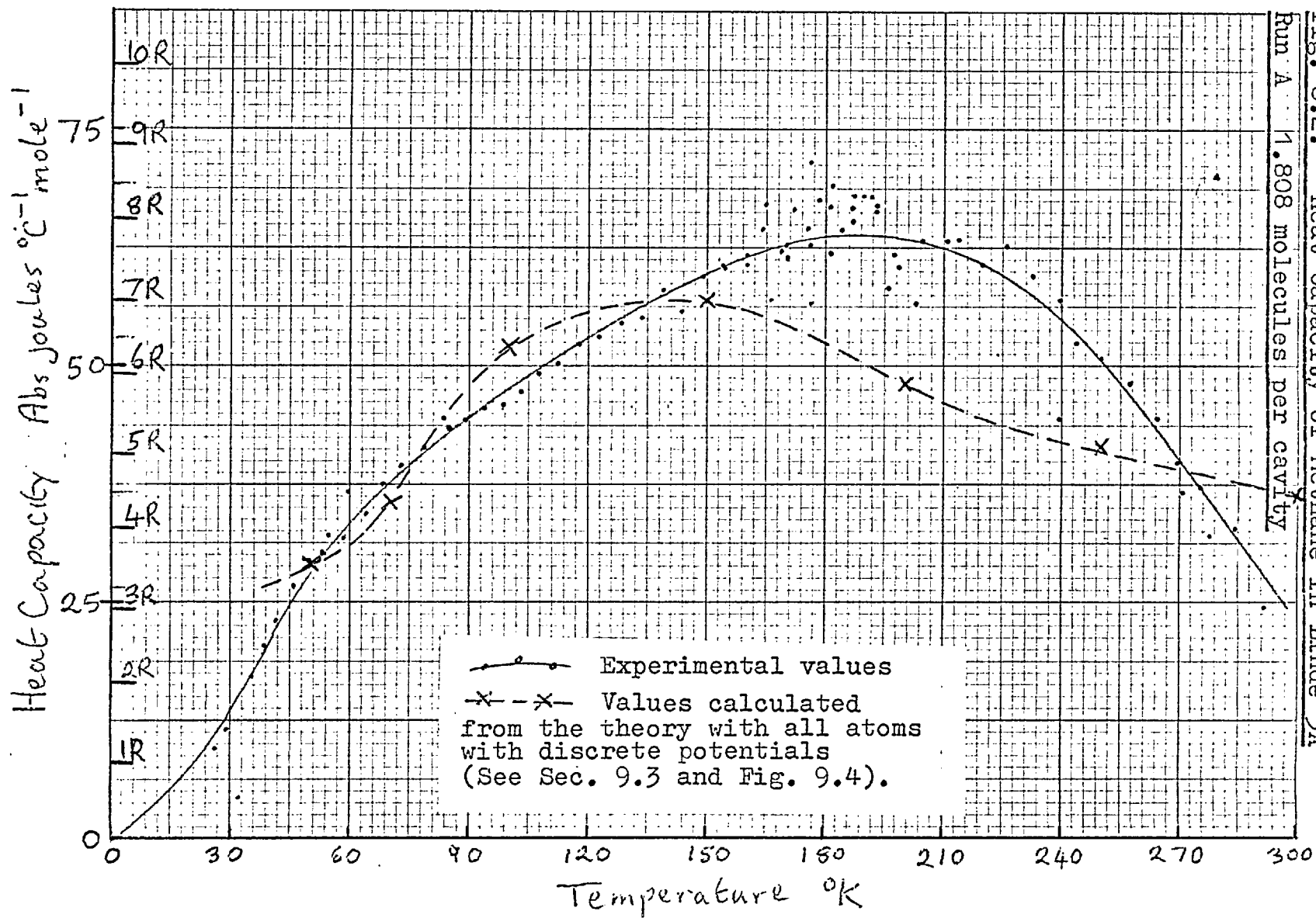
Fig. 8.2. Heat Capacity of Methane in Linde 5A

Run A 1.808 molecules per cavity

Experimental values

Values calculated from the theory with all atoms with discrete potentials (See Sec. 9.3 and Fig. 9.4).

207

$60 - 105^{\circ}K$. Its actual commencement is difficult to
determine because of the very rapid fall-off in the
methane heat capacity at these temperatures. The
decrease in the heat capacity at high temperatures
is very marked, and indeed at $300^{\circ}K$ it approaches
the value for methane in the gaseous phase.

8.3. Methane in Linde 5A: Run B.

For this set of measurements .012829 moles of
methane were added to the vessel. equivalent to
an average cavity occupancy of .8933 molecules.
The results from the 61 heat capacity experiments
are given in Table 8.2. The partial pressure of the
methane in the vessel was calculated at various
temperatures and it is shown in Fig.8.3. From these
calculations, as for the previous run, the contribution
to the heat capacity which arises from the sorbed
methane was calculated (Table 8.4 and Fig. 8.4).

All the points were determined after the system
had been cooled as slowly as conveniently possible.
The heat capacity of the methane at this dosage
showed the same general variation with temperature
as that for the larger dosage of run A. There were
significant differences however. The maximum in
the curve occurred at a lower temperature of between
$165 - 170^{\circ}K$. The associated increase in duration
of the equilibration times also, as would be expected,
was evidenced at a lower temperature, although only
slightly so.

Fig. 8.3. The Partial Pressure of Methane in the Calorimeter Vessel: Run B

Fig. 8.4. Heat Capacity of Methane in Linde 5A
Run B .8933 moles per cavity

Experimental values

—x——x—— Values calculated
from the theory with all atoms
with discrete potentials
(See Sec. 9.3 and Fig. 9.4).
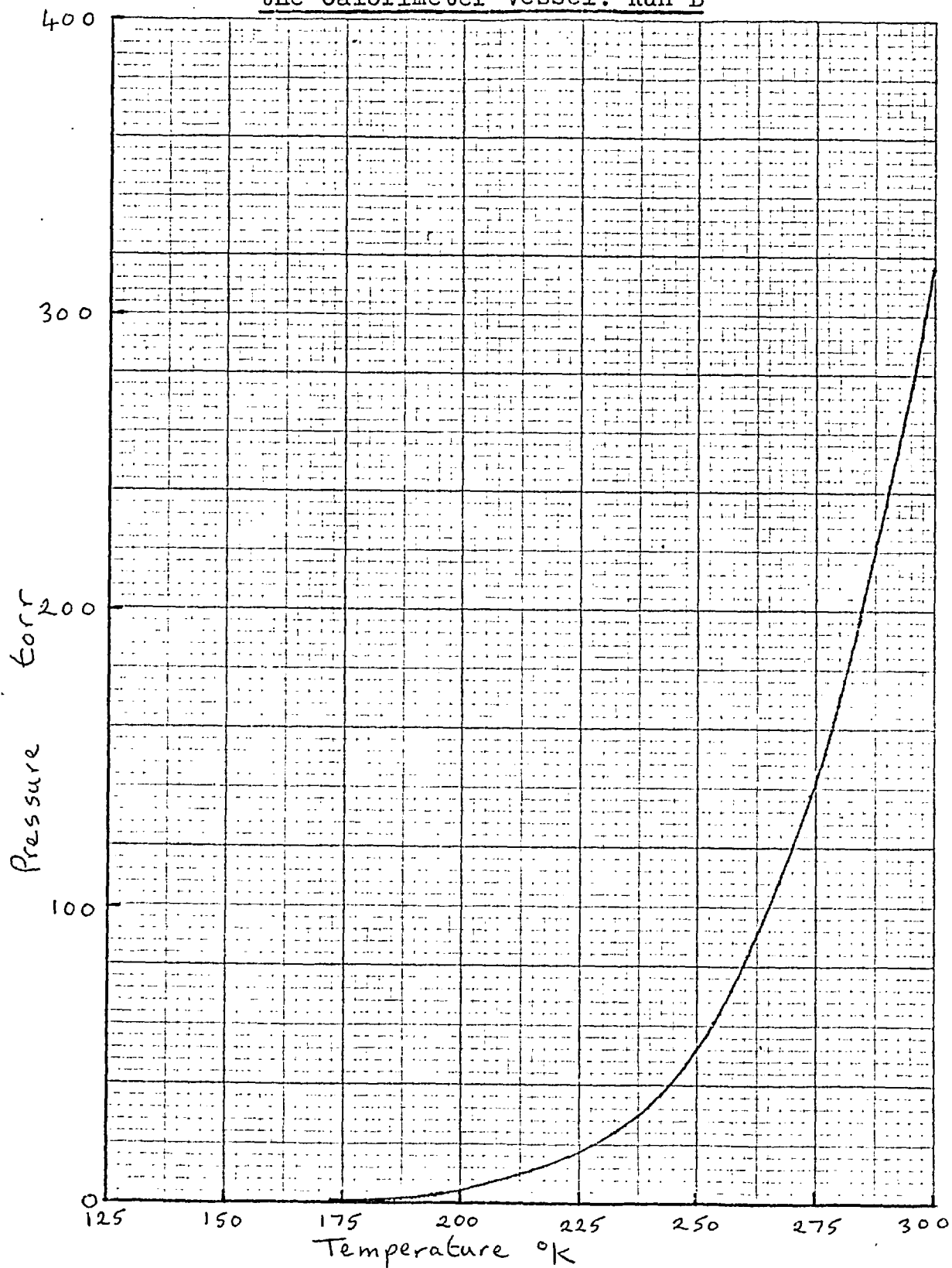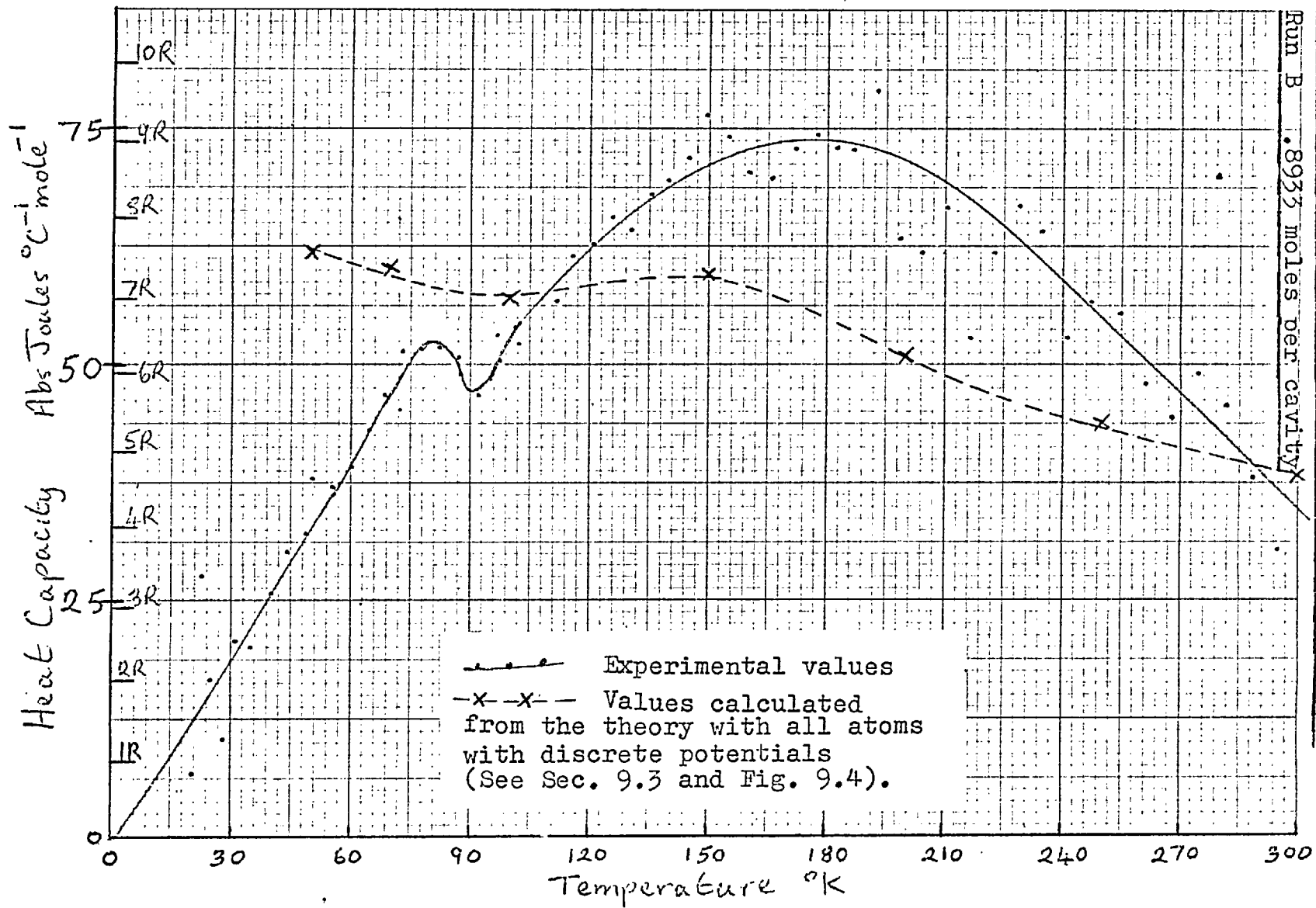
The major difference in the two curves was at
lower temperatures. The 12 heat capacity experiments
using solid hydrogen refrigerant extended over 15
hours because from $23^{o}K$ to about $40^{o}K$ the equili-
bration times were abnormally long (often over 60
minutes) during which period the thermometer was cooling.
The region of anomalously high heat absorption was
much more pronounced than before, and occurred between
$45 - 100^{o}K$, that is at a lower range of temperature
than for run A. Again the low temperature tail
of this region is lost in the fall-off of the total
methane heat capacity.

The contribution to the total heat capacity
from the methane was quite small for this run,
falling from 4.48% at $50^{o}K$, to 3.15% at $100^{o}K$,
3.1% at $170^{o}K$ and only 2.4% at $250^{o}K$. Thus
uncertainties of .1% in each of the bulk heat
capacities from which these results are obtained
causes an uncertainty of about 8% in the total heat
capacity at $250^{o}K$.

TABLE 8.1. – EXPERIMENTAL VALUES OF THE HEAT CAPACITY
OF METHANE SORBED IN LINDE 5A. in Abs.
Joules $^{\circ}C^{-1}$

Wt. of dehydrated zeolite = 23.4338g (in vacuo).
No of moles of methane used = .025966
Approximate amount of helium in vessel = 2.6×10^{-4} moles.
C is the bulk heat capacities.
The last column is the total heat capacity due
to the methane.

Run No.	Temp. $^{\circ}K$	ΔT	C	C (methane)
*1	86.31	4.584	19.040	1.169
*2	90.92	4.595	19.952	1.214
*3	95.56	4.657	20.809	1.252
*4	100.35	4.840	21.609	1.250
*5	105.28	4.862	22.404	1.249
*6a	110.18	4.699	23.156	1.243
*6b	110.21	4.748	22.917	1.000
*6c	110.22	4.776	22.782	0.863
*7	115.09	4.700	24.063	1.428
8	170.48	5.098	30.666	1.626
9	175.62	5.169	31.193	1.680
10	180.84	5.236	31.705	1.736
11	186.15	5.344	32.150	1.730
12	191.55	5.413	32.642	1.765
13	196.95	5.345	33.032	1.608
14	202.48	5.689	33.282	1.468
15	98.09	4.626	21.168	1.185
16	102.83	4.849	21.997	1.233
17	107.70	4.870	22.810	1.277

TABLE 8.1. (continued)

Run No.	Temp. °K.	$\triangle$T	C	C (methane)
18	112.59	4.898	23.574	1.303
19	117.50	4.921	24.341	1.363
20	122.46	4.959	25.035	1.380
21	128.74	4.771	25.899	1.416
22	133.62	4.984	26.503	1.431
23	138.63	5.031	27.164	1.506
24	143.70	5.107	27.690	1.451
25	148.83	5.169	28.363	1.550
26	154.04	5.243	28.952	1.574
27	159.42	5.536	29.542	1.602
28	164.98	5.591	30.266	1.748
29	170.65	5.712	30.744	1.592
30	176.43	5.813	31.222	1.627
31	180.87	5.572	31.584	1.615
32	186.47	5.626	32.139	1.693
33	192.16	5.751	32.654	1.721
34	198.10	6.109	33.010	1.569
35	204.16	6.047	33.565	1.645
36	210.29	6.205	34.052	1.645
37	213,14	6.181	34.295	1.649
38	219.39	6.311	34.728	1.583
39	225.85	6.632	35.264	1.625
40	232.58	6.824	35.745	1.550
41	239.47	6.945	36,181	1.480
p42	54.64	4.787	11.457	0.841
p43	59.50	4.794	12.868	0.956
p44	64.13	4.428	13.938	0.893
p45	68.61	4.547	15.079	0.974
p46	73.21	4.664	16.171	1.032

TABLE 8.1 (continued)

Run No.	Temp.$^\circ$K	ΔT	C	C (methane)
p47	78.13	5.157	17.283	1.074
p48	83.30	5.205	18.441	1.163
49	84.46	4.747	18.640	1.133
50	89.29	4.904	19.591	1.154
51	94.09	4.688	20.486	1.186
52	98.85	4.826	21.305	1.194
h53	15.11	1.239	0.414	
h54	18.30	1.026	0.701	
h55	20.41	1.229	1.049	
h56	22.60	1.886	1.532	
h57	24.52	1.718	2.142	
h58	26.79	2.844	2.976	0.255
h59	29.48	2.570	3.766	0.296
h60	32.19	2.842	4.260	0.112
h61	35.32	3.399	5.483	0.452
h62	38.60	3.150	6.516	0.526
h63	41.88	3.418	7.552	0.601
h64	4.547	3.723	8.673	0.694
h65	49.32	3.939	9.847	0.760
h66	53.62	4.643	11.118	0.784
h67	58.53	5.165	12.488	0.824
68	154.63	5.444	29.006	1.565
69	159.83	4.944	29.562	1.580
t70	163.62	2.621	30.063	1.679
t71	166.25	2.615	30.129	1.487
t72	168.85	2.582	30.508	1.617
73	172.15	3.999	30.926	1.727
74	176.35	4.345	31.038	1.467
t75	176.12	2.506	31.423	1.861

TABLE 8.1. (continued)

Run No.	Temp.$^{\circ}$K	$\triangle$ T	$\dot{C}$	C (methane)
t76	178.65	2.494	31.543	1.754
t77	181.32	2.827	31.807	1.793
t78	184.16	2,815	31.929	1.677
t79	186.97	2.784	32.257	1.769
t80	189.84	2.934	32.510	1.770
t81	192.78	2.912	32.727	1.745
t82	195.70	2.908	32.751	1.520
83	235.59	6.849	35.921	1.220
84	243.40	6.757	36.347	1.363
85	250.21	6.860	36.837	1.323
86	257.13	6.971	37.263	1.259
87	264.04	6.864	37.715	1.156
88	269.85	4.773	38.180	1.037
89	275.61	6.745	38.459	0.972
90	270.76	6.780	38.152	0.951
91	277.60	6.922	38.462	0.838
92	284.54	7.619	39.025	0.849
93	291.70	7.326	39.442	0.638
94	298.99	7.262	39.781	**

** Correction for desorption unknown.

TABLE 8.2. – HEAT CAPACITY OF THE SORBED METHANE
AS A FUNCTION OF TEMPERATURE: RUN A

The run numbers correspond to those of Table 8.1.
C_{vs} is in abs Joules $^\circ C^{-1}$ per mole of methane.

Run No.	Temp $^\circ K$	C_{vs}	Run No.	Temp $^\circ K$	C_{vs}
1	86.31	45.02	20	122.46	53.15
2	90.92	45.75	21	128.74	54.53
3	95.56	48.22	22	133.62	55.11
4	100.35	48.14	23	138.63	58.00
5	105.28	48.10	24	143.70	55.88
6a	110.18	47.87	25	148.83	59.69
6b	110.21	38.51	26	154.04	60.62
6c	110.22	33.24	27	159.42	61.70
7	115.09	55.00	28	164.98	67.32
8	170.48	62.62	29	170.65	61.31
9	175.62	64.70	30	176.43	62.66
10	180.84	66.86	31	180.87	62.20
11	186.15	66.63	32	186.47	65.20
12	191.55	67.97	33	192.16	66.28
13	196.95	61.93	34	198.10	60.43
14	202.48	56.54	35	204.16	63.35
15	98.09	45.64	36	210.29	63.35
16	102.83	47.49	37	213.14	63.51
17	107.70	49.18	38	219.39	60.96
18	112.59	50.18	39	225.85	62.58
19	117.50	52.49	40	232.58	59.69

TABLE 8.2. (continued)

Run No.	Temp^{o}K	C_{vs}	Run No.	Temp^{o}K	C_{vs}
41	239.47	57.00	70	163.62	64.66
42	54.64	32.39	71	166.25	57.27
43	59.50	36.82	72	168.85	62.27
44	64.13	34.39	73	172.15	66.51
45	68.61	37.51	74	176.35	56.50
46	73.21	39.74	75	176.12	71.67
47	78.13	41.36	76	178.65	67.55
48	83.30	44.79	77	181.32	69.05
49	84.46	43.63	78	184.16	64.58
50	89.29	44.44	79	186.97	68.13
51	94.09	45.68	80	189.84	68.17
52	98.85	45.98	81	192.78	67.20
58	26.79	9.82	82	195.70	58.54
59	29.48	11.40	83	239.59	46.99
60	32.20	4.31	84	243.40	52.49
61	35.32	17.41	85	250.21	50.95
62	38.60	20.26	86	257.13	48.49
63	41.88	23.15	87	264.04	44.52
64	45.47	26.73	88	269.85	39.94
65	49.32	29.27	89	275.61	37.43
66	53.62	30.19	90	270.76	36.63
67	58.53	31.73	91	277.60	32.27
68	154.63	60.27	92	284.54	32.70
69	159.83	60.85	93	291.70	24.57

TABLE 8.3. — EXPERIMENTAL VALUES OF THE HEAT CAPACITY
OF METHANE SORBED IN LINDE 5A. in Abs.
Joules $°C^{-1}$

Wt. of dehydrated zeolite = 23.4338g. (in vacuo)
No of moles of methane used = .012829
Approximate amount of helium in vessel = 2.6×10^{-4} moles.
C is the bulk heat capacities.
The last column is the total heat capacity due
to the methane.

Run No.	Temp. $°K$	ΔT	C	C (methane)
1	87.39	4.516	18.707	0.626
2	92.00	4.712	19.539	0.606
3	96.78	4.878	20.447	0.682
4	101.58	4.694	21.251	0.691
5	97.32	4.855	20.497	0.642
6	102.17	4.843	21.328	0.672
7	111.25	4.363	22.797	0.726
8	115.71	4.556	23.510	0.788
9	120.53	5.061	24.198	0.803
10	125.53	4.915	24.899	0.843
11	130.39	4.797	25.499	0.823
12	135.21	4.853	26,134	0.872
13	139.53	4.753	26.655	0.893
14	144.52	5.234	27.256	0.924
15	149.70	5.107	27.892	0.984
16	154.94	5.365	28.437	0.963
17	160.26	5.272	28.926	0.902
18	165.72	5.686	29.464	0.897

TABLE 8.3. (continued)

Run No.	Temp.$^{\circ}K$	ΔT	C	C (methane)
19	171.37	5.643	30.038	0.934
20	177.03	5.671	30.566	0.957
21	182.66	5.583	31.035	0.935
22	186.59	5.504	31.361	0.933
23	192.22	5.785	31.911	1.013
24	198.09	5.926	32.193	0.816
25	204.02	6.032	32.641	0.794
26	210.08	6.181	33.165	0.853
27	216.29	6.311	33.547	0.676
28	222.59	6.418	34.038	0.796
29	229.04	6.585	34.552	0.858
30	234.11	6.830	34.890	0.824
31	240.82	6.735	35.328	0.678
32	247.56	6.882	35.742	0.726
33	254.31	6.794	36.206	0.712
34	261.06	6.941	36.594	0.616
35	267.87	6.866	36.979	0.574
36	274.70	6.997	37.445	0.627
37	281.56	6.920	37.848	0.585
38	288.33	6.863	38.142	0.487
39	295.03	6.786	38.533	0.391
40	301.58	6.642	39.008	0.597
p41	50.51	5.319	9.923	0.483
p42	55.50	4.666	11.327	0.473
p43	60.07	4.474	12.560	0.501
p44	64.48	4.349	13.685	0.553
p45	68.89	4.482	14.767	0.598
p46	73.23	4.188	15.801	0.658
p47	77.65	4.604	16.766	0.660
p48	82.33	4.762	17.748	0.663

TABLE 8.3. (continued)

Run No.	Temp. ^{o}K	$\triangle T$	C	C (methane)
p49	87.07	4.722	18.671	0.651
h50	15.29	1.823	0.369	
h51	17.94	0.595	1.131	
h52	19.11	1.213	1.230	
h53	20.72	2.068	1.444	0.086
h54	22.75	2.162	2.073	0.354
h55	25.13	2.800	2.509	0.210
h56	27.80	3.047	3.112	0.132
h57	30.97	3.698	4.086	0.268
h58	35.34	5.155	5.297	0.258
h59	39.91	4.059	6.705	0.331
h60	44.18	4.503	7.996	0.385
h61	48.36	3.884	9.215	0.413

TABLE 8.4. - HEAT CAPACITY OF THE SORBED METHANE AS A FUNCTION OF TEMPERATURE: RUN B

The run numbers correspond to those of Table 8.3. C_{vs} is in abs Joules $^{\circ}C^{-1}$ per mole of methane.

Run No.	Temp$^{\circ}$K	C_{vs}	Run No.	Temp$^{\circ}$K	C_{vs}
1	87.39	48.80	22	186.59	72.73
2	92.00	47.24	23	192.22	78.96
3	96.78	53.16	24	198.09	63.61
4	101.58	53.86	25	204.02	61.89
5	97.32	50.04	26	210.08	66.49
6	102.17	52.38	27	216.29	52.69
7	111.25	56.62	28	222.59	62.05
8	115.71	61.42	29	229.04	66.88
9	120.53	62.59	30	234.11	64.23
10	125.53	65.57	31	240.82	52.85
11	130.39	64.15	32	247.56	56.59
12	135.21	67.97	33	254.31	55.50
13	139.53	69.61	34	261.07	48.02
14	144.52	72.02	35	267.87	44.74
15	149.70	76.70	36	274.70	48.87
16	154.94	74.06	37	281.56	45.60
17	160.26	70.31	38	288.33	37.96
18	165.72	69.92	39	295.03	30.48
19	171.37	72.80	40	301.58	46.54
20	177.03	74.60	41	50.51	37.65
21	182.66	72.88	42	55.50	36.87

TABLE 8.4. (continued)

Run No.	Temp $^\circ$K	C_{vs}	Run No.	Temp $^\circ$K	C_{vs}
43	60.07	39.05	54	22.75	27.59
44	64.48	43.11	55	25.13	16.37
45	68.89	46.61	56	27.80	10.29
46	73.23	51.29	57	30.98	20.89
47	77.65	51.45	58	35.34	20.11
48	82.33	51.68	59	39.91	25.80
49	87.07	50.74	60	44.18	30.01
53	20.72	6.70	61	48.36	32.19

CHAPTER 9

DISCUSSION OF CERTAIN THERMODYNAMIC
PROPERTIES OF METHANE IN LINDE 5A

9.1. Introduction.

The elucidation of the experimental data given
in the previous chapter presents many interesting
problems. The data is understandably more complex
than that for, say, methane occluded in quinol
clathrates because of the multiple occupancy of
cells, the more heterogeneous potential within each
cell and the much greater mobility allowed to the
guest molecules. Since the statistical thermodynamic
theory formulated in Chapter 3 only applies to
equilibrium states, it cannot be employed as a
description of the slow relaxation processes which
occur in this system. A correct treatment should
account for the magnitude of the heat capacity at
various temperatures and compositions, and furthermore
it should predict the correct form of the equilibrium
isotherms and isosteric heats. In Section 9.2 numerical
values are given for some of these quantities based on
the intermolecular potential data presented in Section
2.3 and using the equations of Chapter 3. An appraisal
of these results in terms of the experimental data
reported in this thesis and later calculations
(Parsonage 1969) is given in Section 9.3.

A study of the relaxation processes should, in

itself, be of great interest because they reflect the mobility allowed to the sorbate. Normally the time required for the calorimeter vessel to become thermally equilibrated is determined by the rate at which the heat supplied to the vessel by the vessel heater is transferred to and then through the sample, and on the amount of heat involved. Thermal equilibration is deemed to be complete when the drift in temperature is either zero or at the smallest steady value attainable with the apparatus in that temperature range. Thus these time periods are small at very low temperatures where the amount of heat involved is small and the thermal conduction efficient, and also at high temperatures because of the high radiative transfer which is possible. Abnormally long equilibration times at a particular temperature suggest that the molecular rearrangement which the sample is attempting in order to allow itself to assume an equilibrium configuration is being hindered by large free energy barriers.

At least three such processes have been recorded for methane occluded in Linde 5A. These occur at (1)low temperatures ($23 - 45^{\circ}$K) with associated cooling drifts,
(2) $160 - 200^{\circ}$K when the drifts were warming, and
(3) above 98°K when the sample of Run A was cooled rapidly and large warming drifts were evidenced.

It is thought that there are several slow processes which could cause these effects. These are as follows: (a) The restricted movement or hopping of the sorbate molecules within the cavities from one site

to another. Here it should be remembered that the
cavities are not spherical but have regions which the
methane molecules would find energetically favourable.
These are near the cations and the eight-membered
rings of oxygens. Also movement between these regions
within multi-occupied cavities is probably comparatively
slow. This process could also involve slight movement
of the cations. (b) The intercavity migration of
molecules by passage through the eight-membered rings.
Lastly (c) the migration of molecules from one crystallite
to another via the crystallite surface and the gaseous
phase. This diffusion process involves several steps,
any one of which could be a slow stage. The process
will be slow if the concentration of methane either on
the outer surface of the crystallites or in the gas
phase is small.

The second of these effects presupposes that there
is a tendency for the molecules to alter their dis-
tribution among all the cavities, whilst the last
effect presumes that the sorbate free energy in any
one cavity is a function of the filling of adjacent
cavities, perhaps causing sorbate clustering or
dispersion. The theoretical discussion of the following
sections indicates that the intercavity redistribution
is significant, but it can give no information about
the last effect because the cavities are assumed
independent. That is, the interaction energy between
two neighbouring cavities is taken as negligible.

At least part of the sorbate rearrangement which
takes place in (a) must precede that of (b), and
similarly (b) that of (c). Thus (a) cannot commence

to take place at a higher temperature than (b), and
likewise the last effect must start at the highest
temperature. However the intracavity liberation
does not have to be complete before intercavity migration
becomes significant. The energy barrier between two
neighbouring cavities could be lower than that between
two parts of a single cavity. All that is required
is that any regions of high energy within a cavity
should not forbid molecules in more favourable energy
wells from passing through the large windows. Since
methane is sorbed in this sample of Linde 5A at a
reasonable rate at $194.6^{\circ}K$ (see Chapter 4), and methane
can pass through the smaller openings between cavities
in Linde 4A at temperatures down to $134^{\circ}K$ (Kvitkovskii
and Sergienko 1962), the above processes (b) and (c)
must be comparatively fast in Linde 5A above $134^{\circ}K$,
as must also be access to at least certain parts of
each cavity.

Hill (1946) has discussed the localized to
mobile transition in physically adsorbed films using
a treatment similar to that mentioned in Section 3.4.5
for hindered rotation. For a barrier of up to 600
cal/mole hindering the movement of the sorbate over
the surface, he concluded that the transition would
occur at temperatures below $50^{\circ}K$. Fig. 2.2 illustrates
that for Limcharoen's intermolecular potential data the
barrier due to the sorbent to a methane molecule moving
around the surface of a cavity in Linde 5A is of this
order, so Hill's conclusion should be valid here also.
However the total interaction potential will contain
intersorbate terms also, and it will be seen later that
modifications to the cavity potential itself might bring
doubt on this conclusion.

Tentatively the slow relaxation processes observed can be accounted for in the following manners. The slow equilibration at hydrogen temperatures can be assigned to a phenomenon akin to the first effect listed above. That is the movement of sorbate in the cavities with perhaps associated small relocations of the cations. Thus as the temperature is raised the system tends to increase in the negative sense its free energy by sorbate becoming less localized. This inevitably leads to the rising of the sorbate energy and ~~this~~ accounts for the cooling drifts observed, and these are slow because of energy barriers between the sorption sites. For this to occur at these very low temperatures these barriers must be very small. At these temperatures the cavities will not only contain methane, but also some of the helium which was added initially to improve thermal equilibration. Helium will not be very firmly sorbed so the relevant energy barriers will be much smaller than for methane which is quite tightly held at these temperatures. It should be remembered also that helium is small enough to enter into the β-cavities in the zeolite framework, and the slow equilibration observed could be either redistribution between the two types of cavity or desorption from the zeolite altogether.

The last mentioned equilibration phenomenon, at around 100°K, is thought to be connected with the intracavity diffusion process. The theoretical discussion later will indicate that the sorbate movement within the cavities, hindered by the heterogeneous cavity potential, is very important, and that the spatial distribution of the molecules is different at different temperatures. If the sample is cooled

very rapidly before the redistribution has taken place the thermal energy of the system can become so low that the diffusion process cannot proceed at a reasonable rate. The sorbate is then held in a meta-stable state of high energy. When the temperature is later increased to the point where intracavity diffusion is again possible, the sorbate will rearrange itself to what is the particular equilibrium distribution for that temperature. This process involves the system moving to a state of lower energy so causing heat to be liberated. This is seen in the warming drifts. In Run A, at $98^{o}K$ the drift was smaller than that given earlier for $110^{o}K$. This was because the rate of heat generation is related to the rate of diffusion, which will clearly increase with temperature.

When the system is cooled very slowly through this temperature range, it will remain in a state which is very nearly an equilibrium one until a low temperature in the region of $98^{o}K$ where again the intracavity diffusion will effectively cease. Now, in this case, when the system is heated passed this temperature so that this rate of diffusion becomes such as to cause significant migration, the system is already very close to an equilibrium state and so no abnormal equilibration process is observed. This assumes that the rate of heating is greater than the rate of cooling, a condition which is always satisfied in the reported experiments.

It was possible to estimate the amount of energy which was frozen into the system because of this slow diffusion process. This was shown in Section 8.2 to be about 1290 cal/mole methane. From the measured

heat capacity it is possible to estimate the difference
in the configurational energy of the sorbed methane
between 90 and 300°K, as the total energy uptake in
the temperature range less the sum of the classical
translational and rotational energies. For Run A
this quantity is about 1600 cal/mole methane. Thus the
amount of heat frozen-in can quite sensibly be
attributed to the configurational energy of the methane.
The difference in these two amounts of energy, about
300 cal/mole, would be due to the amount of sorbate
redistribution which occurred before the rate of
diffusion became too slow, and would depend on the
rate of cooling.

This leaves to be discussed the second mentioned
slow equilibration phenomenon, namely that at 160 –
200°K when the drifts were warming. The effect was
observed in both runs. Analogous to the effect which
has just been discussed above, this must be due to the
freezing-in of some intercavity redistribution which
occurs when the sample is cooled, the warming drift
being due to this energy being liberated when the
sample is later heated. The most obvious explanation
would be that the sample was cooled at a rate such
that within each crystallite of zeolite the diffusion
of sorbate between cavities became too slow to hold
the system in over-all equilibrium and so a certain
amount of intercavity configurational energy became
frozen-in. The effect is not large compared with the
third effect above. This explanation would support
a theoretical approach in which the intercavity redis-
tribution is of little significance. Such is the
case for the lastest calculations based on the theory
given in Chapter 3 and reported later in this discussion.

Evidence was cited at the beginning of this section which indicated that the intercavity migration for methane could be somewhat too fast in this temperature range to cast some doubt on the above explanation, but the intercrystallite migration has been completely ignored here.   Intercavity interactions have been assumed zero in the theoretical discussion which follows to avoid causing the computation from being far more complex, but qualitatitively it can be seen that the freezing in of the sorbate in a distribution among cavities in the same crystallite only or also among those in different crystallites would cause the same type of slow equilibration effects when the system was reheated.

Lastly estimates were obtained from the heat capacity measurements of the standard energy of the sorbate at $300^{\circ}K$ for each degree of cavity filling (n). The values were 12,716 and 14,840 Joules per mole of methane for n = 1.808 and 0.8933 respectively.

9.2.   Some Numerical Results from the Statistical Thermodynamic Theory.

9.2.1.   Introduction.

Here numerical results are presented for the sorption of methane in Linde 5A based on the intermolecular force data from Limcharoen's work (see Chapter 2).   These include the heat capacity at two sorbate concentrations, isosteric heats and equilibrium sorption isotherms.   Considering the indefiniteness which exists in the characterization of just the equilibration times observed in the heat capacity

experiments, it is to be expected that even a quali-
tative discussion of the experimental results would be
difficult.

The results are obtained using the grand partition
function theory (Sec. 3.4.2). This necessitates that
values are known for the various quantities connected
with the canonical partition function for n molecules
per cavity (n = 1 to G, the maximum allowed number),
over a range of temperature. The parameters used to
characterize the intermolecular forces and the crystallo-
graphic properties, of which the various canonical
partition functions are functions, are given in Chapter
2.

In fact, since the thermal energy of the sorbate
molecules is not dependent on their locations, whether
they are sorbed or not, this contribution can be
factorized out of each partition function and the value
of the remaining part, the configurational integral, -
only has to be calculated.

9.2.2.   The Configurational Integral.

By the use of the methods described in Section
3.4.4 some configurational integrals have been
calculated for methane in the α-cavities of Linde 5A
for 5 to 8 molecules per cavity. Reliable values
for up to 4 molecules have been obtained previously
(Limcharoen 1968). The new results are presented
in Table 9.1 and Figure 9.1. For each degree of
cavity filling the primary integral, $q_{n,0}$, was
obtained by the method described in Section 3.4.4.3;
the cut-off parameter, γ, was assigned the value .9

TABLE 9.1. — THE CONFIGURATIONAL FREE ENERGY FOR
5 TO 8 MOLECULES PER CAVITY
based on Limcharoen's data.

|	$-\dfrac{F_c(n,T)}{n\,k}$ in $^{\circ}K$			
n	5	6	7	8
$^{\circ}K$				
40	2489.2	2504.0	2525.3	2545.1
50	2508.2	2521.4	2537.9	2551.3
60	2530.1	2540.0	2551.8	2559.7
70	2554.0	2560.3	2567.1	2568.7
100	2633.0	2627.5	2620.2	2594.2
200	2941.5	2890.6	2840.6	2769.4
300	3273.8	3184.6	3096.0	2976.6

q_n is in the units of A^{3n}

For q_n ($n<5$), see Limcharoen(1968) Chapter 7.
These data include no contribution for the
rotation of the methane molecules.

Fig. 9.1.   The Configurational Free Energy for
Methane in Linde 5A, based on Limcharoen's data.
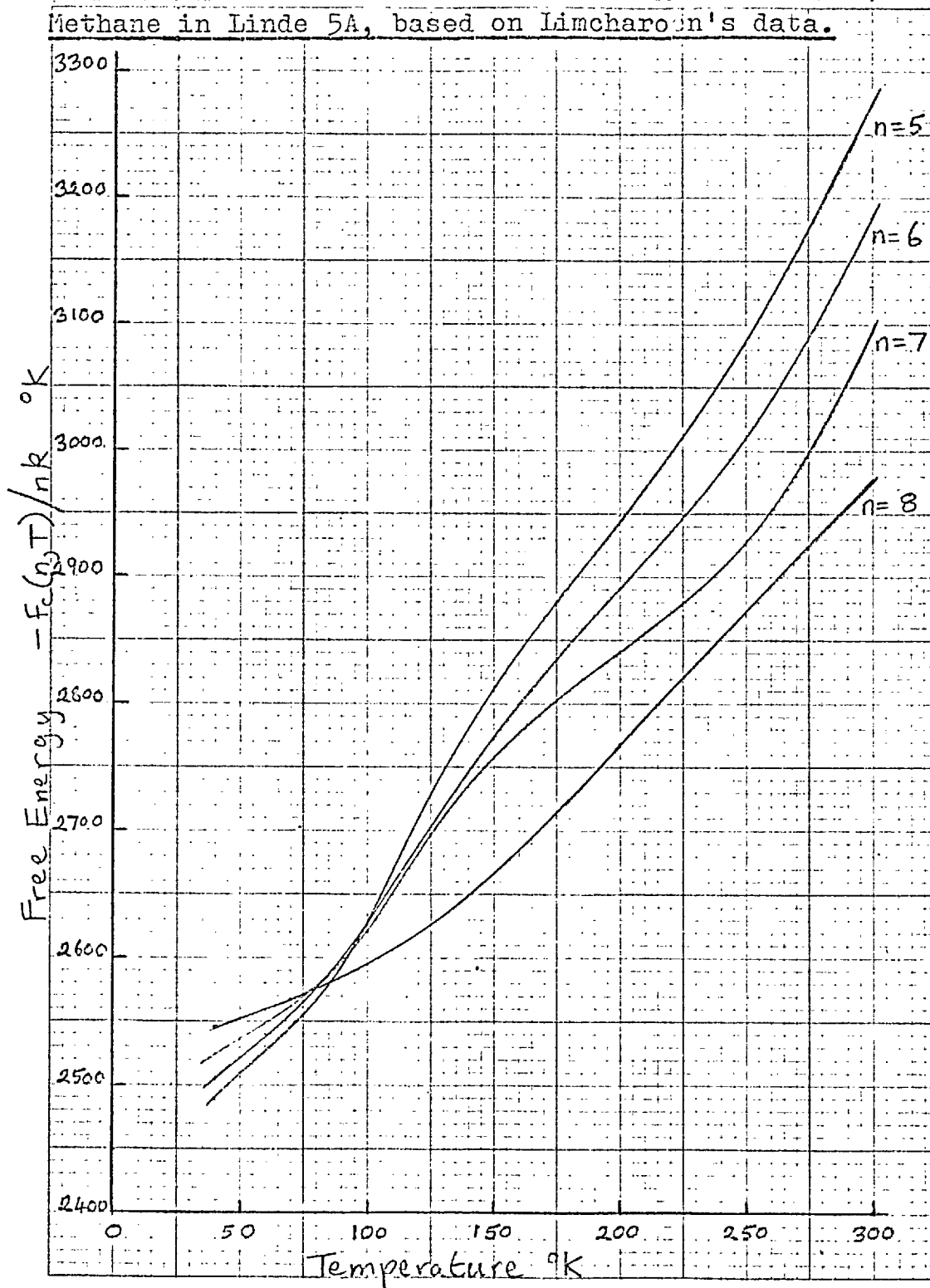
throughout. Limcharoen also used a potential with
a cut-off, his cut-offs corresponding to a γ value
of between .84 and .94. The value used in the present
calculations corresponds to a maximum replusion energy
of about 6.6ϵ in the Lennard-Jones potential used to
calculate $\bar{E}_2(c)$ by the 'integration over temperature'
method. Thus the convergence of $\bar{E}_2(\infty)$ was reasonable,
even in highly filled cavities.

Ideally q_n, the configurational integral, should
be calculated for up to $n = G$, where G is the maximum
allowed number of molecules in the cavity. G is about
9 - 10 for methane, but so far values have been obtained
for up to $n = 8$ only. Nevertheless thermodynamic
properties can be predicted at temperatures which are
not too low since for in these calculations based on
Limcharoen's data the contribution to these properties
from cavities containing 9 and 10 molecules is extremely
small.

The configurational free energy is defined by
the equation

$$F_c(n,T) = -kT \ln(q_n) \quad .$$

It is interesting that these particular calculations
predict that at the lowest temperatures the more
highly populated cavities have a lower free energy
per molecule than the less populated ones. This is
because at these temperatures the molecules take up
their most favoured positions with the maximum inter-
sorbate interaction. It is only at the higher temper-
atures when the molecules become more excited that
the decreased freedom allowed to molecules in the
highly filled cavities causes them to become less

stable compared with the cavities less highly filled.

The configurational free energy found by the 'integration over temperature' method for five molecules per cavity is slightly different to that obtained by the staight-forward simple Monte Carlo method (-3273.8 compared with 3286.0 for $F_c(5,300)/nk$). The difference is small and the error is probably in the latter result because of the very slow convergence of that method at this degree of cavity filling.

The configurational free energy must decrease very sharply at either $n = 9$ or 10 because of the very large repulsive forces which will be present in all the configurations due to the close packing. This will cause great difficulty in the evaluation of these configurational integrals at all temperatures.

9.2.3. The Grand Partition Function and Related Quantities.

Heat capacities, isotherms and isosteric heats are among the quantities which can be estimated from the above configurational integrals by means of the equations derived in Section 3.4.3. These are now given and discussed in terms of the effects which they predict in the system. Isotherms have previously been predicted by Limcharoen(1968) for methane in Linde 5A between 194.65° and $300^{\circ}K$. In fact these results were apparently in very good agreement with the experimental data presented in this thesis (Chapter 4). However they relied on the inaccurate values of the configurational integrals for 5, 6 and

7 molecules per cavity. Also, of course, they employed the statistics formulated by Limcharoen as discussed in Section 3.4.2, and not those suggested by Bakaev (1964), which have been accepted as the correct ones in this work.

Therefore an attempt was made to calculate theoretical isotherms using the equations of Section 3.43.4. At $300^{\circ}K$, the following results were calculated, where $\langle n \rangle$ is the average number of molecules per cavity.

Temp.	Pressure (torr)	$\langle n \rangle$
$300^{\circ}K$	20	1.11
	40	1.95
	80	3.12

Reliable values of $\langle n \rangle$ could not be calculated at significantly higher pressures because they would depend strongly on the known value of q_8, but also the unknown values of q_9 and q_{10}. Clearly at lower temperatures this problem would arise at lower pressures. These points are plotted on the graph of the experimentally measured isotherms (Fig. 4.3). The agreement between the theoretical and experiment values is seen to be poor; it will be discussed in the next section.

The equations of Section 3.4.3.4 also indicate how the isosteric heat can be found from the configurational integrals and various averages of the potential energy of n (n = 1 to G) molecules per cavity. The energy functions themselves were found by Limcharoen (1968) by the method of importance sampling (Sec. 3.4.4.2). The results are presented in Table 9.2 for $\langle n \rangle = .8933$

TABLE 9.2. — THE ISOSTERIC HEAT OF METHANE SORBED
IN LINDE 5A AS A FUNCTION OF TEMPERATURE
based on Limcharoen's data.

$^{\circ}K$	q_{st} in Cal/Mole	
	0.8933 $\langle n \rangle$ 1.808	
40	5092	5093
50	5065	5072
100	4769	4896
200	4783	4888
300	4854	4961

1.808. These compositions were used in these calculations since they were those used in the experimental heat capacity runs.

These results for the isosteric heats show two interesting effects. First at constant concentration of sorbate, with increasing temperature the isosteric heat decreases, passes through a minimum and then increases. This is readily understood since the isosteric heat consists of two contributions. These can be regarded as the energy needed to desorb the sorbate at the given concentration from the sorbent into the gaseous phase at constant molar volume, and then the energy required to expand the gas to the molar volume proper to the equilibrium pressure. For an ideal gas the last term is equal to kT. The increase in the isosteric heat at high temperatures is due to the increasing importance of this last term. At lower temperatures where this term is less significant, the the trend in the first contribution to the isosteric heat appears. This part decreases with temperature because as the temperature rises the average configurational energy per sorbed molecule rises. The configurational energy of an ideal gas is defined to be always zero. Thus the average energy needed to desorb a molecule, ignoring the heat of expansion, is smaller.

Another effect is shown by these results. Within the accuracy of the calculations the isosteric heat at $50^{\circ}K$ is the same at both compositions, but as the temperature rises the difference between them first grows and then declines. The low temperature equality is undoubtedly due to the state of the sorbate being essentially the same, no matter what its concentra-

tion. That is, all the molecules which are desorbed
come from highly filled cavities. As the temperature
increases the distribution of molecules among the cavities
becomes dependent on the sorbate concentration. On
the other hand, at high temperatures the sorbate will
be uniformly distributed no matter what its concentration
and little more redistribution can take place. The
isosteric heats here will be dependent on average
cavity filling because this determines the average
energy of the sorbed molecules, but the difference
between the isosteric heats at two not widely different
degrees of cavity filling should be temperature
independent.

There is an intermediate temperature range when
there is a fairly large difference in the isosteric
heats for two different sorbate concentrations. This
arises because at these temperatures at least one of
the isosteric heats is for a sorbate which is in the
process of redistribution, where the average energy
of sorbate molecules is changing rapidly with temp-
erature as their distribution among the cavities alter.
The actual temperature range in which this effect
occurs depends on the two sorbate concentrations,
since each determines the temperature at which
redistribution commences. The theoretical results
indicate that the redistribution commences at lower
temperatures for the smaller sorbate concentration.

The heat capacity of the sorbate was calculated
by use of the relationship derived in Section 3.4.3.5.
The chemical potential in each case was calculated by
an iterative procedure using the first equation of
Section 3.4.3.2 to give the correct cavity filling.

These results are given in Table 9.3 for the two degrees of cavity filling used in the experimental runs. The first observation is that the calculated molar heat capacity is a function of the degree of cavity filling for all temperatures, as is true of the experimental results. This is in direct contrast to the experimental and theoretical results for a selection of sorbates in clathrate cavities (Grey and Staveley 1963 and references therein). The heat capacity for both sorbate concentrations is predicted to pass through a maximum. The low temperature fall-off in the results is a classical thermodynamic effect as opposed to the quantum fall-off which always occurs in all heat capacities in practice.

The total sorbate heat capacity is obtained by adding to the configurational contribution the kinetic or thermal contribution which is $3/2\,k$ by classical mechanics. A contribution must also be added for poly-atomic molecules which have been assumed spherically symmetric (See Sec. 3.4.3.5). The main contribution to the methane heat capacity, except at low temperatures, is the intercavity redistribution term which goes through a distinctive maximum in the region $60 - 70^{\circ}K$. That is this theory predicts that with Limcharoen's data the distribution of the molecules among the cavities is fairly uniform at high temperatures; whereas at low temperatures the molecules cluster into some cavities. Thus the bulk of the spreading out of the distribution occurs, according to these calculations, in the above temperature region.

At any temperature, the free energy for the clustered system can only be lower than that for the high entropy non-clustered system if the net inter-sorbate energy is favourable, that is attractive.

TABLE 9.3. – THEORETICAL CONFIGURATIONAL HEAT
            CAPACITIES FOR METHANE IN LINDE 5A
            assuming Limcharoen's data.

C_1 and C_v are respectively the intracavity and the total
configurational heat capacity for $\langle n \rangle$ molecules of
methane. $C_v{}^*$ is the configurational heat capacity
per one molecule of methane. These data do not
include contributions from the rotation of the
methane molecules (see page 240).

°K	C_1/k	C_v/k	$C_v{}^*/k$	C_1/k	C_v/k	$C_v{}^*/k$
	$\langle n \rangle = .8933$			$\langle n \rangle = 1.808$		
40	.879	1.562	1.748	1.781	2.793	1.545
50	.934	5.064	5.668	1.888	3.642	2.014
60	.762	11.02	12.34	1.545	23.6	13.06
70	.726	5.20	5.82	1.483	13.17	7.28
100	.4	1.0	1.1	1.8	3.0	1.66
200	.03	.56	.63	.18	1.27	.70
300	.022	.52	.58	.003	.989	.547

$\langle n \rangle$ is the average number of molecules per cavity.
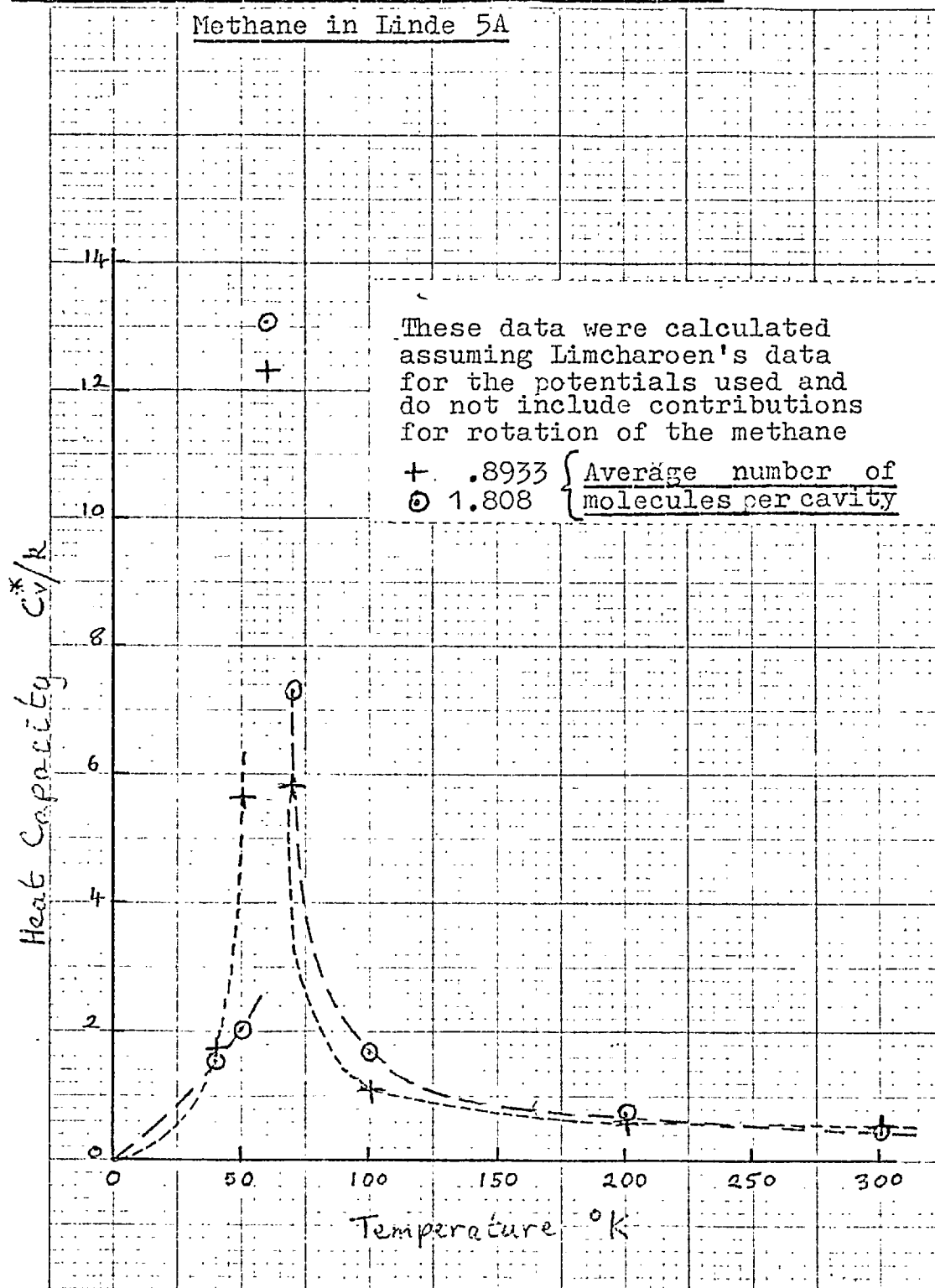
The more highly filled cavities are bound to have
higher sorbate-sorbent energies per methane molecule
than near empty cavities. The intersorbate energy
term is thus very important in these calculations, as
is the shape of the minimum in the sorbate-sorbent
potential well. A consequence of these results is
that the molar energies at very low temperatures are
the same for different overall cavity loadings because
all the molecules will be in packed cavities, that is
each is in an identical environment. At high temper-
atures the molar energy will be higher for systems
with low cavity fillings because of the decreased
intersorbate attraction. It was mentioned previously
that the same effect is seen in the predicted isosteric
heats. Thus the lower the cavity filling the greater
should be the area under the redistribution heat capacity
curve. Since this is by far the larger contribution
to the configurational heat capacity, the same applies
to this curve.

The configurational molar heat capacity is shown
in Fig. 9.2. The actual curves have not been drawn
because of the difficulty of doing so while not
contravening the above argument.

9.3. An Appraisal of These Results.

It has been shown how various thermodynamic
properties can be calculated using the statistical
mechanical equations of Chapter 3. At the outset it
should be remembered that although no quantitative
information on the observed relaxation phenomena can
be deduced from the theoretical calculations, there
should be some correlation since a relaxation effect

Fig. 9.2. Configurational Heat Capacity of Methane in Linde 5A

These data were calculated assuming Limcharoen's data for the potentials used and do not include contributions for rotation of the methane

+ .8933 { Average number of
⊙ 1.808 { molecules per cavity

in a particular temperature range indicates that the
thermal energy being taken up by the system causes a
considerable molecular rearrangement. Therefore this
intra- or intercavity redistribution should be predicted
as altering in these temperature regions.

Since the main criticism of the results of the
previous section concern the intermolecular potentials
used, these are discussed first before comparisons are
attempted with the experimental data. In the above
calculations the major effect predicted is that as the
temperature is lowered the sorbate becomes more localized
in a few cavities which are then, of course, highly
occupied. It is instructive to see the reason for this.
If the cavities were smaller or the sorbate molecules
larger, then clearly the clustering would be much less
pronounced because the maximum number of molecules per
cavity would be less. The concept of size here can be
discussed in terms of potential functions. For instance,
the methane molecule could be said to be larger if the
methane-methane potential was altered in one of two ways.
Firstly it could remain as a Lennard-Jones 12-6 potential,
but with a larger value for the σ parameter (σ being the
finite intermolecular distance which gives zero energy).

The other possibility is to use a different potential
like a Lennard-Jones 12-6 with a cut-off at an inter-
molecular separation near to σ, or, perhaps more
realistically, by using a potential with a differently
shaped well. For example the second virial coefficient
data for methane over a wide range of temperature has
recently been best correlated to a Lennard-Jones
potential of the 18-6 form (Byrne et al 1968, Parsonage
1968). A comparison of experimental data by Roettger
and Hsu (1969) showed that the second virial data for

methane was slightly better accounted for by a two
parameter gaussian-6 function than the classical
12-6 form. It would seem that the 12-6 potential is
probably only adequate for monatomic species like the
heavy inert gases. For instance, Monte Carlo calculations
of the thermodynamic properties of argon in the liquid
state (McDonald and Singer 1969) using this potential
gave better results than the use of either the 18-6
or a Kihara potential (1955) which especially allows
the interacting species to have inpenetratable cores.
On the other hand it is thought that many electron
polyatomic molecules are appreciably harder than
monatomic species, and so one of these potentials with
a repulsive part which increases sharply for small
intermolecular separations is probably more appropriate.

This discussion of intermolecular forces is not
intended to be exhaustive but should serve to illustrate
the complexity of the problem of choosing initially
reasonable potentials and then correct parameters for
them. The inter-methane interaction is the simplest
one involved in the methane-Linde 5A system. Since
there is still debate about its correct form, it can
be imagined that the other more complex potentials
involved are approximate to an even greater extent.

The potential within each cavity with regards to
methane was taken as being spherically symmetrical in the
calculations reported earlier. This was done for
expendiency in order to reduce the complexity of, and
hence the computing time required for, the Monte Carlo
calculations. Since the actual potential is due to
discrete oxygens and cations which form the cavity walls,
the actual potential must be quite heterogeneous.

This means that the true configurational volume could
be in error if the spherically symmetric potential is
not very carefully chosen, and this will again affect
the ratio of sorbate to cavity size which determines
the amount of clustering possible.

Further calculations on this system have recently
been carried out (Parsonage 1969) to investigate the
effect of changes in the intermolecular force parameters.
Since all the sorbent atoms were assumed to be discrete,
the most suitable form of the potential between each
of these atoms and methane could be chosen. Briefly
the changes which were made are as follows. The inter-
methane potential was chosen as a Lennard-Jones 18-6
type as was suggested to be appropriate above. Each
of the methane-metal ion potentials was then chosen
to be of the p-6 type in which the power of the
seperation parameter in the repulsive term was taken
as the root of the product of the ion-ion and the
methane-methane repulsion parameters. For sodium p
was 13 whilst for calcium p=15 is more proper.

The most significant change however is in the
charge allocation between the oxygens and the silicon
atoms. In the previous calculations it was assumed
that the charge that is on the zeolite framework
due to the presence of tetrahedral aluminium was equally
spread over all the oxygens and that all the bonding
in the framework was covalent. This meant that a charge
of .25e was allocated to each framework oxygen. This
would have been the correct charge distribution if the
electronegativities of the framework atoms in this
particular structure were equal. In fact the electro-
negativity of silicon is higher than that of aluminium,

whilst oxygen is far more electronegative than either of
them (Cotton and Wilinson 1962). Thus it would be
expected that the negative charge on the oxygens
suggested above was rather too low. In the new cal-
culations this charge was increased from .25e to 1e.
If the oxygens were present as ions the charge would be
twice this amount. The Si-O bonds in the new suggested
charge structure can thus be described as being 50%
ionic. The effect of this change was to cause the methane-
oxygen potential to take the 14-6 Lennard-Jones form.
The cavity potential with discrete framework atoms
and singly charged oxygens is far from being spherically
symmetric as was assumed in the first calculations.

The validity of any total intermolecular potential
can be ascertained by the calculation, by means of the
equations of Section 3.4, of the thermodynamic data
which has been measured experimentally. The results from
Limcharoen's potential data are not substantiated by
this test. It was pointed out previously that the
theoretical isotherms showed, for a given pressure,
too high a cavity filling. The measured isosteric heat
for methane was 5345 ± 50 cal/mole in the range 200-300°K
which is nearly 500 cal/mole higher than the predicted
value (Table 9.2). Also the theoretical value is
predicted to alter far more sharply with temperature
and degree of cavity filling than was observed in
practice.

A most stringent test of a potential is to compare
predicted and measured heat capacities. In this instance
there was poor agreement. Whereas the experimental heat
capacities had a broad maxima at about 175°K, the

theoretical curves had sharp maxima in the temperature
region around 60°K with the maximum value of the heat
capacity for each degree of cavity filling much higher
than the corresponding experimentally observed highest
values (see Figs. 8.2, 8.4 and 9.2). Nevertheless
the calculated data should not be depreciated too much
since it does at least show maxima in the heat capacities,
but there is clearly much need for improvement.

The results from the new calculations are much
more encouraging. Only the salient points of these will
be presented here just so as to provide a means whereby
the initial calculations reported in this thesis can
be judged. The radical change in the results is that
as the temperature decreases the sorbate is not predicted
as clustering into certain cavities whilst leaving others
empty or nearly so. At high temperatures the sorbate
distribution among the cavities will be such as to allow
the system to take up the maximum entropy, since this
term is the most significant part of the free energy
under these conditions. The molecules will tend to
spread over all possible values of n, the number of
molecules per cavity, but will be forced to group around
$\langle n \rangle$, the average number per cavity. As the temperature
decreases the entropy of the sorbate due to its spread
throughout all the cavities becomes less significant
and then the molecules will spread to large n's if the
cavity energies are favourable for this, if not they
will spread to as low a filling as possible, that is
to $n = \langle n \rangle$.

What will happen in any particular case depends on
the energy of interaction between the sorbate and the
cavity and also that between sorbate molecules within

a particular cavity. In the later case the change will
not be very significant, and will be even less so for
small $\langle n \rangle$. Therefore for this case the redistribution
heat capacity will be a small contribution to the
configurational heat capacity, the bulk of which will
be the intracavity term.

The new calculations show this to be the case for
methane in Linde 5A. Presumably this is mainly due to
the now much increased ion-induced dipole forces between
the methane and the framework oxygens which tend to
localize the former on certain parts of the cavity wall,
and that for there to be any appreciable energy gain
between any two sorbate molecules the distance between
them must be very close to the free equilibrium separation
due to the use of an eighteenth power repulsion potential.
Always any sorbate molecule movement to decrease
(i.e. net gain) the intersorbate energy would result in
a greater increase in sorbate-sorbent energy, and so
this movement will only be viable at relatively high
temperatures, and sorbate association will not be favour-
able.

Using this data sorption isotherms have been
calculated which show much better agreement with experiment
then the former calculations. The new values are as
follows; they are shown in Fig. 9.5.

$200^{\circ}K$		$300^{\circ}K$	
P	$\langle n \rangle$	P	$\langle n \rangle$
1	0.174	100	0.263
10	1.442	300	0.757
20	2.175	1000	2.000
50	3.166		
100	3.807		

Unit pressure is the torr; the gas phase has been

assumed ideal, which for methane is a very reasonable
approximation. The calculated isosteric heats are shown
in Fig. 9.3. Since the value derived from the experimental
data is 5345 ± 50 cal/mole in the range $200-300^\circ K$ and
for small $\langle n \rangle$, there is only a slight improvement
over the previous calculations (Table 9.2). Concerning
the new results, the decrease in q_{st} with $\langle n \rangle$ reflects
the less favourable energy states available to multi-
occupied cavities, an effect which decreases with
increasing temperature due to the increasing importance
of the RT term in q_{st} (see Section 9.2.3) and the
declining significance of the energy states available
to the sorbate in the cavities in determining the
equilibrium distribution. The predicted drop in q_{st}
for $\langle n \rangle = 1.808$ at low temperatures is due to the decline
in the number of cavities containing only one molecule.
The effect is hypothetical since quantum effects make
these calculations quite academic below about $70^\circ K$.

In Figure 9.4 is shown the lastest calculation of
the total heat capacity of the sorbate for the two
degrees of cavity filling used experimentally. The
agreement in the temperature range where quantum effects
are negligible is seen to be quite acceptable for each
composition. Also shown on the graph are the cavity
heat capacities for 1,2,3 and 4 molecules per cavity
(C_n in Section 3.4.3.5). The redistribution of the
molecules among the cavities is predicted as being a
minor contribution. For $\langle n \rangle = .8933$, the redistribution
could be responsible for the hump around $50^\circ K$ (although
the calculations are not accurate in fact due to the
quantum effects which have been ignored and poor
convergence of the configurational integrals) whilst
for more highly filled compositions the effects occur

Fig. 9.3.   Isossteric Heats for Methane in Linde 5A
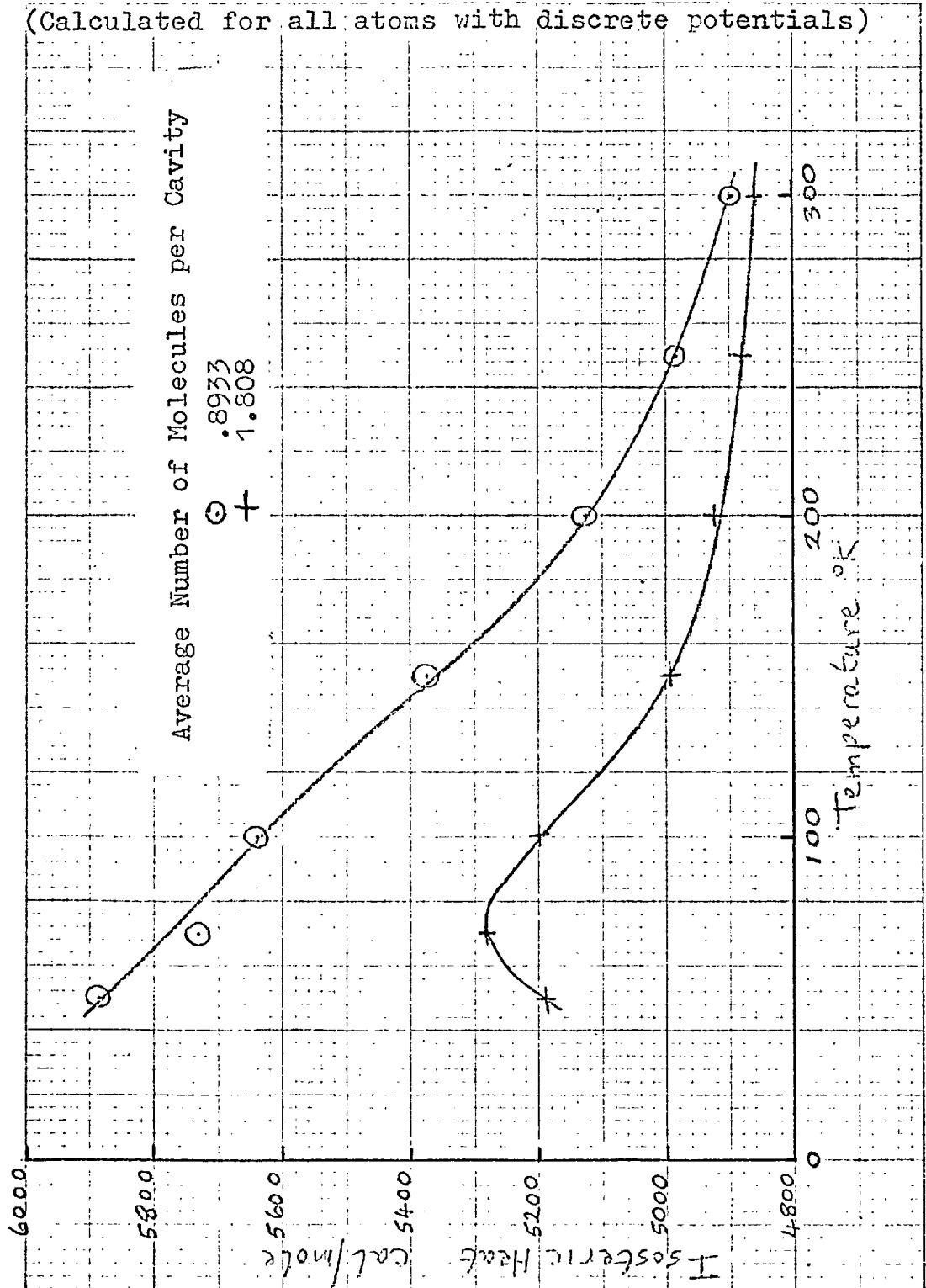(Calculated for all atoms with discrete potentials)

Fig. 9.4.   Heat Capacity of Methane in Linde 5A.
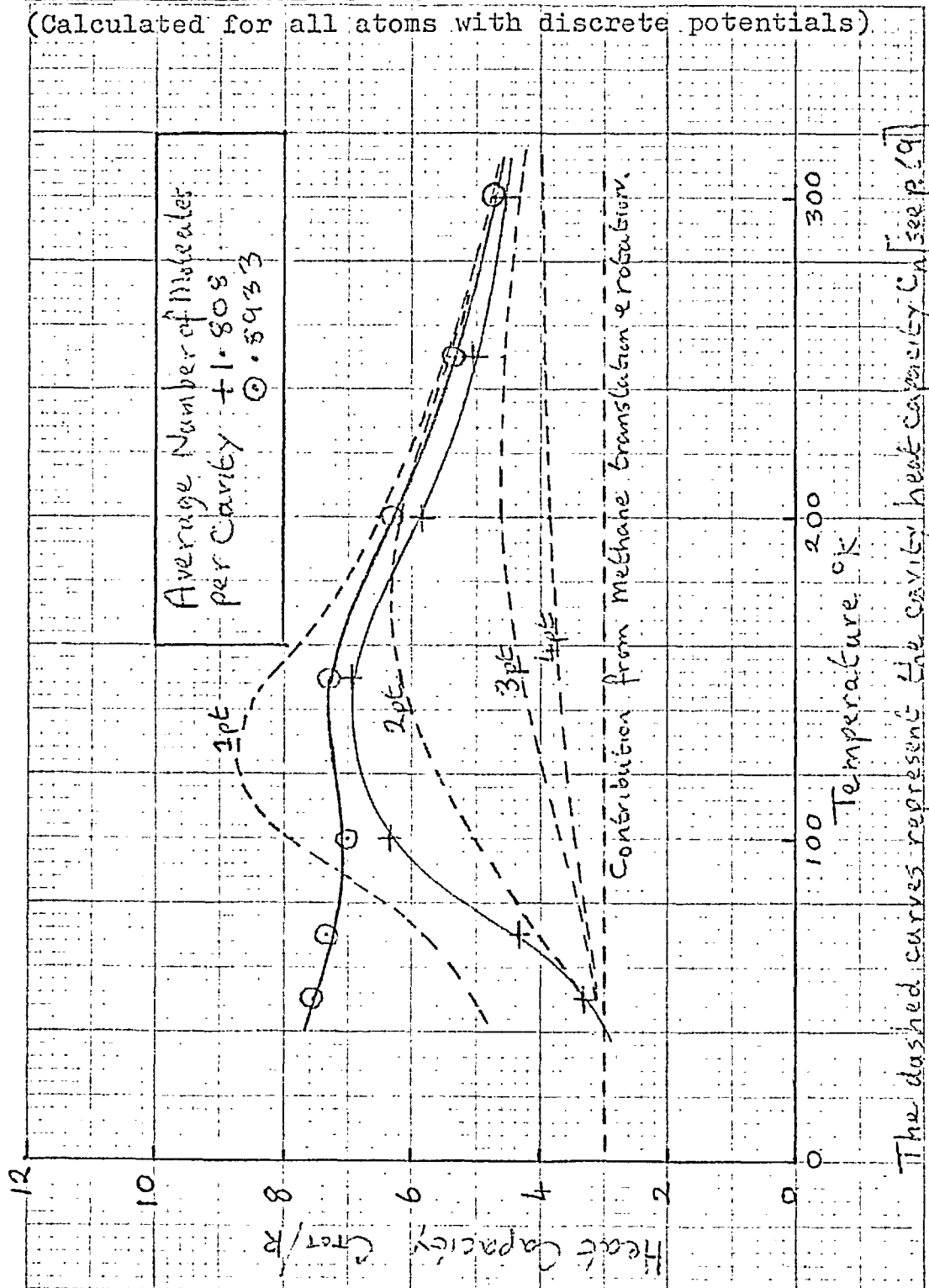
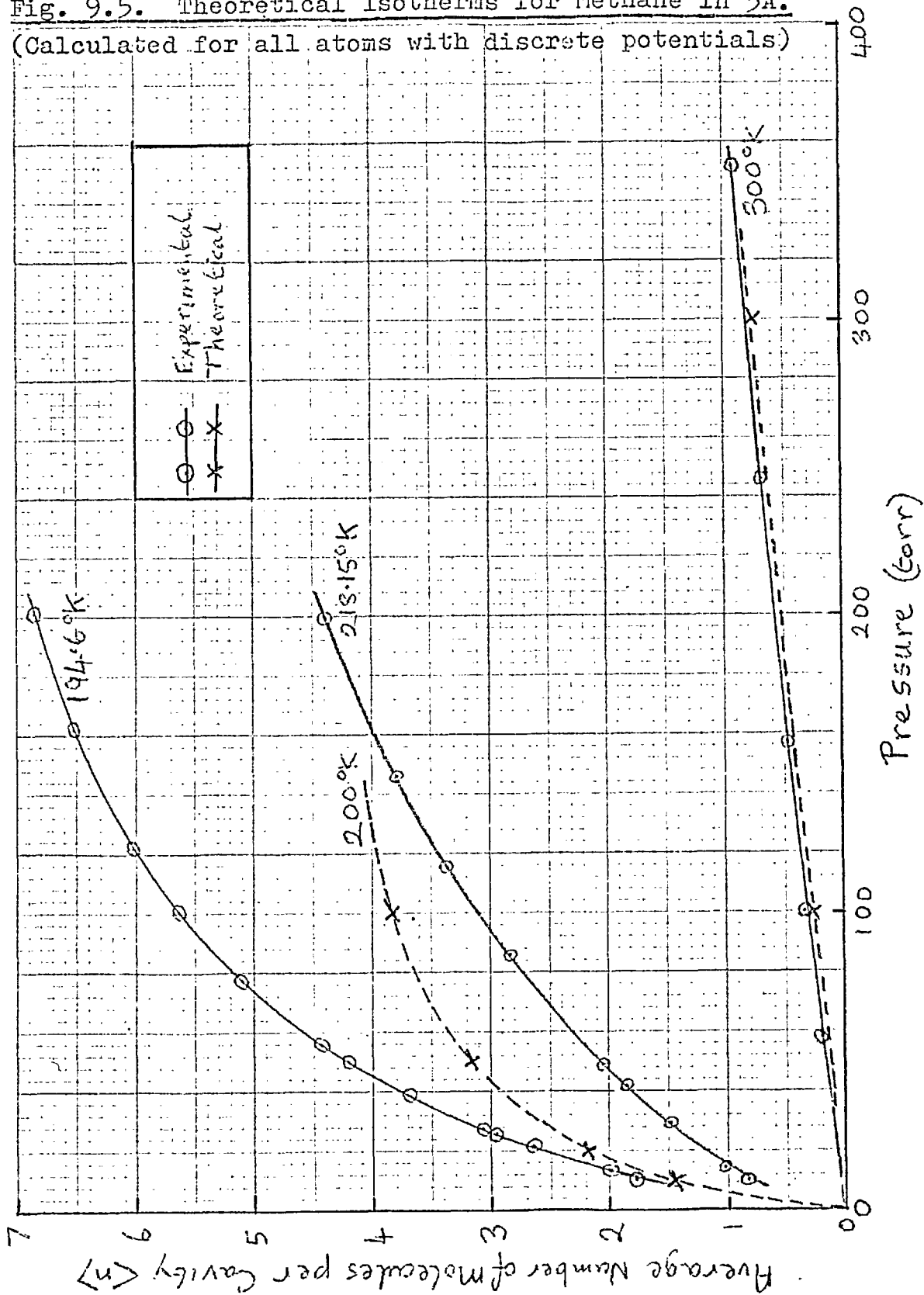

(Calculated for all atoms with discrete potentials)

Fig. 9.5. Theoretical Isotherms for Methane in 5A.
(Calculated for all atoms with discrete potentials)

at a slightly higher temperature.

The heat capacity is a very sensitive function
of the intermolecular potentials used, and a relatively
small error in these could cause the discrepancy shown.
Thus it is reasonable to conclude that the new potentials
definitely give a better representation of the actual
forces present in these complexes, and that the statistics
proposed by Bakaev are applicable to this system.
Also the measure of agreement shown between experiment
and the latter calculated results can be taken as
confirmation that the sorbate does not cluster at low
temperatures but rather spreads itself evenly throughout
the cavities. It also verifies the concept that the
zeolite framework oxygens are fairly ionic, since it is
this notion which is the major difference in the two
sets of potentials which have been studied. There is
also here justification for the reasons given in
Section 9.1 of some of the various observed slow
relaxation effects, for it was mentioned that they
required a very heterogeneous cavity potential and
much intracavity redistribution at around $100^{\circ}K$. Of
course, these calculations can shed no light on the
very low temperature relaxation effect due to the
presence of quantum effects.

The author thanks Dr Parsonage for making the
results from these new calculations available to him.

9.4.   Conclusion.

The studies embodied in this thesis were designed
to probe the sorbed phase rather more deeply than
the case had often been in the past when little more
has been done other than the correlation of the data
obtained from sorption isotherms in terms of well-
known isotherm equations. These equations are derived
by taking, for example, the sorbate has being either
localized on sorption sites or non-localized, or with
or without intersorbate forces being operative.
This approach is clearly very limited when applied to
sorption in microporous substances like zeolites in
which there are several ways in which the sorbate could
be said to be localized. For example, it has been
shown that the sorbate can be localized on certain
parts of the cavity walls or within certain cavities.
The sorption isotherm cannot give information about states
where the sorbed phase cannot equilibrate with the
gaseous phase.

Statistical thermodynamic equations have been
derived and used to allow the calculation of various
macroscopic properties in terms of the intermolecular
force parameters. The usefulness of this approach
is limited at present both by the lack of experimental
data and the dearth of reliable atomic parameters.
Nevertheless this method has enabled several significant
properties of the methane-Linde 5A system to be
observed. This is particularly true for the interpret-
ation of the calorimetric data which was first used
to select the best intermolecular potential parameters
to achieve agreement between the experimental and the
theoretical heat capacities, and then an analysis of

the finally accepted theoretical curve showed that
the intracavity redistribution of the sorbate was more
important in this system than intercavity effects
as was thought to be the case at the outset.

Now that the technique of measuring this calori-
metric data has been developed, it is hoped that many
more investigations will be undertaken. More work on
the methane-Linde 5A system at different degrees of
cavity filling would be useful; as would studies
involving different sorbents and sorbates. The noble
gases would be interesting due to their simplicity in
having no rotational contributions and their inter-
molecular force parameters being better known. Use of
type A zeolites with different cations and hence different
window sizes and force properties would be a useful
area for future work. A calorimeter vessel designed
to operate with an internal pressure of several
atmospheres would be required for the extended work at
higher cavity fillings or with less strongly sorbed
species.

The theoretical calculations are very time consuming
both on the part of the investigator and the computer.
It is hoped that better mathematical techniques and the
more versatile computers which will be available will
make it possible to calculate more data more quickly.

Taken as a whole this field of study seems very
promising both from the viewpoint of gaining a deeper
insight into the sorbed state, especially those in micro-
voids, and also in the more precise characterization of
the intermolecular forces which are present in these

complex sorbents.

Since these zeolites are finding an ever increasing
number of uses in the chemical industry both as sorbents
and as catalysts (often containing precious metals),
it is hoped that this work will eventually be of some
small benefit to the progress of chemistry in these
fields also.

REFERENCES

Bakaev,V.A.   Dokl.Akad.Nauk.SSSR 167(1964)369

Barrer,R.M.   "The Structure and Properties of Porous
                     Materials" in Proc 10th Symp Colston
                     Research Soc,Butterworths (London)1958,8

Barrer,R.M &   Trans.Faraday Soc.54(1958)1074
Meier,W.M.

Barrer,R.M.   in "Non-stoichiometric Compounds"
                     Ed. L.Mandelcorn,Academic Press N.Y.1964,309

Barrer,R.M. & Paterson,D.L.   Proc.Roy.Soc.A280(1964)466

Birkenhead   "The Prof in Two Worlds" Collins 1961

Bobka,R.J. et al.   J.Phys.Chem.61(1957)1646

Breck,D.W. et al.   J.Amer.Chem.Soc.78(1956)5963

Breck,D.W. & Smith,J.V.   Scientific American 200(1959)85

Broussard,L & Shoemaker,D.P. J.Amer.Chem.Soc.82(1960)1041

Brunnauer,S.   "The Adsorption of Gases and Vapours"
                    Clarendon Press (Oxford)1945

Busey,R.H. et al.   J.Amer.Chem.Soc.78(1956)3263

Byrne,M.A. et al.   Trans.Faraday Soc.64(1968)1747

Chemical Society   Interatomic Distances, Special
                    Publication 11(1958)

Cole,A.G. et al.   J.Amer.Chem.Soc.82(1960)4807

Cope,A.F.G.   Ph.D. Thesis,Univ.of London(1967)

Cotton,F.A. &   "Advanced Inorganic Chemistry"
Wilkinson,G   J.Wiley London (1962)92

Coulter,L.V. et al.   J.Phys.Chem.Solids24(1963)171

Dauphinee,T.M.   Can.J.Phys.31(1953)577

Denbigh,K.G.   Trans.Faraday Soc.36(1940)936

Eastman,G.Y.   Scientific American 218(1968)38

Flavell,W & Yarsley,V.E   Chem.in Brit.3(1967)375

Fosdick,L.D.   Methods in Computational Physics 1(1963)245

Furukawa,G.T et al. J.Res.Nat.Bur.Standards 47A(1951)256

Gallant,R.W.   Physical Properties of Hydrocarbons
                    Vol 1 Gulf Publishing Co Houston (1968)

Garden,L.A. & Kington,G.L.   Proc.Roy.Soc.A234(1956)24

Garden,L.A. et al.   Proc.Roy.Soc.A234(1956)35

Ginnings,D.C & Furukawa,G.T.   J.Amer.Chem.Soc.75(1953)522

Ginnings,D.C. & West,E.D.   Rev.Sci.Instr.35(1964)965

Grey,N.R. & Staveley,L.A.K.   Mol.Phys.6(1963)83

Hill,T.L.   J.Chem.Phys.14(1946)441

Hill,T.L.   J.Chem.Phys.17(1949)520

Hill,T.L.   Statistical Mechanics McGraw-Hill
                N.Y. (1956)191

Hill,T.L.   Adv.Catalysis 4(1959)212

Herschfelder,J.O. et al. Molecular Theory of Gases and
                Liquids J.Wiley N.Y. (1954)1110

Howell,P.A.   Acta Cryst.13(1960)737

Kihara,T.   Rev.Mod.Phys.25(1953)831

Kington,G.L. & Aston,J.G.   J.Amer.Chem.Soc.73(1951)1929

Kiselev,A.B. & Lopatkin,A.A.   Confer.on Molecular
                Sieves S.C.I. London (1967)

Kvitkovskii,L.N. &Sergienko,S.R.   Dokl.Akad.Nauk.SSSR
                147(1962)1399

Landolt-Bornstein   Physikalisch-Chemische Tabellen
                1,Auflage (1950)401

Lange,F   Z.Physik Chem.110(1924)343

Lennard-Jones,J.E & Devonshire,A.F.   Proc.Roy.Soc.
                A163(1937)53

Lewis,P.H.   J.Phys.Chem.63(1959)527

Limcharoen,P.   Ph.D. Thesis Univ.of London (1968)

Loewenstein,W.   Min. Mag.39(1954)92

Marvel,C.S.   Soc.Plastics Engineers Trans.5(1965)29

McDonald,I.R. & Singer,K.   J.Chem.Phys.50(1969)2308

Meier,W.M.   Conference on Molecular Sieves
                S.C.I. London (1967)

Metropolis,N et al.   J.Chem.Phys.21(1953)1087

Moelwyn-Hughes,E.A.   Physical Chemistry Pergamon
                Oxford (1961)297

Morrison,J.A. & Szasz,G.J.   J.Chem.Phys.16(1948)280

Osborne,N.S. et al.   J.Amer.Chem.Soc.77(1955)2737

Pace,E.L.   The Solid-Gas Interface Vol 1
                Ed.E.A.Flood Arnold (London) (1967)105

Parsonage,N.G. & Staveley,L.A.K.   Mol.Phys.2(1959)212

Parsonage,N.G. & Staveley,L.A.K.   Mol.Phys.3(1960)59

Parsonage,N.G.   Private Communication (1969)

Pemberton,R.C.   Ph.D. Thesis Univ.of London (1965)

Parsonage,N.G.   Ann.Rep.Chem.Soc.65(1968)33

Pitzer,K.S.   Adv.Chem.Phys.2(1959)59

Pitzer,K.S. & Gwinn,W.D.   J.Chem.Phys.10(1942)428

Reed,T.B. & Breck,D.W.   J.Amer.Chem.Soc.78(1956)5972

Rees,L.V.C. & Williams,C.J.   Trans.Faraday Soc.60(1964)1973

Roettger,G.E. & Hsu,H.W.   J.Chem.Eng.Data 14(1969)44

Rowlinson,J.S. & Townley,J.R.   Trans.Faraday Soc.
                49(1953)20

Rushbrooke,G.S.   Introduction to Statistical Mechanics
                O.U.P. Oxford (1949) (a)Ch7, (b)49

Schirmer,W. et al.   Conference on Molecular Sieves
                S.C.I. (London) (1967)

Siebert,A.R. & Pace,E.L.   J.Amer.Chem.Soc.60(1956)828

Southard,J.C. & Andrews,D.H.   J.Franklin Inst.209(1930)349

Southard,J.C. & Brickwedde,F.G.   J.Amer.Chem.Soc.
                55(1933)4378

Stansbury,E.E. et al.   Rev.Sci.Instr.36(1965)480

Stepakoff,G.L. & Coulter,L.V.   J.Phys.Chem.Solids
                24(1963)1435 ·

Sterret,K.F. et al.   J.Res.Nat.Bur.Stand.69C(1965)19

Waals van der,J.H.   Trans.Faraday Soc.52(1956)184

Waals van der,J.H. & Platteew,J.C.   Adv.Chem.Phys.
                2(1959)1

Wentorf,R.H. Jr. et al.   J.Chem.Phys.18(1950)1484

West,E.D.   J.Res.Nat.Bur.Stand.67A(1963)331

Wood,W.W. & Parker,F.R.   J.Chem.Phys.27(1957)720

Young,D.M. & Crowell,A.D.   Physical Adsorption of
                Gases, Butterworth London (1962)7